THE DYNAMICS AND PHASE BEHAVIOR OF SUSPENSIONS OF STIMULI- RESPONSIVE COLLOIDS

A Dissertation
Presented to
The Academic Faculty

by

JAE KYU CHO

In Partial Fulfillment
of the Requirements for the Degree
Doctor of Philosophy in the
School of Chemical & Biomolecular Engineering

Georgia Institute of Technology
December 2009

THE DYNAMICS AND PHASE BEHAVIOR OF SUSPENSIONS OF STIMULI-RESPONSIVE COLLOIDS

Approved by:

Dr. Victor Breedveld, Advisor
School of Chemical & Biomolecular Engineering
Georgia Institute of Technology

Dr. J. Carson Meredith
School of Chemical & Biomolecular Engineering
Georgia Institute of Technology

Dr. Hang Lu
School of Chemical & Biomolecular Engineering
Georgia Institute of Technology

Dr. Eric R. Weeks
Department of Physics
Emory University

Dr. L. Andrew Lyon
School of Chemistry & Biochemistry
Georgia Institute of Technology

Date Approved: July 17, 2009

Dedicated to beloved my wife, daughter, mom, brother and parents-in-law.

Especially, to the memory of my father

HEE SEO CHO
(July 17, 1949 ~ December 15, 2006)

ACKNOWLEDGEMENTS

My life at Georgia Tech has been excellent and successful because of the luck enough to get supported and inspired by great deal of insightful, enthusiastic, and open-minded faculty members and students. I would like to first thank my advisor, Dr. Victor Breedveld for his support, willingness, and encouragement. If I think back a moment, there were lots of trials and errors. He provided an opportunity how overcome obstacles and how to learn from the mistakes. His attitude and philosophy toward research motivated me to be a real expert. I also would like to thank Dr. L. Andrew Lyon for allowing me to use excellent facilities almost at anytime as well as thoughtful discussions and valuable comments. I wish to thank Dr. Hang Lu for collaboration and sharing various facilities. Also thank to other committee members, Dr. J. Carson Meredith and Dr. Eric W. Weeks for all the helpful comments and suggestions.

During my journey, I received various supports from a number of people, especially colleague students. Thanks to the Complex Fluids Research Group members, Dr. Jun Sato, Dr. Ryan Slopek, Balamurali Balu, Kayode Orlanrewaju, Enrique Michel-Sanchez, Tracie Owens, Dr. Raymond Tu, Dr. Jeng-Shiung (James) Jan, Dr. Santosh Rahane, Dr. Vikram Prasad. We have been a great team and grown together over many years. Also thanks to Dr. Lu group members, Kwanghun, Ed, Matt, Gina, Alison, Jeff, Ivan, Hyewon, and Jan for being a pseudo group members. Another thanks to Dr. Lyon group students, Stella, Jonathan, Bart, Zhiyong, Toni, Grant, and Mike for providing me a great deal of help.

I would like to express my special thanks to my wife, Hyesun. We have gone through many obstacles and we enjoyed all the happiness, difficulties, and sorrow together. Without her endless love, encouragement, compassion, and persistent endurance, I would not be here today. My another special thanks go to my parents for providing me various opportunities, observing my growth with great care, and understanding me in every moments. Especially, I am very indebted to my father, who now stays near God in peace. I cannot express with any words how much I loved my father. In the moment I was in deep sorrow for losing my father, the birth of my daughter, Eileen, gave me a reason to come back to life. I also would like to thank my brother, Moon Kyu, for sharing wonderful childhood and encouraging me in all endeavors. I also would like to acknowledge my parents in-law for providing continual supports and love. My other thanks are reserved for brothers in-law and sisters in-law, especially Panya and Michelle for being buddies beyond monotonous life in Atlanta.

My last thanks go to my friends and Korean Mobs in ChBE for refreshing me beyond research. I cannot image my life without them.

TABLE OF CONTENTS

LIST OF TABLES

LIST OF FIGURES

Page

LIST OF SYMBOLS

2D	2-Dimensionion
3D	3-Dimensionion
D	Diffusion coefficient
D_o	Bulk diffusion coefficient
$D_{//}$	Lateral diffusion coefficient
d	Dimensionality of space
ε_0	Dielectric permittivity of a vacuum
ε_r	Dielectric permittivity of a medium
$f_{//}$	Hindrance coefficient
$f_{//,1}$	Hindrance coefficient near a wall
$f_{//,2}$	Hindrance coefficient between two walls
$\overline{f_{//,2}}$	Average hindrance coefficient between two walls
G'	Storage Modulus
G''	Loss Modulus
g(r)	Radial (Pair) distribution function
H	Height
h	Position of a sphere
$\bar{h}$	Average height
η	Viscosity of a suspension
η_r	relative viscosity
η_s	Solvent viscosity
I	Ionic Strength

k	Shift factor
k_B	Boltzmann constant
k^{-1}	Debye screening length
MW	Molecular weight
n	Refractive index
n_m	Refractive index of medium
n_p	Refractive index of polymer
Δn	Refractive index difference
ϕ_{eff}	Effective volume fraction
ϕ_f	Freezing point
ϕ_g	Glass transition point
ϕ_m	Melting point
$\phi_{\max}$	Maximum packing fraction
σ	Surface charge density
τ	Relaxation (Lag) time
ψ	Electric potential
ψ_0	Surface electric potential
R_H	Hydrodynamic radius
R_o	completely collapsed radius of microgel
T	Temperature
$u(\mathrm{r})$	interparticle potential
u_C	Coulombic interparticle potential
u_{DLVO}	interparticle potential in DLVO theory
u_s	hard sphere interparticle

u_{vdW}	van der Waals interparticle potential
τ	Relaxation (Lag) time
wt%	weight fraction
w (r)	multi-body interaction
z_i	ion valency
z^*	effective charge

LIST OF ABBREVIATIONS

AAc	Acrylic acid
AFM	Atomic force microscopy
APS	Ammonium persulfate
BCC	Body centered cubic
BCO	Body centered orthogonal
BIS	*N,N'*-Methylene bisacrylamide
C	Concentration
CCD	Charge-coupled device
CGC	Critical gel concentration
CGT	Critical gel temperature
CMC	Critical micelle concentration
CMT	Critical micelle temperature
C/S	Core/shell
DI	Deionized
DIC	Differential interference contrast
DLS	Dynamic light scattering
DLVO	Derjaguin-Landau-Verwey-Overbeek
DNA	Deoxyribonucleic acid
DOF	Depth of focus
EM	Electrson microscopy
EO	Ethylene oxide
FCC	Face-centered cubic
FT	Fourier Transformation

LCST	Lower critical solution temperature
LSA	Linear superposition approximation
MSD	Mean squared displacement
N.A.	Numerical aperture
NIPAm	*N*-isopropylacrylamide
OT	Optical tweezers
PCR	Polymerase chain reaction
PCS	Photon correlation spectroscopy
PDMS	Polydimethylsilosane
PEG	poly(ethylene glycol)
PEO	poly(ethylene oxide)
PEO-PPO-PEO	poly(ethylene oxide)- poly(propylene oxide)- poly(ethylene oxide)
PMMA	poly(*methyl methacrylate*)
pNIPAm	poly(*N*-isopropylacrylamide)
pNIPAm-*co*-AAc	poly(*N*-isopropylacrylamide-*co*-acrylic acid)
PO	propylene oxide
PPO	poly(propylene oxide)
PS	polystyrene
PTVM	Particle tracking video microscopy
RHCP	Random hexagonal close-packed
SANS	Small-angle neutron scattering
SAXS	Small-angle x-ray scattering
SEM	Scanning electron microscopy
SFA	Surface force apparatus
STM	Scanning tunneling microscopy

TEM	Transmission electron microscopy
TIRM	Total internal reflection microscopy
VPT	Volume Phase Transition

SUMMARY

The role of colloids in science has changed dramatically over the past few decades as they are being used as novel advanced materials for various applications *e.g.* paint/coating, electronics, cosmetics, and pharmaceutics. Direct observation and manipulation of colloids are now very common and colloidal dispersions are being used as model systems for studying equilibrium/non-equilibrium thermodynamics and kinetics of molecular and atomic systems. While most original pioneering works in colloidal science has been performed with a focus on hard sphere systems, researchers now devote considerable attention to more complex soft colloids. Aqueous microgels form one of the most extensively studied classes of soft materials due to their unique tunability and responsiveness. However, the fundamental knowledge about microgels is still rather poor, in particular for multi-responsive systems, and there are a variety of open questions that need to be answered. As a contribution to this field, this thesis describes studies of the dynamics, phase behavior, interparticle interactions, and hydrodynamics of stimuli-responsive pNIPAm-*co*-AAc microgels. Since these microgels are multi-responsive to the external stimuli temperature, pH, and ionic strength, one can tune their interparticle interactions and size. These colloidal particles serve as excellent model systems to probe the relationship between colloidal interactions and phase behavior. As a first step, we established our core experimental methodology, by demonstrating that particle tracking video microscopy is an effective technique to quantify various parameters in colloidal systems, such as the hydrodynamic particle radius, local temperature of a dilute

suspension, and rheological/micro-structural properties of the embedding medium. Then we used the technique in combination with a microfluidic device that provides in situ control over sample pH to probe the phase behavior of pNIPAm-*co*-AAc microgel suspensions. In essence, the experimental set-up enables changes in effective particle volume fractions by changing pH, which can be used to construct the phase diagram. In order to explain the unique features of the microgel phase diagram, we measured the underlying pairwise interparticle potential of pNIPAm-*co*-AAc microgels directly in quasi-2D suspension and proved that the interactions are pH dependent and can range from weakly attractive to soft repulsive. Finally, the hindered Brownian diffusion due of colloidal particles confined by hard walls was investigated systematically and striking differences between hard sphere and soft sphere were found, with soft pNIPAm-*co*-AAc microgels showing surprising mobility even under strong confinement.

CHAPTER 1

INTRODUCTION

A colloidal particle is a microscopic entity ranging in size between 10 nm and 1 μm. Colloids are very common in everyday life; for example, paint, ink, smoke, cosmetics, pharmaceutics, and many food dispersions such as ketchup, milk, and mayonnaise are all classified as colloidal systems. The study of colloids aims to obtain a better understanding of the stability, flow behavior, interactions, and phase behavior of these materials. The history of colloidal research goes back to the mid-nineteenth century, to experiments with colloidal gold sols by Michael Faraday and liquid diffusion studies by Thomas Graham. The term colloid was coined by Graham in 1861 based on the Greek word κολλα (which means "glue") to differentiate between substances that could diffuse through membranes and substances that could not [1, 2]. Since then, the definition of colloid has been used quite leniently to describe any particle that undergoes Brownian motion. As long as they meet the size criteria, colloids can consist of any kind of material and appear in many different shapes, for instance, spheres, ellipsoids, platelets, and rods.

In general, colloidal particles exhibit constant irregular motion, which is often described mathematically with a stochastic equation. Due to continuous thermally driven collisions between solvent molecules and colloidal particles, the latter exhibit random Brownian motion driven by energy of magnitude $k_B T$. Einstein first related the diffusion coefficient (D) of a colloidal suspension to this thermal energy [3]. By considering Stokes' law for the hydrodynamic mobility, the diffusion coefficient for colloids in dilute dispersions can be rewritten in term of their hydrodynamic radius (R_H) and the viscosity of medium (η), so called Stokes-Einstein-Sutherland relation,

$$D = \frac{k_B T}{6\pi\eta R_H} \tag{1.1}$$

Colloidal particles are very unique since they are sufficiently large and slow to be observed by optical techniques, such as conventional light microscopy. Thus, many researchers have used colloidal suspensions as a model system for a large variety of processes, such as nucleation, growth and melting of crystals [4-8]. Interparticle forces between colloids are strong enough to promote macroscopic ordering, leading the formation of a sequence of phases. Slight variations in environmental conditions can trigger phase changes that in turn induce major changes in macroscopic properties. Understanding the relation between colloidal particle interactions and phase behavior is essential for developing predictive models of the macroscopic behavior of colloidal systems. The following section will discuss the interaction forces that govern colloidal systems at the microscopic level.

1.1 Forces in colloidal systems

Many applications of colloids require control over the various interparticle forces that play a role in these systems, *e.g.* electrostatic forces, van der Waals forces, and hydrophilic/hydrophobic forces [9]. Consequently, scientists have devoted considerable effort experimentally and theoretically to understand this topic. Overall forces between colloids are the result of a complex interplay between many chemical and physical processes at the molecular level. Practically, the total force can be obtained by summing intermolecular forces of all types that are present in the system. In this section, we will first discuss the various intermolecular forces separately and then describe the effects of their combined actions in the following section.

1.1.1 Electrostatic forces

In some cases when a colloid is dispersed in a solvent, it acquires surface charges due to the dissociation of chemical groups at the surface or due to the adsorption of ionic species, *e.g.* electrolytes or ionic surfactants [10, 11]. For simplicity, the resulting surface charge is often considered to be homogeneous, although in reality the charges are discrete and heterogeneously distributed. In solution, charged materials attract counterions, in which form an immobile layer of ions close to the surface that is usually called the Stern or Helmholtz layer. This layer, in turn, controls the ion distribution nearby and gives rise to a diffuse counterion atmosphere, the electric double layer. In general, charged surfaces can be characterized by a surface charge density σ and surface potential Ψ_0. To describe the potential or distribution of ions in the solutions, one must solve the Poisson equation, a non-linear second order partial differential equation that requires two boundary conditions. Although there is no general solution of this equation, in the limit of low, constant surface potential Ψ_0, the solution is:

$$\Psi(x) \approx \Psi_0 e^{-\kappa x} \tag{1.2}$$

with

$$\kappa^{-1} = \left(\frac{\varepsilon_0 \varepsilon_r k_B T}{\sum_i c_{\infty i} e^2 z_i^2} \right)^{1/2} \tag{1.3}$$

where ε_r is the solvent relative dielectric constant, ε_0 the dielectric permittivity of a vacuum, $c_{\infty i}$ the concentration of ion species *i* at the reference point (normally chosen to be the bulk concentration), and z_i ion valency; the summation must be carried out over all ion species in solution. The parameter κ^{-1}, as defined in Eq. (1.3), is referred to as the Debye screening length and defines the characteristic distance from the surface over which electrostatic forces are felt. It is a function of electrolyte concentration and ion

valency as shown in Table 1.1. For instance, a 10 mM 1:1 electrolyte solution has κ^{-1} = 3.04 nm and for an 0.1 mM 1:1 electrolyte solution κ^{-1} = 30.4 nm. Generally speaking, the Debye screening length is inversely proportional to electrolyte concentration and valency of electrolyte. These lengths quantify the range of electrostatic interactions and can be significant compared to the size of colloidal particles.

Table 1.1 Values of κ^{-1} for various electrolyte concentrations and valencies for aqueous solution at 25 °C.

C (mM)	**Symmetric electrolyte** (*e.g.* NaCl, $MgSO_4$, $FePO_4$)		**Asymmetric electrolyte** (*e.g.* $CaCl_2$, $LaCl_3$, Ag_2S_3)	
	$Z_+ : Z_-$	$\kappa^{-1}(nm)$	$Z_+ : Z_-$	$\kappa^{-1}(nm)$
100	1:1	0.961	1:2, 2:1	0.556
	2:2	0.481	1:3, 3:1	0.393
	3:3	0.320	2:3, 3:2	0.249
10	1:1	3.04	1:2, 2:1	1.76
	2:2	1.52	1:3, 3:1	1.24
	3:3	1.01	2:3, 3:2	0.787
1	1:1	9.61	1:2, 2:1	5.56
	2:2	4.81	1:3, 3:1	3.93
	3:3	3.20	2:3, 3:2	2.49
0.1	1:1	30.4	1:2, 2:1	17.6
	2:2	15.2	1:3, 3:1	12.4
	3:3	10.1	2:3, 3:2	7.87

1.1.2 Van der Waals forces

All interfacial phenomena in colloidal system are influenced significantly by forces that have their origin at atomic or molecular level interactions due to dipole or

induced dipole of molecules [12, 13]. Collectively, these forces are often referred to as van der Waals forces. They have a shorter effective range than electrostatic forces, but play an important role in all aspect of materials including atoms, molecules, and particles. For example, van der Waals forces contribute to numerous interfacial and colloidal phenomena, *e.g.* adsorption of materials, surface tension, stability of liquid films, adhesion, and colloidal aggregation. Van der Waals forces are usually attractive and consist of Keesom interactions (permanent dipole-permanent dipole), Debye interactions (permanent dipole-induced dipole), and London or dispersion interactions (induced dipole-induced dipole). Two permanent dipoles, which have two equal charges of opposite sign can rotate easily in a solvent over all orientations. To maximize the electrostatic interaction between dipoles, they align themselves parallel but opposite direction and this alignment generates net attractive force. In a similar manner, when permanent dipole is resent next to non-permanent dipole, a permanent dipole generates an electric field, by which it induces non-permanent dipole into induced-dipole and aligns themselves oppositely parallel direction, providing another type of attraction between permanent dipole and induced dipole. Even between molecules without a permanent dipole, such as non-polar hydrocarbons, fluctuations of the electron cloud around the nuclei can generate instantaneous dipoles, resulting in London forces.

1.1.3 Miscellaneous colloidal forces

Other important colloidal forces include solvation forces (hydrogen bonding), hydrophilic/hydrophobic forces and steric forces [9, 14-16]. Solvation forces arise when a liquid is confined to a gap between two surfaces and solvent orientation at the surfaces introduces short range repulsive forces which are stronger than attractive van der Waals forces. This short range stabilizing force was observed between solid surfaces, such as silica and mica, across water [17-19]. For instance, when two mica plates are brought together at close separation (normally less than about 10 solvent molecule diameters),

they experience repulsive force rather than attractive van der Waals. Although the molecular origin of solvation forces is not clear, most researchers consider the ordering of the solvent molecules into semi-ordered layers the surfaces as a main cause. Since the structured solvent layers are stabilized by effective orientation associated with multi-body interactions, any disruption or change of this ordering is not favorable due to considerable entropic penalty, which in turn generate a repulsive force. Hydrogen bonding is a special type of solvation force, namely the attractive force between one electronegative atom and a hydrogen atom covalently bonded to another electronegative atom. Hydrogen bondings are weaker than covalent bonds, but strong enough to be of significance on molecular and colloidal scales, as evidenced by the high boiling point and surface tension of water in comparison to other solvents, and by the double helical structure of DNA which is stabilized by multiple hydrogen bondings.

Hydrophilic/hydrophobic forces are also of importance in colloidal systems. The origin of these forces can be explained by strong electrostatic cohesion in water. Water molecules tend to form hydrogen bondings with each other, thus excluding non-polar molecules that are incapable of forming hydrogen bondings, *e.g.* alkanes, hydrocarbons, and fluorocarbons. In other words, formation of hydrogen bondings around non-polar molecules requires reorientation or restructuring of water molecules and it costs high entropic and enthalpic penalty. For this reason, hydrocarbons are poorly soluble in water and water molecules are highly immiscible with most organic solvents.

Lastly, when colloidal particles with hairy surfaces (*e.g.*, grafted or adsorbed polymers) approach each other, they experience a repulsive force once the outer surface layers begin to overlap. This phenomenon is caused by the unfavorable entropic penalty associated with compression or overlap of polymer chains and is referred to as steric repulsion. Experimentally, surfactants or polymer additives are added in colloidal suspensions and if they are soluble in the solvent, the added materials cover the surfaces of colloidal particles by adsorption or covalent attachment. The parts of the materials that

are not in direct contact with the surfaces tend to extend out from the surface to maximize their degree of freedom. Once the colloidal particles are fully covered, the colloidal particles can see one another through the hairy outer layer part. In general, the dimension of adsorbed molecule determines the range of the force and the onset of the repulsive force.

1.2 Colloidal phase behavior and interparticle potentials

Colloidal suspensions exhibit remarkably interesting phase behavior, with a variety of phase transitions between gas, liquid, crystal, and liquid-crystal coexistence phases, similar to atoms and molecules. As a result, colloids have been widely used as a model system for phase behaviors [6, 16, 20, 21], intermolecular interactions [22, 23], and crystallization kinetics [4]. The key advantages of colloidal particles over atomic and molecular systems are their large size, slow dynamics, and the tunability of their interactions. Colloids are sufficiently large to scatter visible light. Unlike atomic systems, which require special instruments like ultrafast spectroscopy, atomic force microscopy (AFM), and scanning tunneling microscopy (STM), colloidal systems can directly be observed with relatively simple experimental techniques, such as light scattering and optical microscopy. Whereas the characteristic time scale of processes in atomic systems usually are on the order of femto-seconds, the dynamics of colloids are much slower, spanning a range of time scales from milliseconds to several months. It is therefore no surprise that the Brownian motion of colloids was first observed in the 19^{th} century with a rather rudimentary experimental apparatus, while the first direct observation of atoms occurred much later. Furthermore, the chemical and physical properties of colloids and solvents in which they are dispersed can be easily tuned in order to engineer the forces between colloids. For instance, by grafting ionic groups, DNA, or small polymer

segments on the surface of colloidal particles, one can introduce electrostatic forces, specific binding forces, or steric forces [24-26]. Modification of solvent viscosity can be used to manipulate the time scale of colloidal dynamics. By controlling the density and refractive index difference between solvent and colloids, one can not only minimize gravitational effects, but also suppress attractions arising from van der Waals interactions.

1.2.1 Intermolecular interactions

Many researchers have tried to predict colloidal phase behavior and proposed models for interparticle interactions. A major advance in quantitatively studying the interactions between colloidal particles was achieved by Derjaguin, Landau, Verwey, and Overbeek (DLVO theory) who provided insights in the stability of charge-stabilized colloidal suspensions [27, 28]. According to DLVO theory, the interaction potential between two colloidal particles can be explained by the interplay of three force components: excluded volume interaction due to the finite diameter of colloids (Eq. (1.5)), screened Coulombic repulsion with screening length κ^{-1} (Eq. (1.6)), and short range van der Waals attraction (Eq. (1.7)):

$$u_{DLVO}(x) = u_S(x) + u_{vdW}(x) + u_C(x) \tag{1.4}$$

with

$$u_s(x) = \begin{cases} 0 & x > 2r \\ \infty & x \le 2r \end{cases} \tag{1.5}$$

$$\frac{u_C(x)}{k_B T} = Z^{*2}\left(\frac{e^{\kappa r}}{1+\kappa r}\right)^2 \frac{e^2}{4\pi\varepsilon_0\varepsilon_r k_B T}\frac{e^{-\kappa x}}{x} \tag{1.6}$$

$$\frac{u_{vdW}(x)}{k_B T} = -\frac{A}{6}\left(\frac{2r^2}{x^2-4r^2} + \frac{2r^2}{x^2} + \ln\left(\frac{x^2-4r^2}{x^2}\right)\right) \tag{1.7}$$

where Z^* is effective charge on the particle surface and r is the radius of the colloidal particles. Although the DLVO theory has a simple mathematical form and requires several assumptions, it has been applied successfully to many colloidal systems [23, 29, 30].

1.2.2 Hard sphere system

When the interaction between colloidal particles is zero at all separations except for a strong repulsion at physical overlap, as described by Eq. (1.5), these particles are referred to as hard spheres. The hard sphere model is the simplest theoretical model for a colloidal system. Experimentally, it has been realized by using refractive index-matched solvents with monodisperse, sterically stabilized colloids for which the thickness of the stabilizing polymer segment is much smaller than the radius of the particles [16, 31, 32]. The phase diagram of a hard sphere suspension can be predicted by a single parameter, the particle volume fraction (ϕ), as shown in Fig. 1.1 [16, 33]. The upper limit for ϕ is the maximum packing density ($\phi_{\max}$), which is realized when hard spheres are arranged in close-packed layers with twelve-nearest neighbors. While $\phi_{\max,\,cp} = 0.7404$ can be achieved for regularly packed monodisperse spheres, random close packing renders $\phi_{\max,rcp} = 0.637$. Hexagonal packing with six in-plane neighbors maximizes the local entropy for each particle, which is the driving force towards crystallization of hard sphere systems with increasing ϕ. It has been proven theoretically and shown experimentally that above the freezing point, $\phi_f = 0.494$, hard spheres begin to form such entropically favorable crystals and that the entire suspension becomes crystalline above the melting point, $\phi_m = 0.545$. However, the predicted equilibrium phase diagram is not always realized; hard sphere systems can get trapped kinetically in a glassy non-equilibrium phase beyond the glass transition, $\phi_g \approx 0.57$ [34-36]. While thermodynamics dictates the equilibrium structure, kinetics determines if and how fast this equilibrium structure is

reached. If an unordered suspension is created at these concentrations, lack of particle mobility frustrates the evolution of an equilibrium crystalline structure.

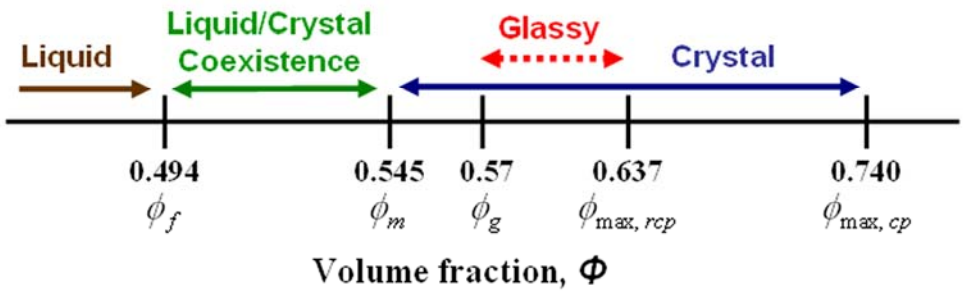

Figure 1.1 The phase diagram of hard sphere system as a function of volume fraction.

1.2.3 Soft sphere system

Recently, soft and deformable particles have been extensively studied, because of their rich phase behavior and associated opportunities for the synthesis of advanced materials. Examples are star polymers [37-39], polymer microgels [40-45], vesicles and micelles [46, 47], and dendrimers [48, 49]. Due to the unique characteristics of soft spheres, in particular their compressibility, deformability, and inter-penetrability, researchers have put forward numerous efforts to investigate the relationship between soft sphere interactions and their phase behavior. As discussed earlier, hard spheres only have three thermodynamically equilibrium phases which are governed by ϕ (Fig. 1.1). In contrast, soft spheres, for instance star polymers, have more complex phase diagrams. Numerical studies have predicted body centered cubic (BCC), face-centered cubic (FCC), body-centered orthogonal (BCO), and diamond structures for star polymers [38]. The phase behavior of these systems can no longer be predicted with a single parameter. Due to their deformability and compressibility, the volume occupied by soft spheres is somewhat ill-defined; soft spheres have been found to crystallize at (effective) volume

fractions well above $\phi_{max} = 0.7404$ [50]. An effective volume fraction is often defined based on the hydrodynamic particle radius in dilute suspensions.

1.2.3.1 Hydrogels - Overview

Among the various types of soft colloids, our attention is directed at hydrogels because of the growing interest in these materials for applications in fields like drug delivery [51], bio/chemical sensing [52], and contact lenses [53]. Hydrogels are water soluble, physically or chemically cross-linked polymers. Depending on size, they are divided into colloidal microgels (10 nm ~ 10 μm) and non-colloidal macrogels (larger than 10 μm). Significant advances in synthetic methodology now enable fabrication of microgels with a broad range of chemical components, morphologies, and sizes. Microgels are particularly known for their responsiveness to external stimuli such as temperature, pH, and ionic strength. One of the most extensively studied polymers for microgels is poly(*N*-isopropylacrylamide) (pNIPAm) because of physical/morphological changes of the polymer in aqueous media in response to temperature [54, 55]. Colloidal pNIPAm microgels undergo a volume phase transition (VPT) at the lower critical solution temperature (LCST, ca. 32 °C). While pNIPAm is in a swollen, hydrated state below the LCST, heating changes the solvent quality of water from good to poor, resulting in a polymer collapse and expulsion of water molecules from the polymer network. To introduce additional functionality to the polymer network, one can copolymerize NIPAm with other monomers, for example styrene, methyl methacrylate and acrylic acid, as shown in Fig. 1.2. Aqueous-based free radical polymerization of pNIPAm-based microgels is normally performed at elevated temperature (ca. 50~70 °C, to ensure effective decomposition of thermo-initiator) under a N_2 blanket (to prevent oxygen from inhibiting polymerization) and results in microgels with a globular structure [54, 56, 57].

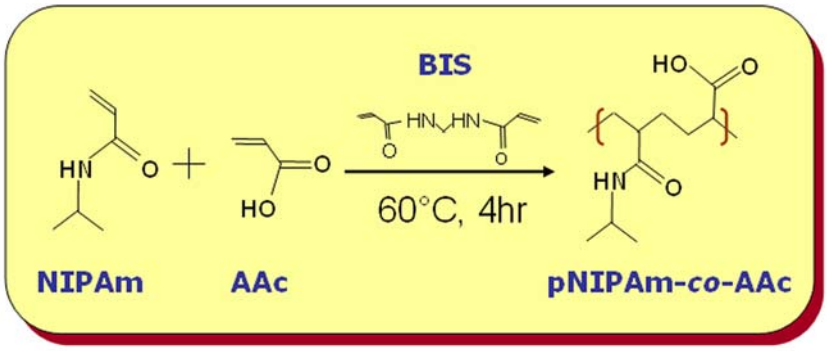

Figure 1.2 Schematic of Synthesis of pNIPAm-*co*-AAc microgel.

Incorporation of acrylic acid (AAc) into the microgel network introduces additional responsiveness to pH and ionic strength. Figure 1.3 depicts the volume phase transition of pNIPAm-*co*-AAc microgels as a function of pH, temperature, and ionic strength. Due to the presence of NIPAm, pNIPAm-*co*-AAc microgels still undergo a VPT at elevated temperature. Addition of ionizable AAc groups provides not only pH-responsiveness due to electrostatic repulsion between deprotonated acid groups and osmotic pressure of counterions, but also responsiveness to ionic strength because of counterion screening. In chapter 2, we will discuss the dynamic swelling-deswelling transition of pNIPAm-*co*-AAc microgels as a function of AAc content induced by pH change.

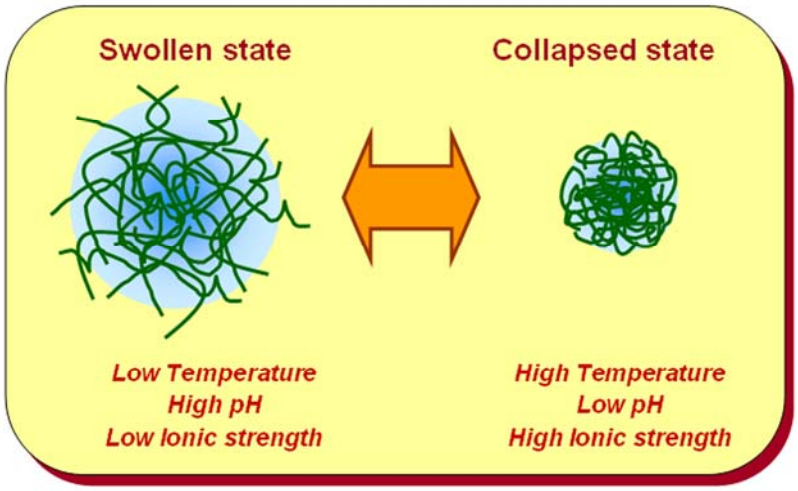

Figure 1.3 The Volume phase transition of pNIPAm-*co*-AAc microgels.

1.3 Motivation and structure of thesis

As discussed before, soft colloidal particles have becoming an important area of interest, both scientifically and technically. To date, sterically stabilized and charged stabilized colloidal suspensions have been studied as model systems for hard spheres [16, 31, 32] and long-range repulsive spheres [58-61], respectively. More recently, researchers have begun to use microgels, in particular pNIPAm-based microgels, as a model system for soft spheres because of the tunability of their softness and the volume phase transition induced by temperature changes. Significant work has been devoted to the phase behavior [45, 50, 62], structural properties [63-67], and rheological properties [44, 68, 69] of pNIPAm microgels. It has been shown that interactions between pNIPAm microgels can be described as a soft repulsive interaction and the phase behavior of pNIPAm microgels has been found to differ significantly from that of hard spheres due to microgel deformability [44]. Nuclear magnetic resonance experiments have revealed structural inhomogeneities inside pNIPAm microgels [67] and small-angle neutron scattering of dilute microgel suspensions showed that radial concentration gradient decays toward the surface with dangling polymer chains attached to the particle surface [64]. These results suggest that the softness of pNIPAm colloidal microgels arises primarily from dangling chains on the surface and from an elastic, deformable corona. We expect that the incorporation of AAc functional group into pNIPAm microgel will introduce another complexity into the system

In this thesis, we investigate the dynamics, phase behavior, hydrodynamics of colloidal suspensions of multi-responsive pNIPAm-*co*-AAc microgels. From prior research [45, 62-68] it is known that the phase behavior of pNIPAm microgels can be relatively well explained via the effective volume fraction of microgels, analogous to hard spheres. However, incorporation of ionizable groups into the pNIPAm microgel network adds significant complexity to the system, and it is therefore reasonable to expect that such ionizable microgels will show interesting phenomena that deviate from

regular pNIPAm microgels. Indeed, past research in the Lyon group has shown that pNIPAm-*co*-AAc microgel suspensions crystallize at amazingly low concentrations at which pure pNIPAm microgels remain fluidized [50]. This phenomenon cannot be explained by simple hard sphere theory. We note that a key advantage of pNIPAm-*co*-AAc microgels as a model system is that *in situ* manipulation of effective volume fraction of particles can be achieved by changing either temperature or pH. In contrast, for hard sphere suspensions it is difficult to vary particle concentration once a sample has been prepared. For this thesis, we have selected multi-responsive pNIPAm-*co*-AAc colloidal microgels, with the objective to provide meaningful insight in the properties of these soft colloids. The ultimate goal is to use this knowledge to enhance control over colloidal phase behavior and facilitate fabrication of ordered colloidal structures for various applications.

The structure of the thesis is as follows. In chapter 2, we introduce particle tracking video microscopy (PTVM) as an experimental technique for various colloidal systems. We will demonstrate that PTVM can be used to characterize various physical properties of materials, in particular the hydrodynamic radius of particles and the temperature or viscosity (micro-structural information) of the suspending medium. Chapter 3 focuses on the phase behavior of concentrated pNIPAm-*co*-AAc microgel dispersions as a function of effective volume fraction. Specifically, by taking advantage of the pH-responsiveness of the microgels and using a microdialysis cell which allows us to modulate solvent composition, we studied the melting/freezing phase transitions by manipulating the effective microgel volume fraction without external mechanical mixing or shear stress. Via gradual particle size (pH) changes we probed the equilibrium phase behavior of these suspensions. In addition, we studied non-equilibrium jammed states that can be generated via abrupt large volumetric expansions of the microgels. In chapter 4, we aim to directly measure the underlying interparticle interactions of the microgel particles in an effort to explain the observed behavior in concentrated systems. By

utilizing a quasi-2D confinement set-up, interparticle interactions between specially synthesized core/shell (polystyrene/pNIPAm-*co*-AAc) particles can be measured as function of pH. In chapter 5, we describe studies of the hindered Brownian diffusion induced by hydrodynamic coupling between particle and walls both for hard sphere and soft sphere suspensions. Finally, in chapter 6, the major conclusions of this thesis are presented and recommendations about future research directions are made.

REFERENCES

1. Russel, W.B., D.A. Saville and W.R. Schowalter, *Colloidal dispersions*, (Cambridge University Press, Cambridge, 1989).

2. Evans, D.F., Wennerström H., *The colloidal domain : where physics, chemistry, biology, and technology meet*. 2nd ed. Advances in interfacial engineering series, (Wiley-VCH, New York, 1999).

3. Einstein, A., *The theory of the Brownian Motion.* Annalen Der Physik, 1906. **19**(2): p. 371-381.

4. Gasser, U., E.R. Weeks, A. Schofield, P.N. Pusey, and D.A. Weitz, *Real-space imaging of nucleation and growth in colloidal crystallization.* Science, 2001. **292**(5515): p. 258-262.

5. Yethiraj, A. and A. van Blaaderen, *A colloidal model system with an interaction tunable from hard sphere to soft and dipolar.* Nature, 2003. **421**(6922): p. 513-517.

6. Weeks, E.R., J.C. Crocker, A.C. Levitt, A. Schofield, and D.A. Weitz, *Three-dimensional direct imaging of structural relaxation near the colloidal glass transition.* Science, 2000. **287**(5453): p. 627-631.

7. tenWolde, P.R., M.J. RuizMontero, and D. Frenkel, *Simulation of homogeneous crystal nucleation close to coexistence.* Faraday Discussions, 1996(104): p. 93-110.

8. Dixit, N.M. and C.F. Zukoski, *Nucleation rates and induction times during colloidal crystallization: Links between models and experiments.* Physical Review E, 2002. **66**(5): p. 051602.

9. Israelachvili, J., *Intermolecular and surface forces*. 2nd ed. (Academic Press, London, 1991).

10. Vanderhoeven, P.H.C. and J. Lyklema, *Electrostatic Stabilization in Non-Aqueous Media.* Advances in Colloid and Interface Science, 1992. **42**: p. 205-277.

11. Roberts, G.S., R. Sanchez, R. Kemp, T. Wood, and P. Bartlett, *Electrostatic charging of nonpolar colloids by reverse micelles.* Langmuir, 2008. **24**(13): p. 6530-6541.

12. Rosenholm, J.B., K.E. Peiponen, and E. Gornov, *Materials cohesion and interaction forces.* Advances in Colloid and Interface Science, 2008. **141**(1-2): p. 48-65.

13. Larson, I., C.J. Drummond, D.Y.C. Chan, and F. Grieser, *Direct Force Measurements Between TiO_2 Surfaces*. Journal of the American Chemical Society, 1993. **115**(25): p. 11885-11890.

14. Mewis, J., W.J. Frith, T.A. Strivens, and W.B. Russel, *The Rheology of Suspensions Containing Polymerically Stabilized Particles.* AIChE Journal, 1989. **35**(3): p. 415-422.

15. Vanderwerff, J.C., C.G. Dekruif, C. Blom, and J. Mellema, *Linear Viscoelastic Behavior of Dense Hard-Sphere Dispersions.* Physical Review A, 1989. **39**(2): p. 795-807.

16. Pusey, P.N. and W. Vanmegen, *Phase-Behavior of Concentrated Suspensions of Nearly Hard Colloidal Spheres.* Nature, 1986. **320**(6060): p. 340-342.

17. Israelachvili, J. and H. Wennerstrom, *Role of hydration and water structure in biological and colloidal interactions.* Nature, 1996. **379**(6562): p. 219-225.

18. Israelachvili, J.N. and R.M. Pashley, *Molecular Layering of Water at Surfaces and Origin of Repulsive Hydration Forces.* Nature, 1983. **306**(5940): p. 249-250.

19. Parry, A.O. and R. Evans, *Critical Amplitudes for Critical Wetting with Short-Ranged Forces - the Approach to D=3-.* Journal of Physics-Condensed Matter, 1990. **2**(37): p. 7687-7698.

20. Woodcock, L.V. and C.A. Angell, *Diffusivity of the Hard-Sphere Model in the Region of Fluid Metastability.* Physical Review Letters, 1981. **47**(16): p. 1129-1132.

21. Stradner, A., H. Sedgwick, F. Cardinaux, W.C.K. Poon, S.U. Egelhaaf, and P. Schurtenberger, *Equilibrium cluster formation in concentrated protein solutions and colloids.* Nature, 2004. **432**(7016): p. 492-495.

22. Larsen, A.E. and D.G. Grier, *Like-charge attractions in metastable colloidal crystallites.* Nature, 1997. **385**(6613): p. 230-233.

23. Crocker, J.C. and D.G. Grier, *Microscopic Measurement of the Pair Interaction Potential of Charge-Stabilized Colloid.* Physical Review Letters, 1994. **73**(2): p. 352-355.

24. Derjaguin, B. and L. Landau, *Theory of the Stability of Strongly Charged Lyophobic Sols and of the Adhesion of Strongly Charged-Particles in Solutions of Electrolytes.* Progress in Surface Science, 1993. **43**(1-4): p. 30-59.

25. Kim, A.J., P.L. Biancaniello, and J.C. Crocker, *Engineering DNA-mediated colloidal crystallization.* Langmuir, 2006. **22**(5): p. 1991-2001.

26. Kim, A.J., V.N. Manoharan, and J.C. Crocker, *Swelling-based method for preparing stable, functionalized polymer colloids.* Journal of the American Chemical Society, 2005. **127**(6): p. 1592-1593.

27. Verwey, E.J.W., Overbeek, J.Th.G., *Theory of the stability of lyophobic colloids; the interaction of sol particles having an electric double layer*, (Elsevier Publication Company, New York, 1948).

28. Derjaguin, B. and L. Landau, *Theory of Stability of Highly Charged Liophobic Sols and Adhesion of Highly Charged Particles in Solutions of Electrolytes.* Zhurnal Eksperimentalnoi I Teoreticheskoi Fiziki, 1945. **15**(11): p. 663-682.

29. Vondermassen, K., J. Bongers, A. Mueller, and H. Versmold, *Brownian-Motion - a Tool to Determine the Pair Potential between Colloid Particles.* Langmuir, 1994. **10**(5): p. 1351-1353.

30. Denton, A.R., *Effective interactions and volume energies in charged colloids: Linear response theory.* Physical Review E, 2000. **62**(3): p. 3855-3864.

31. Oxtoby, D.W., *New Perspectives on Freezing and Melting.* Nature, 1990. **347**(6295): p. 725-730.

32. Raynaud, L., B. Ernst, C. Verge, and J. Mewis, *Rheology of aqueous latices with adsorbed stabilizer layers.* Journal of Colloid and Interface Science, 1996. **181**(1): p. 11-19.

33. Alder, B.J., W.G. Hoover, and D.A. Young, *Studies in Molecular Dynamics .V. High-Density Equation of State and Entropy for Hard Disks and Spheres.* Journal of Chemical Physics, 1968. **49**(8): p. 3688.

34. Vanblaaderen, A. and P. Wiltzius, *Real-Space Structure of Colloidal Hard-Sphere Glasses.* Science, 1995. **270**(5239): p. 1177-1179.

35. Vanmegen, W. and S.M. Underwood, *Change in Crystallization Mechanism at the Glass-Transition of Colloidal Spheres.* Nature, 1993. **362**(6421): p. 616-618.

36. Kegel, W.K. and A. van Blaaderen, *Direct observation of dynamical heterogeneities in colloidal hard-sphere suspensions.* Science, 2000. **287**(5451): p. 290-293.

37. Likos, C.N., H. Lowen, M. Watzlawek, B. Abbas, O. Jucknischke, J. Allgaier, and D. Richter, *Star polymers viewed as ultrasoft colloidal particles.* Physical Review Letters, 1998. **80**(20): p. 4450-4453.

38. Watzlawek, M., C.N. Likos, and H. Lowen, *Phase diagram of star polymer solutions.* Physical Review Letters, 1999. **82**(26): p. 5289-5292.

39. Likos, C.N., N. Hoffmann, A. Jusufi, and H. Lowen, *Interactions and phase behaviour of polyelectrolyte star solutions.* Journal of Physics-Condensed Matter, 2003. **15**(1): p. S233-S238.

40. Meng, Z.Y., J.K. Cho, S. Debord, V. Breedveld, and L.A. Lyon, *Crystallization behavior of soft, attractive microgels.* Journal of Physical Chemistry B, 2007. **111**(25): p. 6992-6997.

41. Wu, J.Z., B. Zhou, and Z.B. Hu, *Phase behavior of thermally responsive microgel colloids.* Physical Review Letters, 2003. **90**(4): p. 048304.

42. Gottwald, D., C.N. Likos, G. Kahl, and H. Lowen, *Ionic microgels as model systems for colloids with an ultrasoft electrosteric repulsion: Structure and thermodynamics.* Journal of Chemical Physics, 2005. **122**(7): p. 074903.

43. Gottwald, D., C.N. Likos, G. Kahl, and H. Lowen, *Phase behavior of ionic microgels.* Physical Review Letters, 2004. **92**(6): p. 068301.

44. Senff, H. and W. Richtering, *Temperature sensitive microgel suspensions: Colloidal phase behavior and rheology of soft spheres.* Journal of Chemical Physics, 1999. **111**(4): p. 1705-1711.

45. Alsayed, A.M., M.F. Islam, J. Zhang, P.J. Collings, and A.G. Yodh, *Premelting at defects within bulk colloidal crystals.* Science, 2005. **309**(5738): p. 1207-1210.

46. Yatcilla, M.T., K.L. Herrington, L.L. Brasher, E.W. Kaler, S. Chiruvolu, and J.A. Zasadzinski, *Phase behavior of aqueous mixtures of cetyltrimethylammonium bromide (CTAB) and sodium octyl sulfate (SOS).* Journal of Physical Chemistry, 1996. **100**(14): p. 5874-5879.

47. Wanka, G., H. Hoffmann, and W. Ulbricht, *Phase-Diagrams and Aggregation Behavior of Poly(Oxyethylene)-Poly(Oxypropylene)-Poly(Oxyethylene) Triblock Copolymers in Aqueous-Solutions.* Macromolecules, 1994. **27**(15): p. 4145-4159.

48. Schenning, A.P.H.J., C. Elissen-Roman, J.W. Weener, M.W.P.L. Baars, S.J. van der Gaast, and E.W. Meijer, *Amphiphilic dendrimers as building blocks in supramolecular assemblies.* Journal of the American Chemical Society, 1998. **120**(32): p. 8199-8208.

49. Karatasos, K., *Self-organization in dendrimer polyelectrolytes.* Macromolecules, 2008. **41**(3): p. 1025-1033.

50. Debord, S.B. and L.A. Lyon, *Influence of particle volume fraction on packing in responsive hydrogel colloidal crystals.* Journal of Physical Chemistry B, 2003. **107**(13): p. 2927-2932.

51. Hoffman, A.S., *Hydrogels for biomedical applications.* Advanced Drug Delivery Reviews, 2002. **54**(1): p. 3-12.

52. Holtz, J.H. and S.A. Asher, *Polymerized colloidal crystal hydrogel films as intelligent chemical sensing materials.* Nature, 1997. **389**(6653): p. 829-832.

53. Compan, V., A. Andrio, A. Lopez-Alemany, E. Riande, and M.F. Refojo, *Oxygen permeability of hydrogel contact lenses with organosilicon moieties.* Biomaterials, 2002. **23**(13): p. 2767-2772.

54. Pelton, R., *Temperature-sensitive aqueous microgels.* Advances in Colloid and Interface Science, 2000. **85**(1): p. 1-33.

55. Saunders, B.R. and B. Vincent, *Microgel particles as model colloids: theory, properties and applications.* Advances in Colloid and Interface Science, 1999. **80**(1): p. 1-25.

56. Debord, J.D. and L.A. Lyon, *Synthesis and characterization of pH-responsive copolymer microgels with tunable volume phase transition temperatures.* Langmuir, 2003. **19**(18): p. 7662-7664.

57. Jones, C.D. and L.A. Lyon, *Dependence of shell thickness on core compression in acrylic acid modified poly(N-isopropylacrylamide) core/shell microgels.* Langmuir, 2003. **19**(11): p. 4544-4547.

58. Schope, H.J., T. Decker, and T. Palberg, *Response of the elastic properties of colloidal crystals to phase transitions and morphological changes.* Journal of Chemical Physics, 1998. **109**(22): p. 10068-10074.

59. Aastuen, D.J.W., N.A. Clark, L.K. Cotter, and B.J. Ackerson, *Nucleation and Growth of Colloidal Crystals.* Physical Review Letters, 1986. **57**(14): p. 1733-1736.

60. Ackerson, B.J., J.B. Hayter, N.A. Clark, and L. Cotter, *Neutron-Scattering from Charge Stabilized Suspensions Undergoing Shear.* Journal of Chemical Physics, 1986. **84**(4): p. 2344-2349.

61. Dux, C., S. Musa, V. Reus, H. Versmold, D. Schwahn, and P. Lindner, *Small angle neutron scattering experiments from colloidal dispersions at rest and under sheared conditions.* Journal of Chemical Physics, 1998. **109**(6): p. 2556-2561.

62. St John, A.N., V. Breedveld, and L.A. Lyon, *Phase behavior in highly concentrated assemblies of microgels with soft repulsive interaction potentials.* Journal of Physical Chemistry B, 2007. **111**(27): p. 7796-7801.

63. Berndt, I., J.S. Pedersen, P. Lindner, and W. Richtering, *Influence of shell thickness and cross-link density on the structure of temperature-sensitive - Poly-N-isopropylacrylamide-poly-N-isopropylmethacrylamide core-shell microgels investigated by small-angle neutron scattering.* Langmuir, 2006. **22**(1): p. 459-468.

64. Stieger, M., W. Richtering, J.S. Pedersen, and P. Lindner, *Small-angle neutron scattering study of structural changes in temperature sensitive microgel colloids.* Journal of Chemical Physics, 2004. **120**(13): p. 6197-6206.

65. Berndt, I., J.S. Pedersen, and W. Richtering, *Temperature-sensitive core-shell microgel particles with dense shell.* Angewandte Chemie-International Edition, 2006. **45**(11): p. 1737-1741.

66. Eckert, T. and W. Richtering, *Thermodynamic and hydrodynamic interaction in concentrated microgel suspensions: Hard or soft sphere behavior?* Journal of Chemical Physics, 2008. **129**(12): p. 124901.

67. Guillermo, A., J.P.C. Addad, J.P. Bazile, D. Duracher, A. Elaissari, and C. Pichot, *NMR investigations into heterogeneous structures of thermosensitive microgel particles.* Journal of Polymer Science Part B-Polymer Physics, 2000. **38**(6): p. 889-898.

68. Crassous, J.J., M. Siebenburger, M. Ballauff, M. Drechsler, O. Henrich, and M. Fuchs, *Thermosensitive core-shell particles as model systems for studying the flow behavior of concentrated colloidal dispersions.* Journal of Chemical Physics, 2006. **125**(20): p. 204906.

69. Deike, I. and M. Ballauff, *Rheology of thermosensitive latex particles including the high-frequency limit.* Journal of Rheology, 2001. **45**(3): p. 709-720.

CHAPTER 2

PARTICLE TRACKING VIDEO MICROSCOPY AND ITS APPLICATION TO COLLOIDAL SYSTEMS

Particle tracking video microscopy (PTVM) uses the mobility of colloidal particles to extract information about the particles themselves or about the local environment explored by these particles. One can either use intrinsic colloidal particles which are naturally present in a system or embed tracer particles. PTVM experiments can be divided into two categories: one class involving the active manipulation of particles via externally applied forces (*e.g.*, optical or magnetic) and another class exploiting the inherent Brownian motion of particles due to their thermal energy $k_B T$. Regardless of whether PTVM is carried out in active or passive mode, the technique records, identifies, and analyzes the trajectories of colloidal particles. In the following sections, we will discuss the experimental technique in more detail. For this thesis, we primarily focus on the passive version of PTVM and provide various examples of how the method can be applied in colloidal systems.

2.1 Particle tracking video microscopy

Particle tracking video microscopy (PTVM) is an analytical technique that monitors the motion of individual colloidal particles in a suspending medium. It converts the motion of colloidal particles into useful physical information, for example diffusion coefficient, viscosity, temperature, hydrodynamic radius, and micro-structural morphology/heterogeneity. Due to the versatility of the method for soft materials and complex fluids, PTVM has been utilized in numerous applications, such as biophysics [1-

4], microfluidics [5], colloid physics [6, 7], rheology [8-10], and polymer science [11]. PTVM can provide both ensemble-averaged information and local spatially-resolved information from individual tracer particles. Monitoring the mobility of tracer particles can be useful for interpreting the dynamics of a system. For example, tracking of single proteins within a mammalian cell by epifluorescence microscopy unveiled the dynamics of intracellular macromolecules [12]. Imaging of diffusive motion of embedded dye molecules revealed cell membrane dynamics [13, 14]. In another study, PTVM was successfully applied *in-situ* to determine sol-gel transition during photo-polymerization [11]. The observation of particles slowing down during the polymerization was utilized to evaluate the underlying reaction mechanism. Moreover, PTVM can be used as a visualization tool to investigate micro-structural characteristics of a media. The random Brownian dynamics of embedded tracer particles display characteristics of the microenvironments that the tracers explore. It has been reported that 3D positions/trajectories of tracer particles could visualize deformation of cross linked *F*-actin networks, which form a major structural component of eukaryotic cells [2]. Under shear stress, the deformed trajectories of tracer particles were used to visualize the mechanical relaxation of the cell. When the characteristic length scale of a system is similar to the size of the colloidal probes, PTVM can also be used to obtain detailed information about morphological properties of the sample, such as heterogeneity and pore/mesh size [3, 15].

The PTVM method consists of recording a movie, identifying particles in each frame of the movie via computational algorithms, combining the information in separate images to create trajectories of individual particles, and is completed by statistical analysis of these trajectories[16]. In general, PTVM utilizes one of the following four image analysis algorithms to detect particle positions and displacements: cross-correlation, sum-absolute difference, centroid, and direct Gaussian fit [17]. Although various groups have developed in-house algorithms for analyzing movies, the strategies

generally fall into these four categories. While centroid and direct Gaussian fit algorithms estimate the positions of particles based on single images, cross-correlation and sum-absolute difference algorithm identify the locations of particles by comparing consecutive images. Generally speaking, the centroid algorithm is known as the most robust against noise and particularly appropriate for micron size colloidal particles. For this thesis, we utilized a brightness-weighted centroid algorithm developed in Interactive Data Language (IDL; ITT Visual Information Solutions, Boulder, CO). Various codes for particle tracking with either IDL or Matlab can be found online [18]

A typical PTVM experiment for this thesis proceeded as follows. First, movies of moving colloids were captured with a CCD camera attached to the microscope and stored directly on a PC. Because Brownian motion can easily be obscured by external vibrations, we used an air-floated optical table to minimize vibrational noise from the microscope. The image analysis procedure in IDL consists of four stages; image restoration, locating particles, refining particle positions/eliminating unwanted particles, and connecting particle positions into trajectories [16]. The first stage aims to reduce low/high spatial frequency noise and the second stage detects the location of particle centers with multiple brightness-weighted centroids, as shown in Fig. 2.1(a). Original images are distorted by noise as a result of microscope optics and the imaging process during digitization. Such noise is minimized by computerized algorithm [16, 19]. During the second stage, locating the particles, all local brightness maxima are identified as potential particles. The third stage applies additional selection criteria such as eccentricity (aspect ratio) and minimum/maximum brightness in order to distinguish between actual in-focus particles and other objects in the image that are not single particles. Aggregates, for instance doublets and triplets, have higher eccentricity and brightness than single particles and are eliminated effectively by using eccentricity and brightness as selection criteria. In general, to ensure robust particle identification and accurate positioning with sub-pixel accuracy, the particle diameter in the image must be larger than 5 pixels. In that

scenario the algorithm used in this thesis can determine the center of particles to the order of 0.1 pixels. The third stage creates particle trajectories from the particle position data for the individual images, shown in Fig. 2.1(b). Finally, the trajectories can be used to calculate mobility and to investigate various mechanical/physical properties of the colloidal suspensions.

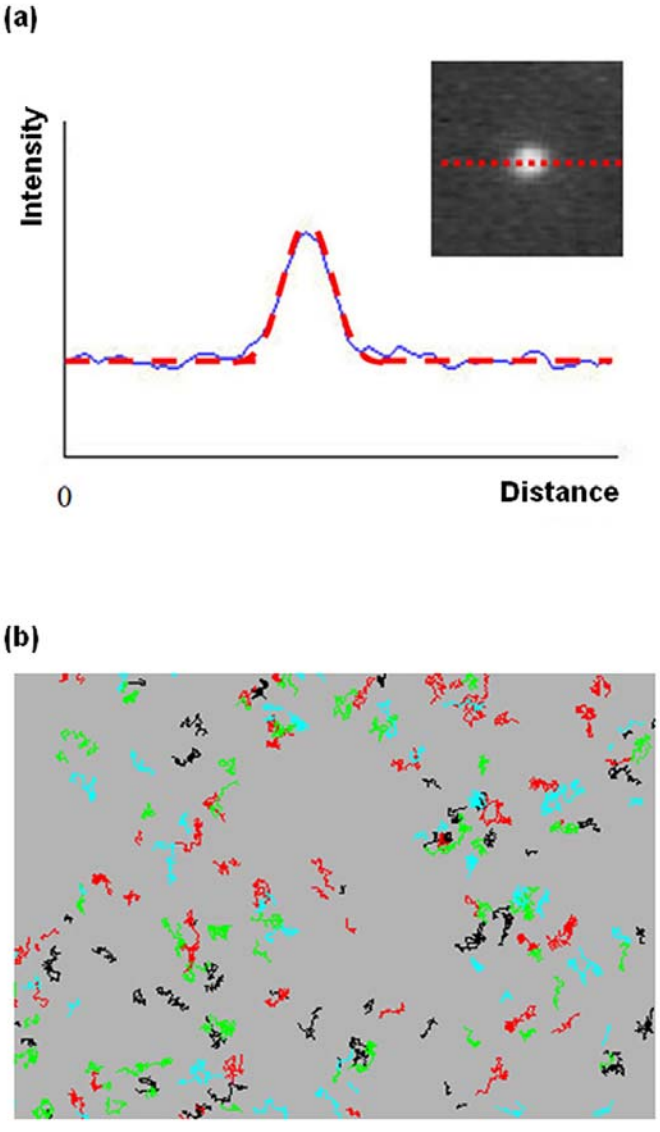

Figure 2.1 Particle Tracking Video Microscopy (PTVM) (a) Intensity profile of 1 μm Nile Red carboxylate-modified fluorescent particle observed with 100× emulsion oil objective; the dashed line on the intensity profile represents the brightness-weighted

centroid algorithm and the inset shows the image of the fluorescent colloidal particle. (b) Trajectories of individual fluorescent particles.

When analyzing the trajectory of a colloidal particle, one can calculate the average squared displacement particles travel in a given time interval, often referred to as the mean squared displacement (*MSD*):

$$MSD(\tau) = \left\langle \Delta \mathbf{r}_i^2(\tau) \right\rangle_k = \left\langle \left(\mathbf{r}_i(t_j + \tau) - \mathbf{r}_i(t_j) \right)^2 \right\rangle_k \tag{2.1}$$

where $\mathbf{r}(t)$ and τ represent the position vector of the colloidal particle and lag time, respectively [19]. The bracket represents the ensemble-average over all particles and all starting times t_j. Since the displacement of colloidal particles undergoing Brownian motion is the result of their thermal energy of magnitude $k_B T$, via the Stokes-Einstein relation Eq. (1.1), in the Newtonian regime *MSD*, which reflects that the diffusion coefficient can be related to various physical properties of the colloidal suspension: hydrodynamic radius of the particle R_H, temperature of the medium T, and mechanical/rheological properties of the medium η, as depicted in Fig. 2.2. While the *MSD* of a particle in a Newtonian fluid is directly proportional to τ, analysis of the diffusion in non-Newtonian fluids requires the use of a generalized, frequency dependent version of the Stokes-Einstein relation [20]; in this thesis, we will either use the Stokes – Einstein relation or use raw *MSD* data without rheological interpretation. In the following sections, we discuss the practical applications of PTVM via three examples: 1) determination of hydrodynamic radius R_H for colloidal particles, 2) temperature measurements with colloidal particles in microfluidics devices, and 3) micro-structural characterization of complex fluids with colloidal particles.

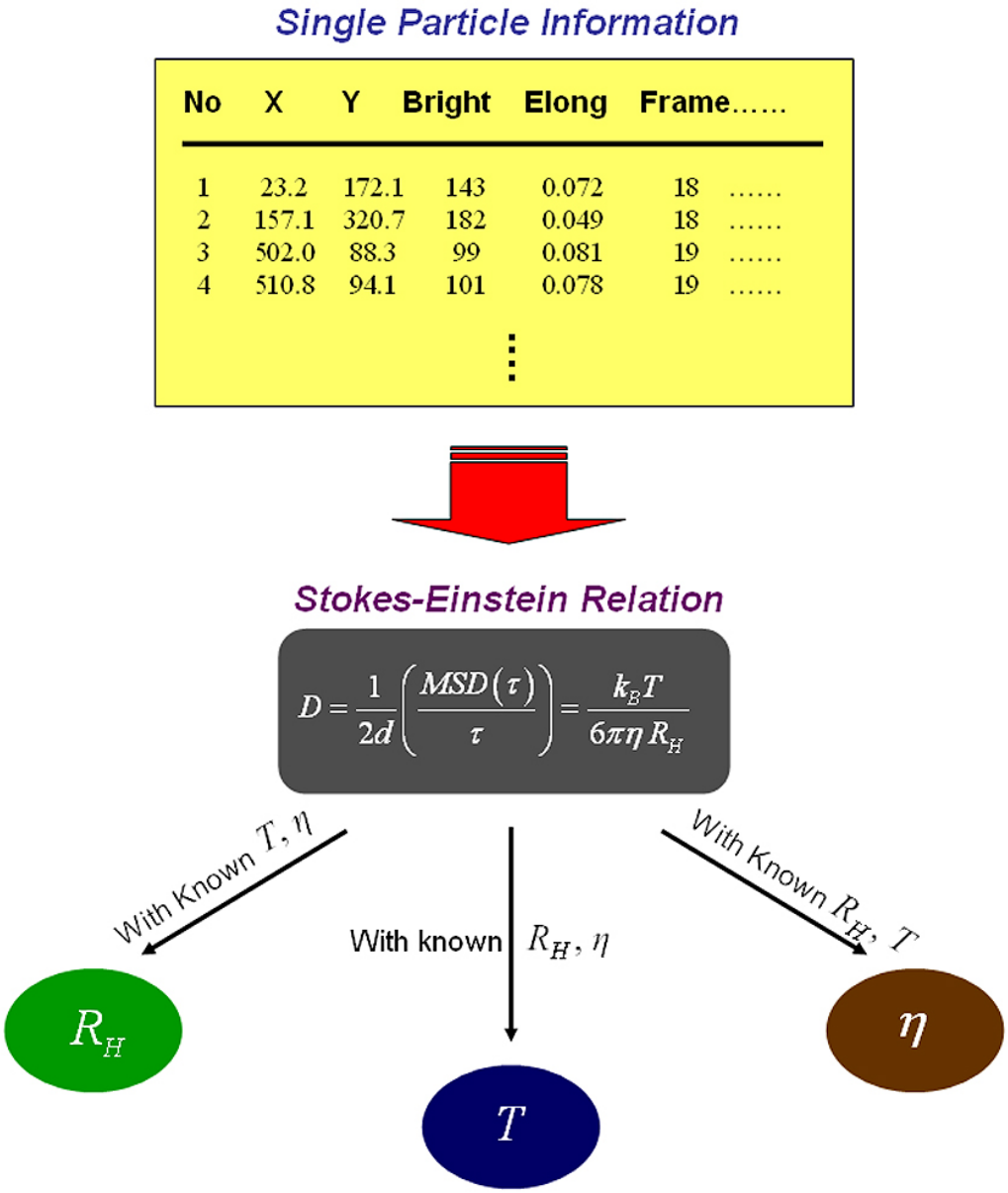

Figure 2.2 Physical properties characterization of colloidal suspensions via PTVM. In Stokes-Einstein Relation, d is the dimensionality of trajectories ($d = 2$ for optical microscopy).

2.2 Characterization of colloidal particle size

The most common methods to characterize colloidal particle size are photon correlation spectroscopy (PCS, often referred to as DLS, Dynamic Light Scattering), Atomic Force Microscopy (AFM) and Electron Microscopy (EM) [21-24]. PCS measures intensity fluctuations of scattered light to determine a diffusion coefficient, which it is then converted to hydrodynamic radius via Eq. (1.1). EM utilizes a beam of electrons to produce images, from which one can measure feature sizes directly. AFM scans across sample surfaces with a cantilever to render a topographic representation of the surface. For colloidal suspensions, each of these techniques has drawbacks. PCS is very sensitive to impurities; it ensemble-averages the scattered laser intensity over the scattering volume and large particle aggregates or dust in the sample generate very strong scattering, thus overwhelming the signal from single particles. EM often involves deposition of metal elements on the sample surface and generally requires sample drying, which is not suitable for hydrated materials that collapse during drying. AFM applies external forces through the cantilever, which can be detrimental for soft, deformable samples. In this study, we applied PTVM as an alternative technology to characterize the hydrodynamic radius of various colloidal particles. First, we evaluate PTVM as a characterization technology by comparing the results with PCS, followed by the application of our current method to monitor dynamic swelling-deswelling transitions of stimuli-responsive microgel particles upon pH change in a microfluidic device.

2.2.1 Experimental Section

Material

Fluorescent carboxylate-modified polystyrene FluoSpheres® (Molecular probes, Inc.) with 0.50 μm and 1.0 μm diameters and 3 % polydispersity were used. Acrylic acid (AAc, Sigma-Aldrich), *N,N'*-methylenebis (acrylamide) (BIS, Fluka), and ammonium

persulfate (APS, Sigma-Aldrich) were used as received. *N*-isopropylamide (NIPAm, Sigma-Aldrich) was recrystallizaed from hexane (J.T. Baker) and dried in vacuum. Water for all experiments was prepared by filtering deionized water (18 MΩ, Barnstead E-Pure system) through a 0.2 μm filter to remove particulate impurities.

Preparation of p(NIPAm-co-AAc) Microgels

Colloidal microgel particles, pNIPAm-*co*-AAc, were synthesized via aqueous precipitation polymerization under nitrogen atmosphere at 60 °C for 4 hours [25, 26]. A precursor mixture without initiator was premixed at ratios shown in Table 2 with 100 *mL* water in a round bottom flask and pre-heated for 30 min under N_2 blanket. The reaction was initiated by adding the APS initiator and allowed to proceed for 4 hours at 60 °C under N_2 blanket. After the reaction, all colloidal particles were filtered and exhaustively purified via centrifugation, supernatant exchange and resuspension with DI water at least four times in order to get rid of unreacted components, linear polymer and impurities.

Table 2.1 Composition of pNIPAm-*co*-AAc microgels

Type	NIPAm (g)	BIS (mg)	AAc (mg)	APS (mg)
AAc 1%	1.980	30	20	50
AAc 3%	1.940	30	60	50
AAc 5%	1.900	30	100	50
AAc 7%	1.860	30	140	50
AAc 10%	1.800	30	200	50
AAc 15%	1.700	30	300	50

Characterization of colloidal particles

Photon Correlation Spectroscopy (PCS). PCS (DynaPro, Protein Solutions, Inc.) was used to obtain hydrodynamic radii of colloidal particles in aqueous solution. Samples were analyzed with a three-sided quartz cuvette and the temperature of the sample was controlled via a Peltier-heater coupled to the sample holder. Before the measurements, samples were extensively sonicated. The scattering angle was 90° and the wavelength of light was 784.8 nm. Between measurement at different temperatures, samples were allowed to equilibrate for 5 minutes. Each data point consists of 25 measurements that were each obtained with a 15 s collection time.

Static Characterization via PTVM. The fluorescent styrene particles were suspended in DI water and pNIPAm-*co*-AAc microgel particles were suspended in various buffer solutions with pH values ranging from 2.0 to 8.0 and constant ionic strength I = 15 mM. Diluted colloidal suspensions were placed between a microscope slide and cover slip with parafilm spacers of about 100 μm thickness. An optical video microscope (Leica DM-IRB) was used in the combination with Peltier-controlled thermal microscope stage (PE100-LI2, Linkam Scientific Instruments Ltd.) and objective heater (PN150819, Bioptechs, Inc.). Movies of 1500 frames were collected for each sample with a CCD camera (Cohu, Poway, CA; 30 frame/s, 640 × 486 pixels) and analyzed. Our optical microscope-based PTVM can detect particles with a spatial resolution of 4~5 nm. While the fluorescence imaging mode was applied to the polystyrene particles, pNIPAm-*co*-AAc particles were imaged in Differential Interference Contrast (DIC) mode.

Dynamic Characterization via PTVM coupled with a Microfluidic Set-up. To control and manipulate the solvent composition *in situ*, our group has previously developed a microfluidic microdialysis cell [27]. For this study, a modified transparent version of microdialysis cell was fabricated with soft-lithography techniques based on polydimethylsilosane (PDMS; Sylgard 184, Dow Corning). In contrast to the original, non-transparent device based on a silicon wafer and cleanroom etching technology, the

new microdialysis design enabled us to visualize colloidal particles without fluorescent labeling, which would require undesirable modifications of surface chemistry. The manufacturing process of the dialysis cell is shown in Fig. 2.3(a). The mold for the microdialysis cell was made with Photoresist (SU-8 2100, Microchem) on a 5" silicone wafer. As shown in Fig. 2.3(b), the microdialysis cell consists of three main structural elements: a reservoir channel connected to an external flow system, a nanoporous membrane, and the sample chamber. The main PDMS body of the microdialysis cell has three features: a rectangular reservoir channel, a circular insert for the membrane, and two holes for inlet/outlet ports. An Anodisc^{TM} 13 (Whatman plc. England) aluminum oxide membrane with 20 nm pore sizes was inserted into PDMS body and below the membrane a sample chamber was created with glass coverslips. Two flexible tubes were connected to the inlet/outlet ports. To control the flow of different buffer solutions, a four-way switching valve (V-101D, Upchurch Scientific) and syringe pump (KDS210C, KD Scientific Inc.) with two syringes were utilized. The sample volume of the micro-dialysis cell set-up is about 1 μL. The height of the reservoir channel small compared to its width, so that a uniform quasi-2D parabolic flow develops across the membrane and convective-diffusive mass transport occurs through the nanoporous membrane into the sample chamber [27], as shown in Fig. 2.3(c).

(a)

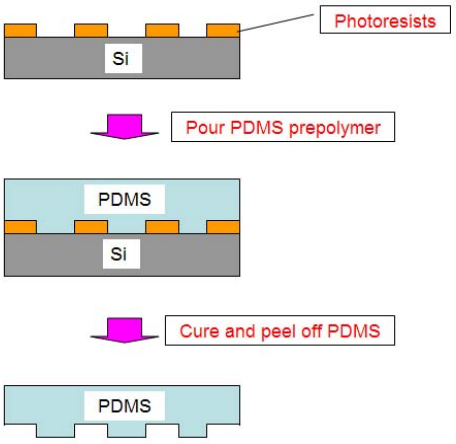

(b)

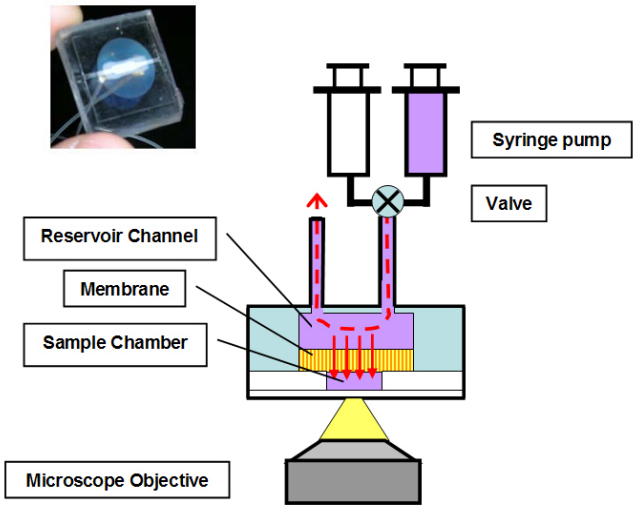

(c)

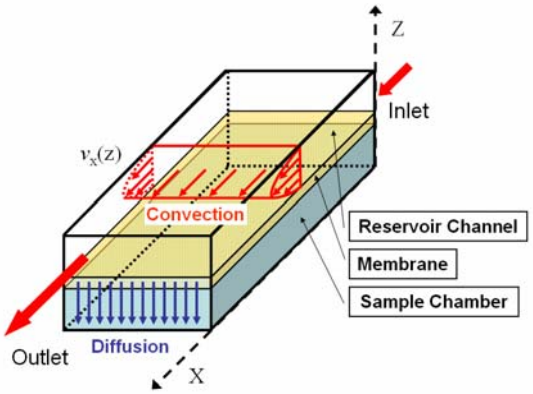

Figure 2.3 Microdialysis Cell: (a) Schematic of fabrication of microdialysis cell via soft-lithography. (b) Schematic representation and photograph (inset) of the microdialysis cell. (c) 3-D geometry of microdialysis cell and flow profile; while parabolic convective flow develops in the reservoir channel, the fluid remains quiescent in both membrane and sample chamber.

2.2.2 Results and discussion

Validation of PTVM against PCS

The reliability of PTVM versus PCS was tested with two different sizes mono-disperse fluorescent polystyrene particles at very dilute particle concentrations (~ 0.001

wt%). Although the motion of fluorescent particles in aqueous media displays random Brownian motion in 3D, conventional optical microscopy monitors only the projection of the 3D motion. From the trajectories of colloidal particles, we obtained the hydrodynamic radius (R_H) from *MSD* via Stokes-Einstein relation as,

$$R_H = \frac{k_B T}{6\pi\eta D} = \frac{dk_B T}{3\pi\eta\left(\frac{MSD(\tau)}{\tau}\right)} \tag{2.2}$$

where D represents the diffusion coefficient and dimensionality $d = 2$ for our PTVM.

According to the manufacturer's product specifications, the nominal R_H of the fluorescent polystyrene particles was 1.0 μm and 0.50 μm, characterized by EM [28]. It is obvious from the data in Fig. 2.4 that the R_H of polystyrene particles suspended in DI water measured via PTVM is in good agreement with PCS results at temperatures ranging from 20 °C to 35 °C. In principle, the result from PCS, which averages over the entire scattering volume, could be biased by aggregates and other impurities. In PTVM, such impurities can explicitly be excluded by the computerized image analysis algorithms. The results imply that there are very few di-mers, tri-mers, or dust in the sample, which is expected since carboxyl-modified polystyrene particles are well-dispersed in DI water due to Coulombic repulsions between charged surface groups. Fig. 2.4 also shows that R_H does not depend on temperature, which is also expected for polystyrene in water.

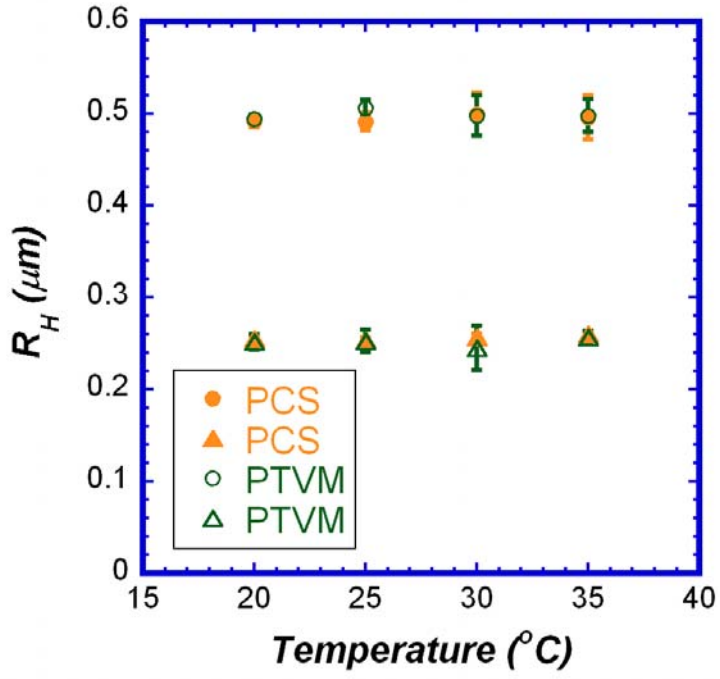

Figure 2.4 Hydrodynamic radius (R_H) of fluorescent polystyrene particles from PCS and PTVM; open symbols represent PTVM and solid symbols represent PCS result. Spheres and triangles represent polystyrene particles of 0.50 μm and 0.25 μm in radius, resp.

Static characterization of hydrodynamic radius of microgels

After the initial benchmarking, PTVM was applied to a more interesting material, the PNIPAm-*co*-AAc microgels. As discussed in Chapter 1, microgels are physically or chemically cross-linked macromolecules with ~ 90 % of their volume occupied by solvent, in our case water. In contrast to polystyrene particles, microgels are soft and compressible, and deform easily when external force is applied. PCS has been widely used as a method to characterize R_H of microgels in aqueous suspension, because application of EM and AFM is very challenging for hydrated microgels. For example, particles collapse during SEM, resulting in dehydrated flat "pancake" structures that provide little meaningful information about microgel size in suspension. Standard TEM also fails to characterize R_H of microgels because sample preparation involves drying [29]. The application of AFM for microgels is also limited because AFM involves physical interaction between sample and cantilever. PCS is therefore the most

appropriate traditional technique for soft hydrated spheres, since it is a non-destructive method and utilizes the inherent thermal energy k_BT of colloids without applying external forces [25, 29, 30]. However, PCS is challenging for swollen microgels due to lack of refractive index contrast. At low pH, when pNIPAm-*co*-AAc microgels are protonated and collapsed, there is a reasonable refractive index contrast, which makes PCS measurements possible. As pH increases, the microgel refractive index approaches that of water and the particles provide insufficient scattering for PCS. The refractive index of microgels suspended in media depends on the polymer volume fraction and can be approximated as follows [31, 32]:

$$n = n_m\left[1-\left(\frac{R_0}{R_H}\right)^3\right]+n_p\left(\frac{R_0}{R_H}\right)^3 \tag{2.3}$$

where n, n_m, and n_p represent the refractive index of microgel, medium, and polymer, respectively. R_H is radius of a microgel in a solvent (mostly water) and R_0 is the radius of the microgel when completely collapsed; $\left(R_0 / R_H\right)^3$ is therefore the volume fraction of polymer in a swollen microgel. Even if the intrinsic refractive index of pNIPAm-*co*-AAc is 1.53, hydrated pNIPAm-*co*-AAc microgels have a refractive index similar to water (~1.35, $\Delta n \approx 0.02$) [33]. In addition to the contrast issue, ensemble-averaged results from PCS can not distinguish aggregates. PTVM allows direct visualization of single particles with computerized algorithms that enhance image contrast sufficiently to track microgels even in their swollen state. Therefore, we decided to apply PTVM to characterize R_H of microgels as a function of pH and results are shown in Fig. 2.5, which displays the normalized hydrodynamic radius as a function of pH. Below pH = 3.5, pNIPAm-*co*-AAc swells very slightly with increasing pH, at higher pH, microgels swell more rapidly up to pH 7.0, where the size reaches a plateau.

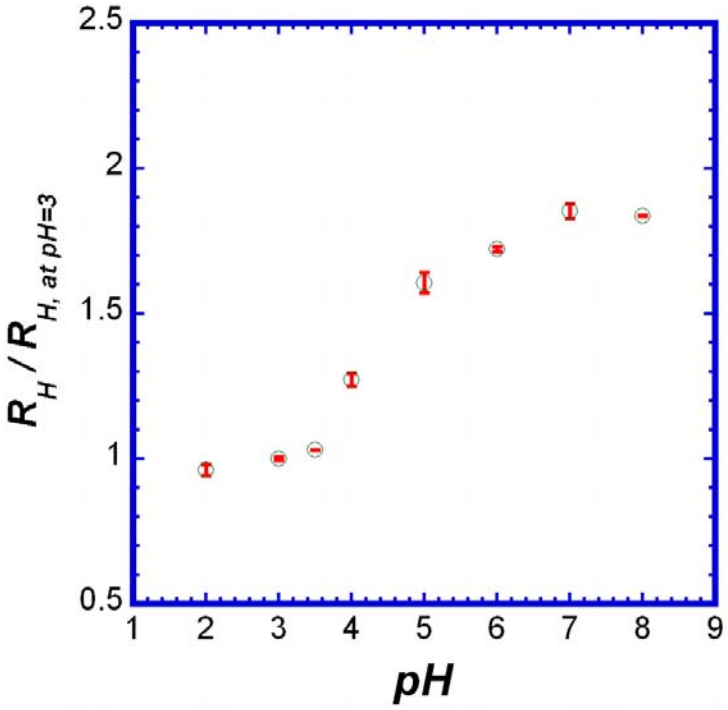

Figure 2.5 Normalized R_H of pNIPAm-*co*-AAc microgels with AAc 10 wt% as a function of pH; measurements were made at 23 °C and normalization is performed based on R_H at pH 3.0.

Dynamic swelling/deswelling of microgels

Dynamic studies of swelling/deswelling behavior of microgels coupled with diffusion inside microgels are of importance for practical applications as drug delivery carriers [34], chemical sensors [35, 36], micro-lenses [37] and as actuator systems in microfluidic devices [38, 39]. While the temperature-responsiveness of pNIAm-based microgels is well understood, the dynamics of pH-responsive microgels upon pH change have not been studied as extensively. By taking advantage of our microdialysis cell that enables solvent manipulation without sample replacement [27], we can manipulate the pH of pNIPAm-*co*-AAc microgel suspensions and apply PTVM to investigate the transient swelling/deswelling *in situ* without the need for mechanical mixing; with conventional methods such reversible pH variations are impossible. Furthermore, PTVM

coupled with the microdialysis cell requires only miniscule amounts of sample (about 1 μL). Due to the small feature size of the sample chamber (~100 μm height), the response time of the microdialysis cell to solvent change occurs less than 10 min.

In figure 2.6, we show the dynamic swelling/deswelling of pNIPAm-*co*-AAc microgels. We measured R_H of the microgels inside the microdialysis cell for various AAc comonomer ratios by alternating the pH between 3.0 and 5.0 repeatedly, as shown Fig. 2.6(a). It is clear that, regardless of the AAc fraction in the polymer network, pNIPAm-*co*-AAc microgel swelling/deswelling is reproducible and reversible. Figure 2.6(b) shows the relative swelling ratio of pH-responsive microgels as a function of AAc concentration. It is clear that microgels swell more as the concentration of AAc increases. However, above 10 wt% AAc, the swelling ratio levels off. This observation implies the existence of critical concentration of AAc for swelling/deswelling. Addition of AAc group into the network beyond this critical concentration is chemically possible but additional swelling is physically constrained by crosslinks inside the polymer network. Additional ionic groups exceeding critical concentration do not play a significant role in the swelling transition. It is important to point out that the reversible changes of sample solvent composition in the sample chamber is achieved by diffusion transport through the nanoporous membrane, as shown in Fig. 2.3 (c). Although we change the solvent composition in the reservoir channel almost instantaneously (within a few seconds) by switching the direction of the valve system, there is an intrinsic delay because of the membrane diffusion. The time dependent swelling/deswelling of all pNIPAm-*co*-AAc microgels occurs on a similar time scale, as can be seen in Fig. 2.6(a), which likely reflects the diffusion of pH buffer through the membrane, not the kinetics of microgels themselves.

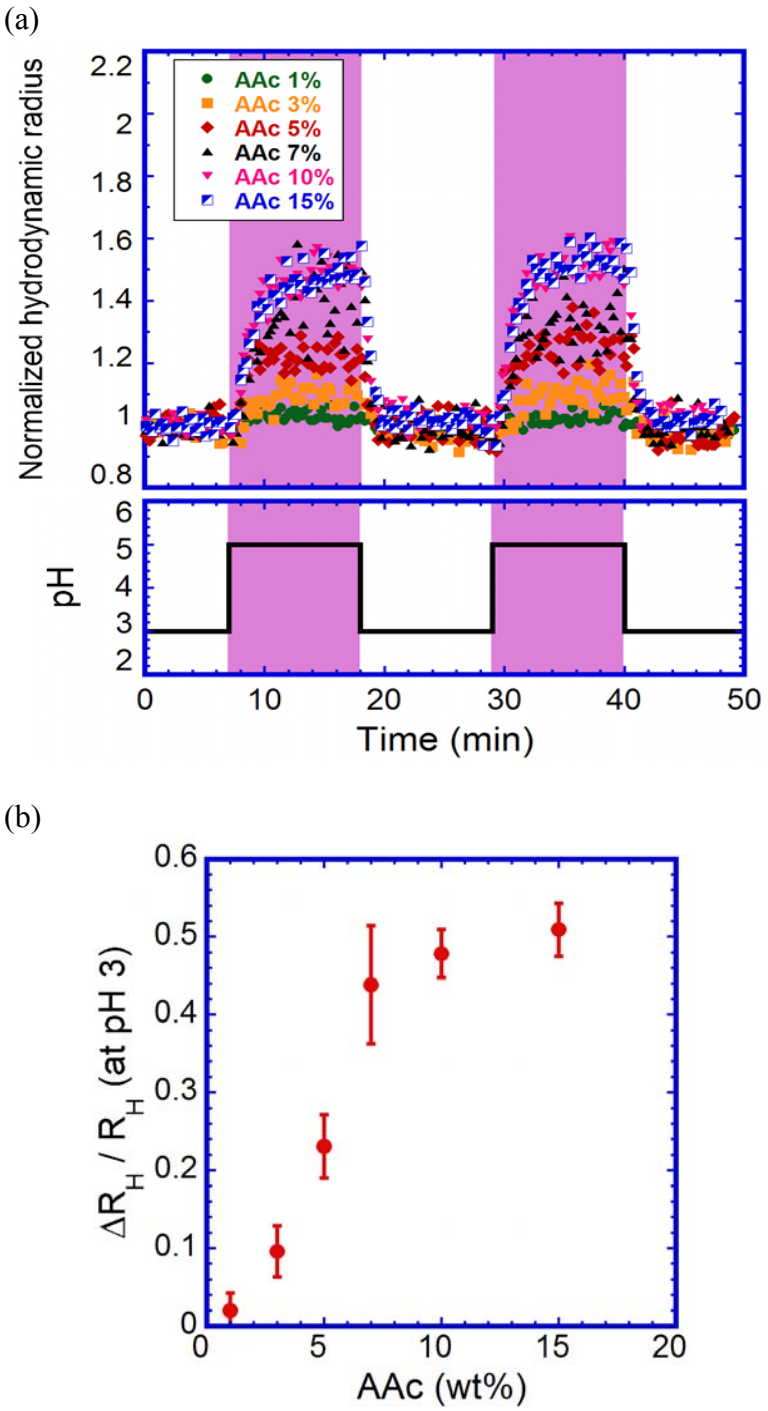

Figure 2.6 Dynamic swelling/deswelling of pH-responsive microgel suspensions in the microdialysis cell. (a) Top: Normalized R_H of pNIPAm-*co*-AAc microgels upon pH changes between 3.0 and 5.0 as a function of. Bottom: imposed pH profile in the reservoir channel. (b) Relative swelling ratio of pNIPAm-*co*-AAc microgels as a function of AAc content. Swelling ratio was normalized with R_H at pH 3.0. All experiments were performed at 23 °C with I = 15 mM.

2.2.3 Conclusion

We have demonstrated the efficacy of PTVM for determining the diffusion coefficient and hydrodynamic radius of colloidal particles. First, we benchmarked PTVM by comparing the results for polystyrene colloids with PCS data and excellent agreement was found. Then we investigated the swelling-transition of pH-responsive pNIPAm-*co*-AAc microgels as a function of pH in regular, static sample chambers and confirmed the pH-responsive changes of R_H for pNIPAm-*co*-AAc microgels upon pH change. We also successfully investigated the dynamics of swelling/deswelling of pH-responsive microgels upon pH change *in situ* by using PTVM in combination with a microdialysis cell that allows direct manipulation of solvent composition in a controlled manner. The results showed that the size changes upon pH change are reversible and reproducible. These dynamic experiments would have been impossible with conventional characterization techniques (PCS, EM). PTVM coupled with the microdialysis cell can be used to explore the kinetics of stimuli-responsive materials upon various environment changes.

2.3 Direct temperature measurement from colloidal suspensions*

Microsystems for chemical and biological analysis require precise control over the temperature inside microfluidic devices, because temperature can significantly affect biological or chemical processes [40, 41]. For example, on-chip amplification of DNA sequences by Polymerase Chain Reaction (PCR) demands precise temperature control over time and space [40] and another study has demonstrated the importance of temperature effects in systems for capillary electrophoresis [41]. A reliable on-chip temperature measurement method is essential to design and operate microsystems effectively. However, current methods have several drawbacks. For instance, microfabricated thermocouples for microfluidic devices can measure temperature only at fixed positions and involve complex lithographic processing steps [42]. A newly developed spectroscopic method can provide temperature measurements with sub-micron spatial resolution by taking advantage of the temperature dependence of material properties of chemicals [43, 44]. However, this spectroscopic method requires a light source with constant fluorescence intensity and a specialized, expensive experimental apparatus, for example multi-photon confocal microscopy. Temperature sensitive dye can also be adsorbed to samples and toxicity makes many of such chemicals unsuitable for biological samples. In this section, we present a novel *in situ* temperature measurement method using the Brownian motion of nanoparticles via PTVM. First, we evaluated the PTVM-based temperature measuring technique by directly comparing is with a currently available method. We then applied the technique towards 2D and 3D temperature mapping in a microfluidic device. This method has several advantages; (i) the video-

---

* The work in this section was published as part of 'Three-Dimensional *in situ* Temperature Measurement in Microsystems using Brownian Motion of Nanoparticles', K. Chung, J.K. Cho, E.S. Park, V. Breedveld and H. Lu, *Anal Chem*, **81**, 991 (2009, equal contribution).

microscopy of colloidal tracer particles is insensitive to fluctuations in fluorescence intensity and can even be performed with brightfield microscopy, (ii) three-dimensionally resolved temperature measurements can be achieved by simply adjusting the focal plane of an optical microscope, and (iii) the properties of tracer particles can be easily tuned for specific applications.

2.3.1 Experimental Section

For PTVM, carboxylate-modified polystyrene particles (FluoSpheres®, Invitrogen) with 0.25 μm radius were used. The fluorescent particles were suspended in DI water for temperature measurement. Before every experiment, the particle suspensions were sonicated for ~30 min to prevent aggregation. For validation of PTVM vs. thermocouple, a sample chamber was created with a microscope slide and coverslip separated by ~300 μm, using parafilm as spacer. The particle suspension was loaded into the chamber, which was sealed with vacuum grease after the insertion of the thermocouple (HH202A, Omega). For temperature measurements in microfluidic devices, the particle suspension was introduced after sonication and the device was sealed with solid metal pins to eliminate evaporation. To create temperature gradients in the devices, hot and cold streams were generated by flowing DI water (hot fluid) and 30 wt% sodium chloride solution (cold fluid) off-chip through temperature-controlled copper tubing, and then introduced into the temperature control channels via constant pressure-driven flow. Temperatures of the copper tubing were controlled using a water-bath for the hot fluid and a Peltier cooler for the cold fluid. The flow rates of the hot and cold streams were set to be high enough (typically 5 ~ 10 *mL*/min) that the temperature differences between inlet and outlet temperature of the streams were less than 1 °C. More detailed information about the microfluidic devices is provided in detail elsewhere [45].

To measure the Brownian motion of fluorescent nanoparticles in the particle channels, an inverted optical microscope (Leica DM-IRB) with 63× air and 63× oil-

immersion objectives was used and movies were captured using a CCD camera (Cohu, Poway, CA) at 30 frame/s and with 640 × 480 pixel resolution. Subsequently the recorded movies were analyzed via PTVM as described in Section 2.1. The spatial resolution of PTVM in the vertical (axial) direction was measured with a 100× oil-immersion objective.

2.3.2 Results and Discussion

Temperature measurement from Brownian motion

Before we apply PTVM to microfluidic devices, the reliability of temperature measurement with PTVM was evaluated by comparing it directly with data from a thermocouple. From the trajectories of colloidal particles, one could obtain the temperature (T) from *MSD* via the Stokes-Einstein relation, provided that the medium is Newtonian and that its viscosity is known as a function of temperature:

$$T = \frac{6\pi\eta(T)D}{k_B R_H} = \frac{3\pi\eta(T)\left(\frac{MSD}{\tau}\right)}{dk_B R_H} \tag{2.4}$$

We measured the *MSD* of the polystyrene particles over a temperature range from 1 °C to 50 °C and values measured via PTVM are in excellent agreement with the corresponding temperature measured by a thermocouple, appearing in Fig. 2.7. When using 500 nm (±15 nm) particles, this method provides an overall accuracy of temperature measurement of less than 2 °C.

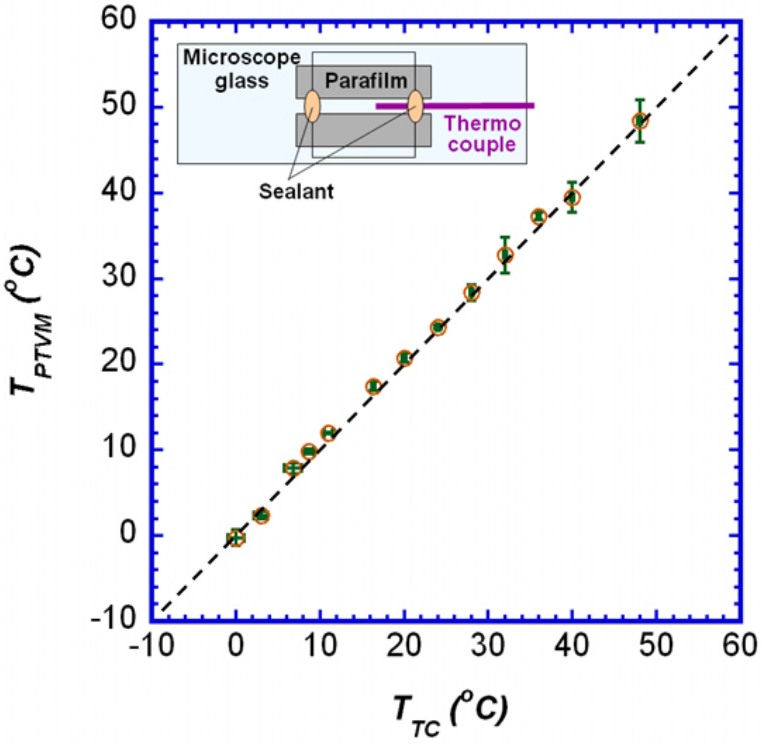

Figure 2.7 Comparison of temperature data by both PTVM and thermocouple temperature (TC). The dotted line, which has a slope of 1, represents perfect agreement between the two methods. The inset depicts the experimental set-up that enables temperature measurement via both PTVM and thermocouple.

2D temperature measurement

As a demonstration of the capability of our method to measure spatial variations of temperature, we first performed temperature measurements in a microfluidic device that was specifically designed to generate a 2D temperature gradient within the field of view of the microscope. Figure 2.8(a) depicts an isolated sample chamber filled with particle suspension, surrounded by two parallel temperature control channels. We first measured the temperature distribution at room temperature without imposed temperature gradient as shown in Fig. 2.8(b). The result shows average temperature of ~ 22 °C with standard deviation of 0.62 °C, which gives another indication of the temperature resolution one can obtain with our technique. To generate a temperature gradient across sample chamber, we used a cold stream of ~ 5 °C and a hot stream of ~ 35 °C. Figure

2.8(c) illustrates the measured temperature distribution in the presence of a temperature gradient. The measured temperatures were compared with numerical predictions and gave a good overlap. Numerical predictions for heat transport were obtained using commercially available finite element software, COMSOL (previously known as Femlab). More details about the numerical calculations are provided in reference 45. This experiment demonstrated that PTVM enables spatially resolved temperature measurements within the field of view of the microscope with a spatial resolution of ~12 μm. Although the theoretical optical resolution for our 63× objective is less than 1 μm and each single particle trajectories can be used to produce local temperatures, we had to discretize the field of view as shown in Fig. 2.8(b) ~ (c) so that each domain contains multiple trajectories of particles in order to obtain meaningful statistics, thus sacrificing some spatial resolution. However, the resolution can be easily improved by using an objective with higher magnification, high-speed camera, or higher particle concentrations in the suspension.

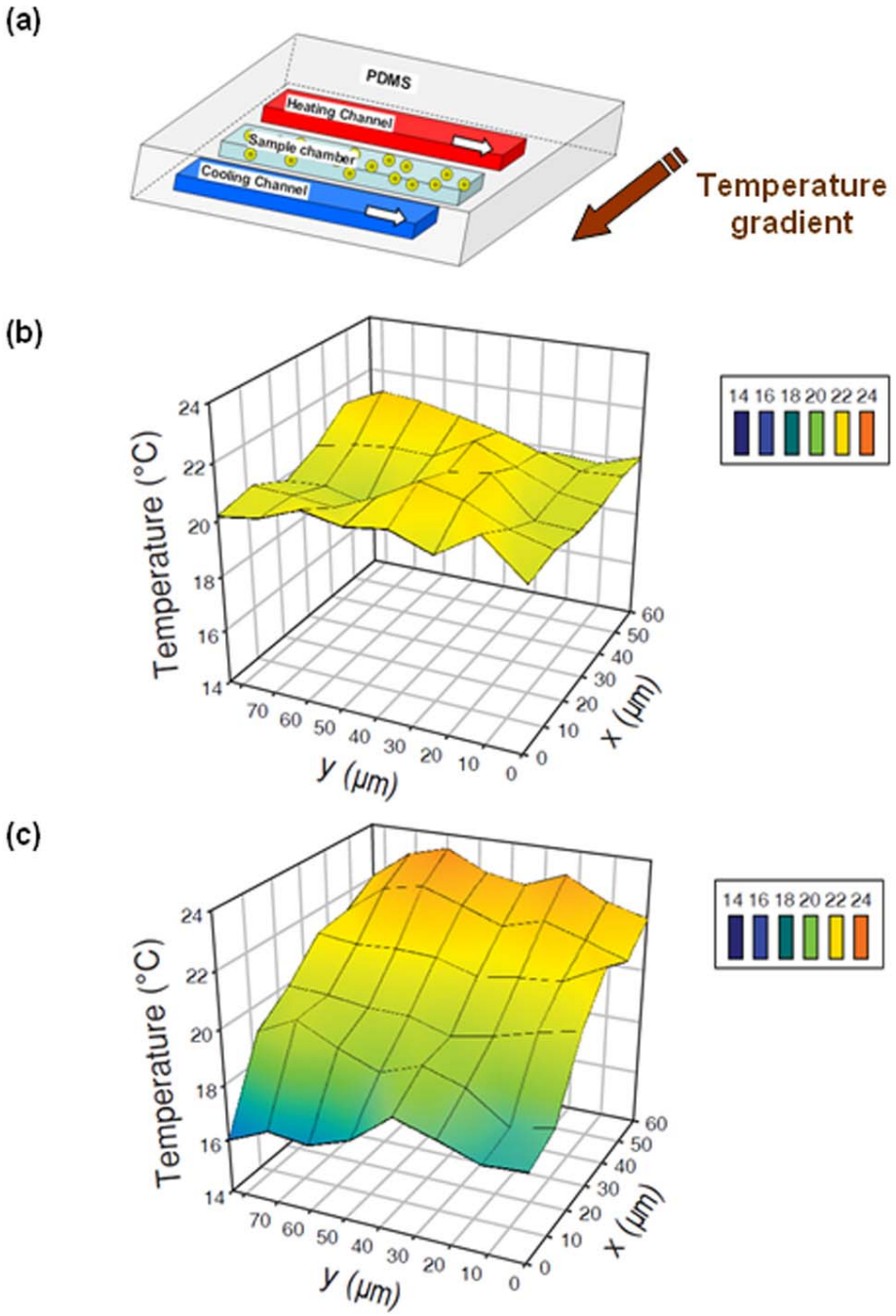

Figure 2. 8 Temperature measurement in 2D (a) Schematic of a microfluidic device. The temperature control channels colored with red (hot stream, 35 °C) and blue (cold stream, 5 °C) was 200 μm × 80 μm (width × height) and the tracer particle loading channel colored with yellow was 60 μm × 80 μm (width × height). (b) 3D contour plot of measured temperature distribution at room temperature. (c) 3D contour plot of measured temperature distribution with temperature gradient.

3*D temperature measurement*

We finally applied our method to measure the temperature distribution in the vertical (out of image plane) direction, to demonstrate potential application of our method for a multi-layered microfluidic device. Before performing temperature measurements in the vertical direction, we first evaluated the inherent spatial resolution of PTVM. To do this, we created a single layer of particles on a substrate and imaged this layer for different focal plane locations, which were controlled by means of a high resolution Piezo-controlled microscope stage. We then analyzed the pictures via PTVM. The results appear in Fig. 2.9 for different particle sizes and objectives. For conventional optical microscopy, the depth of focus (*DOF*) is the essential factor that determines axial resolution, as illustrated in Fig. 2.9(a). Objectives with a high numerical aperture (N.A.) collect more light, which enhances both lateral and axial resolution. Only particles within *DOF* can be observed through conventional microscopy, although it must be noted that the image analysis algorithm can artificially reduce *DOF* by applying strict criteria for particle recognition. Figure 2.9(b) shows the percentage of particles identified via PTVM as a function of focal plane position. As expected, the high NA 100× objective has narrower *DOF* than the 63× objective. Also, the detection efficiency of smaller particle decays faster than for larger particles. It is reasonable to conclude from the Figure that 0.5 μm fluorescent particle provide an axial resolution of ~1 μm, since roughly 50 % of the particles becomes unidentifiable beyond ± 0.5 μm from the focal plane.

To evaluate the ability of our method to resolve axial temperature gradients, we fabricated a multi-layered microfluidic device, shown in Fig. 2.9(c). To ensure uniform lateral temperature in the sample chamber, we sandwiched the sample chamber between two insulating air channels. In the axial direction, the sample chamber was bounded by the cooling channel and the glass cover slip. Temperatures were measured as a function of height by shifting the focal plane across the sample chamber. The results were again compared with predictions from a COMSOL numerical model [45]. We observed a

temperature gradient of ~ 10 °C across the 70 μm thick channel and found good agreement between experimental and numerical results, as shown in Fig. 2.9(d). Deviations from numerical calculation at 1 μm can be easily explained as an artifact due to wall effects. When particles are close to a wall, hydrodynamic coupling between the particles and the wall hinders Brownian motion of particles, resulting in suppressed diffusion, which was erroneously interpreted as a low sample temperature by our technique. This hindered diffusion phenomenon will be discussed more detail in Ch. 5.

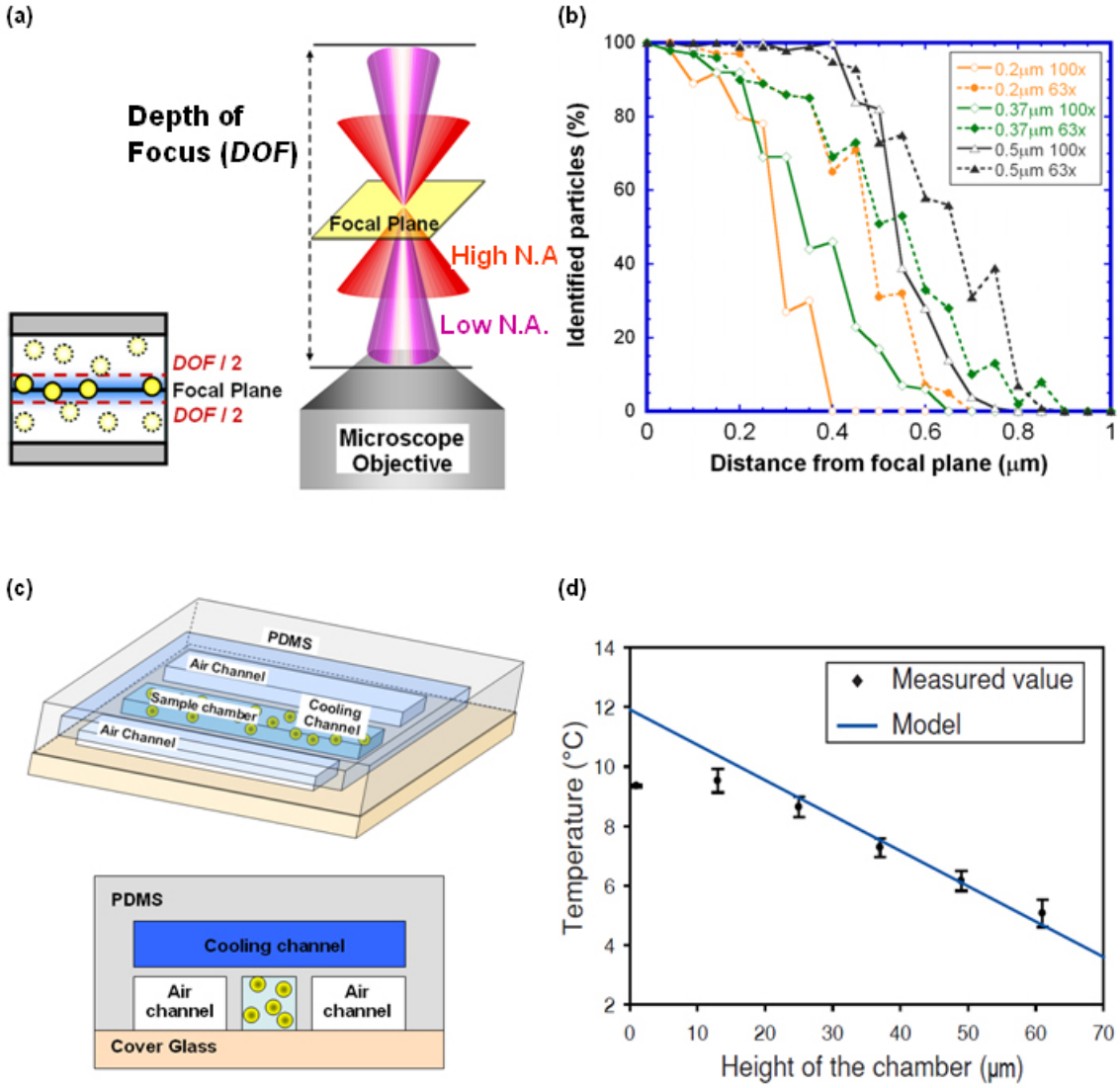

Figure 2.9 Temperature measurement in 3D via PTVM. (a) Schematic representation of *DOF* in conventional optical microscopy. (b) Percentage of particles recognized via PTVM as a function of the position of the focal plane. Spheres, diamonds, and triangles represent data for 0.20 μm, 0.37 μm, and 0.50 μm radius fluorescent polystyrene particles. Solid and dashed lines are for 100× and 63× objectives, respectively (c) Schematic of microfluidic device: (Top) sample chamber is surrounded by two air insulation channels, a cooling channel, and glass cover slip. (Bottom) Cross-section of the microfluidic device. (d) Temperature gradient in axial direction measured with 63× oil-emulsion objective. Symbols represent experimental measurements via PTVM and the line is the prediction from a numerical model.

2.3.3 Conclusion

In this section, we demonstrated that the Brownian motion of colloidal particles analyzed by PTVM can be used to measure the local temperature in microfluidic devices. The comparison with data from a thermocouple showed that PTVM can provide accurate and reproducible temperature measurements. Our method was also applied to measure temperature gradients in-plane and out-of plane in microfluidics devices and the results were in good agreement with predictions from numerical finite element models. Our experimental technique had a lateral (in plane) spatial resolution of ~ 10 μm and axial (out-of-plane) resolution of 1~2 μm. Our method can also be combined with microscopy in DIC mode or bright-field mode. The usage of a high speed camera and smaller particles can further improve both temporal and spatial resolution.

2.4 Rheological property characterization from PTVM

Phase behavior and interactions between nonionic water-soluble polymers have been studied extensively because these materials are of interest as template materials for nanoparticle synthesis [46-49] and as viscosity modifying additives for industrial formulations (*e.g.* paints/coatings, detergents, cosmetics, and pharmaceutics) [50-53]. One particularly interesting class of nonionic polymers are triblock copolymers of poly(ethylene oxide)-poly(propylene oxide)-poly(ethylene oxide) (PEO-PPO-PEO or $EO_nPO_mEO_n$, commercially available under the trade names Pluronics (BASF) and Poloxamers/Synperonics (ICI)). These polymers can self-assemble into various structures in aqueous solution, which has attracted great attention [54, 55]. In summary, the molecular microstructure of solutions of these triblock copolymers is determined primarily by temperature and concentration, as illustrated in Fig. 2.10. At low temperature or low concentration, the copolymers exist in solution as randomly coiled single molecules, unimers. With increasing temperature or concentration the PEO-PPO-PEO copolymers self-assemble to form micelles due to the limited solubility of the PPO block above the critical micelle concentration (CMC) or critical micelle temperature (CMT) [56]. The structure of the triblock copolymer micelles has been investigated by various light scattering techniques and these studies revealed that they consist of a core of hydrophobic PPO with low water content and outer layer with hydrated PEO blocks [57-59]. A further increase of temperature or concentration to values above the critical gel concentration (CGC) or critical gel temperature (CGT) leads to micelle aggregation and gelation.

Recently, the structure and the mechanisms of various gel phases composed of close-packed arrays of micelles have been investigated via light scattering, NMR and rheometry [60-63]. In spite of these studies, the phase behavior and the properties of the triblock copolymer solutions at high concentration and/or high temperature are not well

understood. Small-angle neutron scattering (SANS) studies have suggested that the micelle formation and gelation of the triblock copolymer mimics the phase behavior of hard spheres with a body-centered-cubic crystalline phase (BCC) [61, 63-65]. Although there has been a report using small-angle x-ray scattering (SAXS) that provides no evidence for the existence of micellar cubic crystals [66], most experimental and theoretical results show that the gel is in cubic liquid crystalline mesophases with micelles as building blocks. Other recent studies on the temperature dependence of micellization of the PEO-PPO-PEO copolymers have indicated that the micellization occurs over a broader temperature range, suggesting potential heterogeneity in the gelation process on the macro- or micro-scale [67, 68]. The purpose of this section is to investigate the mechanism and dynamics of gelation of two PEO-PPO-PEO block copolymers (F-127 and F-68) systematically using a combination of conventional rheology (oscillatory shear measurements) and PTVM to obtain rheological properties on different length scales.

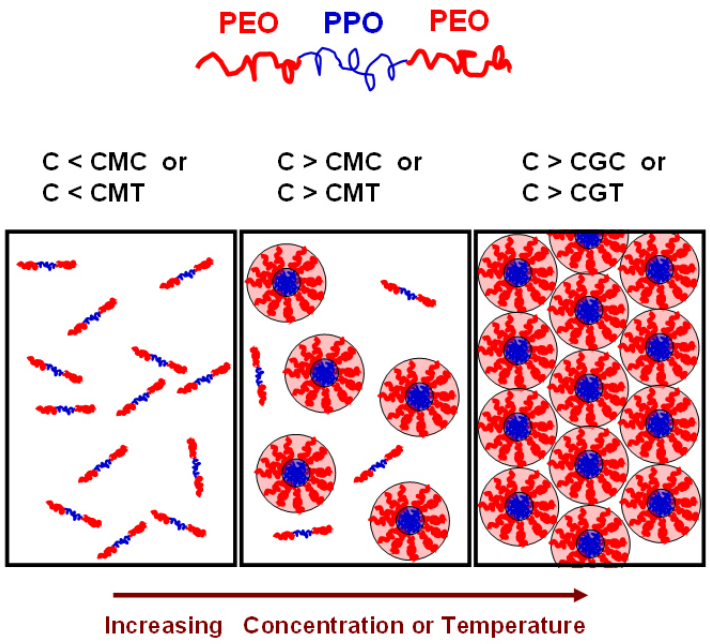

Figure 2.10 Phase behavior of PEO-PPO-PEO triblock copolymers in aqueous solution.

2.4.1 Experimental Section

Materials and sample preparation

Pluronics F-127 ($EO_{100}PO_{70}EO_{100}$, MW ~ 12600 g/mol, 70 wt% of PEO) and F-68 ($EO_{80}PO_{30}EO_{80}$, MW ~ 8350 g/mol, 80 wt% of PEO), both from Sigma Chemicals were used without further purification. Aqueous copolymer solutions at concentrations ranging from 15 to 20 wt% for F-127 and from 35 to 40 wt% for F-68 were prepared in DI water. Since PEO-PPO-PEO triblock copolymers have better solubility in water at low temperatures, the solutions were kept in a refrigerator overnight and then placed on a slow roller until the solutions became homogenous. To prevent bacterial growth, the samples were stored in the refrigerator for no more than 3 days before use.

Macro-rheology measurements

Oscillatory shear measurements were carried out using a Peltier-controlled Rheometer (MCR300, Anton Paar) with cone-plate geometry (50 mm diameter, 1° cone angle). The temperature-induced gelation was studied by increasing the temperature at a heating rate of 0.2 °C/min. A strain amplitude of 1 % was employed to ensure that all oscillatory measurements were conducted in the linear viscoelastic region, where the dynamic storage modulus (G') and loss modulus (G'') are independent of strain amplitude. Strain amplitude sweeps confirmed that non-linear responses are incurred for strain amplitudes above 10 %.

Micro-rheology via Particle Tracking Video Microsocopy

Information about the local rheological properties of the sample was obtained by performing statistical analysis of mobility of colloidal tracer particles via PTVM. To prevent non-specific adhesion of polymers to the particles and particle aggregation, PEG-coated carboxylate-modifed polystyrene microspheres (Invitrogen) of 0.50 μm were dispersed in the aqueous PEO-PPO-PEO triblock copolymer solutions [69]. After mixing the particle suspension in the copolymer solution at ~ 0.06 solid wt%, the mixtures were gently sonicated to prevent particle aggregation. The samples were then loaded into ~ 100

μm thick sample chambers, which were created by placing Parafilm spacers between a microscope slide and a cover slip, and sealed with vacuum grease to prevent evaporation. The samples were placed on the Peltier-controlled thermal microscope stage (PE100-LI2, Linkam Scientific Instruments Ltd.) and an objective heater (PN150819, Bioptech) was used to further improve temperature control. The 100× oil-immersion objective was used for measurements above 33 °C and the 63× air-objective was used below 33 °C. To ensure that there are no artifacts associated with the use of different objectives, we confirmed agreement between data collected with the two objectives at intermediate temperatures. Samples were equilibrated at different temperatures, so that the rheological properties remained constant during the image acquisition.

2.4.2 Results and discussion

Temperature-induced gelation with oscillatory shear measurement

The gelation (sol-gel transition) of F-127 and F-68 solutions as a function of temperature was measured using bulk oscillatory shear measurements (1 rad/s, 1 % strain) at varying concentrations. The storage modulus G' and the loss modulus G'' were monitored as a function of temperature to describe the evolving viscoelastic properties during temperature-induced gelation, as shown in Fig. 2.11. The crossover of loss and storage modulus on a curing curve can be interpreted as a gelation point, a temperature where the system changes from a predominantly viscous liquid to a viscoelastic solid at the specific frequency; careful studies over a wide frequency range are necessary for a more accurate definition of gelation. The results from our rheology measurements show that the gelation temperature and gel strength increase with increasing concentration of polymer. Starting at low temperatures, for all solutions, G' and G'' increase by two or more orders of magnitude with increasing temperature before G' approaches a steady value, indicating that the solution has changed from a liquid to a gel-like state. For F-127, the curves for G' and G'' as a function of temperature show a single transition at

concentrations below 16 wt% and distinct two-step S-shaped rheological transitions for concentration above 16 wt%. For example, for F-127 at 18 wt%, G'' is higher than G' at low temperatures, as typically observed in the case of viscoelastic liquids. At 21 °C, G' shows a relatively abrupt increase, crossing G'' and reaching 10 Pa at 23 °C, the signature of the formation of a weak gel. At higher temperatures, G' and G'' tend towards a first plateau (G' ~ 70 Pa at 25 °C), after which a sharp secondary S-shape transition is detected upon further heating (from 100 Pa at 25.5 °C to 3000 Pa at 27.5 °C). Finally, a second plateau is reached for G' ~ 10 kPa at 35 °C. Apparently, the gelation process involves very complex conformational changes as indicated by two S-shaped transitions: a broad transition at low temperature followed by a sharp transition at higher temperature. Qualitatively similar behavior is observed for F-68 solutions, albeit at much higher polymer concentrations, ranging from 35 to 40 wt%, as shown in Fig. 2.11(b). If we focus on F-68 at 38 wt%, at 30 °C the first transition occurs with both G' and G'' increasing upon heating (G' ~ 0.25 Pa at 30 °C and 350 Pa at 33 °C), with a crossover of G' and G'' at ~ 31 °C. The second, comparatively sharp S-shaped transition is observed above 43 °C and G' finally reaches a plateau of ~ 20 kPa.

(a)

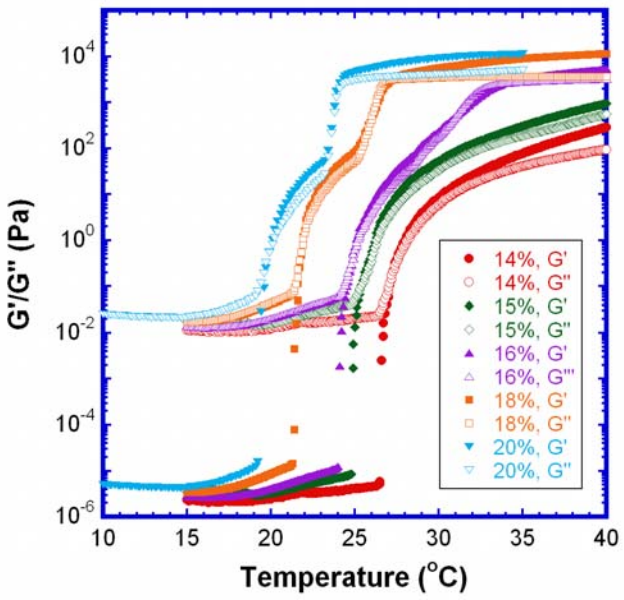

(b)

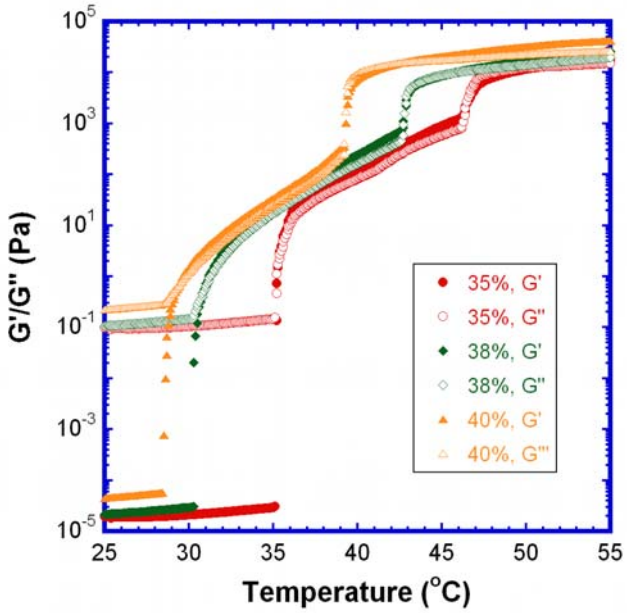

Figure 2.11 Rheological Property of triblock copolymer F-127 and F-68 solutions during oscillatory shear measurement with various concentrations as a function of temperature. (a) aqueous F-127 and (b) aqueous F-68. Solid symbols and Open symbols represent storage modulus (G') and loss modulus (G''), respectively.

Temperature-induced gelation with micro-rheology

We measured morphological changes of the triblock copolymer solution on the micrometer scale during gelation by using PTVM micro-rheology. For F-127, we focused our attention on the intermediate concentration of 18 wt%, which clearly shows a two-step transition of G' and G'' as a function of temperature. It is important to realize that the results from macro-rheology represent an ensemble-averaged result over the entire sample volume in the rheometer and do not reveal details about the local microstructure during gelation. However, as discussed at the beginning of this section, there is a possibility of heterogeneity during phase transition and the PTVM offers the opportunity to investigate sample heterogeneity by calculating *MSD* values for individual tracer particles, similar to the spatially resolved temperature measurements in Section 2.3. Figure 2.12 shows the spatial distributions of tracer mobility in the microscope field of view in the form of contour plots for F-127 and F-68 solutions at various temperatures.

The color scale is consistent for all four images of each sample, with darker colors corresponding to lower tracer mobility. For a homogeneous sample, the mobility of monodisperse tracers at a fixed relaxation time is expected to be homogeneous. However, Fig. 2.12 clearly shows a transition from homogeneous to heterogeneous particle mobilities during gelation. For instance, for the F-127 solution at 18 wt%, at the lowest temperature we found a homogenous distribution of tracer mobility, while at 26 and 27 °C we observed a heterogeneous microstructure with coexisting domains of low- and high-mobility. At even higher temperature of 29 °C the system is much more homogeneous, similar to the situation at 25 °C, albeit at lower average mobility. Interestingly, the onset of microscopic heterogeneity corresponds exactly to the second, sharp S-shaped transition in the bulk rheometry measurements. Figure 2.12 (b) shows the corresponding micro-rheological data for an F-68 solution at 38 wt%. The trend is very similar to F-127: over a very narrow temperature range, between 42 and 43 °C, microscopic heterogeneities appear in the sample and these temperatures again corresponding to the temperature at which the second, sharp transition occurs in macro-rheology. No data are shown above 43 °C for the 38 wt% F-68 solution due to limitations of our objective heater which does not provide reliable sample heating beyond 43 °C under our experimental conditions.

(a)

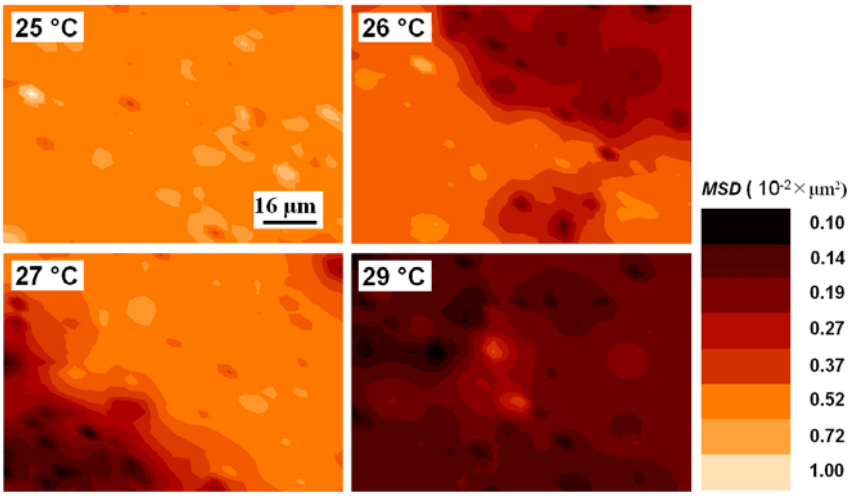

(b)

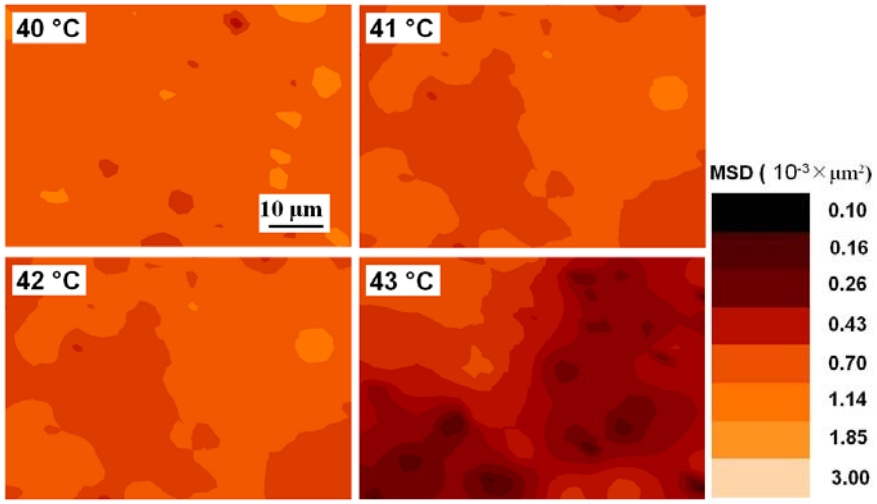

Figure 2.12 Contour plot of the spatial *MSD* distribution (for $\tau = 0.2$ s) of 0.50 μm PEG-coated carboxylate-modified tracer particles for F-127 and F-68 solutions during temperature-induced gelation. (a) in 18 wt% aqueous F-127 and (b) in 38 wt% aqueous F-68 solution at different temperatures.

Another interesting result was obtained by analyzing the *MSD* distributions of tracer particles during gelation more quantitatively, as shown in Fig. 2.13. For a homogeneous sample, the distribution of tracer mobilities is expected to be Gaussian and the corresponding cumulative probability distribution should therefore be S-shaped. Figure 2.13(a) clearly supports the picture that arose in Figure 2.12(a): homogeneous microenvironments for the tracer particles are found at 25 and 29 °C. In contrast, strong heterogeneity is observed at 26 and 27 °C, as indicated by cumulative distributions with two distinct plateaus and a "double S-shape". In fact, Figure 2.13(a) shows that over this entire temperature range, the particles can be divided into two populations, a slow and a fast population. Furthermore, the relative magnitude of the two steps in the cumulative distribution changes, but the location of the steps remains the same. This suggests that the rheological nature of the microenvironment around both particle populations remains the same, but that the balance between the populations shifts with temperature, with a larger fraction of slow particles at higher temperatures. The heterogeneous processes detected by PTVM were reversible and a very similar trend was observed for F-68 as well, shown

in Fig. 2.13(b), although the homogeneously slow sample was beyond our temperature range in this case.

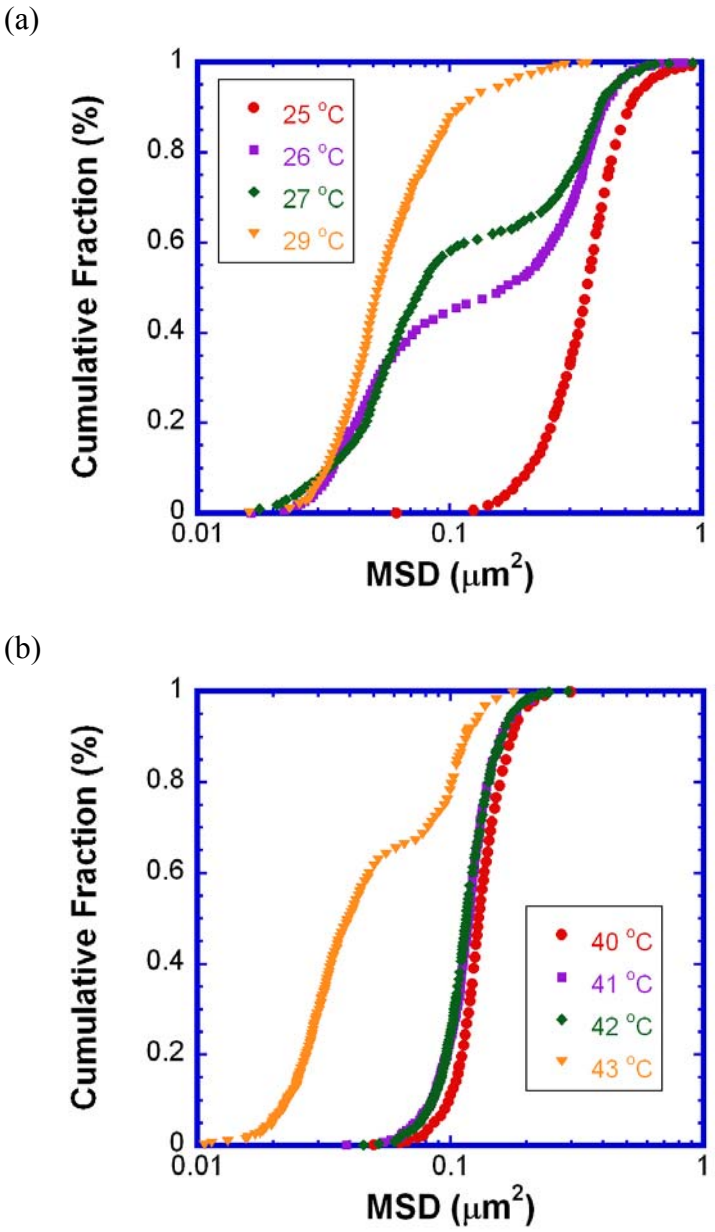

Figure 2.13 Cumulative *MSD* distributions ($\tau = 0.2$ s) as a function of temperature for 0.50 μm PEG-coated carboxylate-modified spheres during temperature-induced gelation of (a) 18 wt% aqueous F-127 solution and (b) 38 wt% aqueous F-68 solution.

Based on results from both macro-rheology and micro-rheology, it is obvious that temperature plays an important role in the micelle formation and following gelation of micelles. Macro-rheology showed a distinctive two-step transition and micro-rheology showed heterogeneous microscopic phase separation during the second transition observed by macro-rheology. It is interesting to point out that the transition was so intricate that fast heating or lack of thermal control resulted in a convoluted phenomenon, one step transition. By using reduced heating rate measurement, we were able to differentiate the two-step transition which is consistent to data for other block copolymer systems [70, 71]. Interestingly, micro-rheology did not show significant changes of sample rheology at temperatures below the microphase separation. Below the second transition temperature detected in the rheometer, microrheology experiments revealed Newtonian behavior, without any signs of elasticity. We explain this apparent discrepancy as follows: Temperature increase above CMT induces micellization of PEO-PPO-PEO copolymers which enhances viscosity of system. At the same time the hydrophobic PPO blocks accumulate to air-water interface at the edge of the sample, eventually the concentrated PPO-PEO-PPO copolymers form ordered layer structure near the interface as shown in Fig. 2.14. The accumulated polymers at the surface enhance the viscoelasticity and the increase in moduli suggests the degree of surface coverage changes as a function of temperature, prior to the formation of bulk gel. This behavior has been reported by many researchers. For instance, Munoz *et al.* studied the adsorption kinetics of PEO-PPO-PEO copolymers at the air-water interface [72]. They showed that a first diffusion-mediated adsorption kinetic process, eventually leading to the formation of brush-like structures at the surface, was followed by slow molecular rearrangements and internal reorganization of the brush. It is therefore reasonable to assume that the increase in both elastic and viscous moduli seen at primary transition temperatures below the gel point could at least partly find their origin from the development of a structured layer air-

water interface. From micro-rheology which only measure in the bulk without interface, we do not observe the behavior.

The second transition, we believe as CGT, is clearly observed by both macro-rheology and micro-rheology. Micro-rheology clearly visualizes the occurrence of a progressive structural reorganization into cubic crystal phase: microscopic phase separation between growing elastic domains (the aggregation of micelles) and shrinking viscous domains (free-fluid with micelles), as evidenced by both Fig. 2.12 and Fig. 2.13. At sufficiently high temperature, the system eventually converts to a homogeneous strong gel. It is also manifest from macro-rheology that sharp increase of moduli reflects the overlap between micelles and intermicellar distances decrease.

(a)

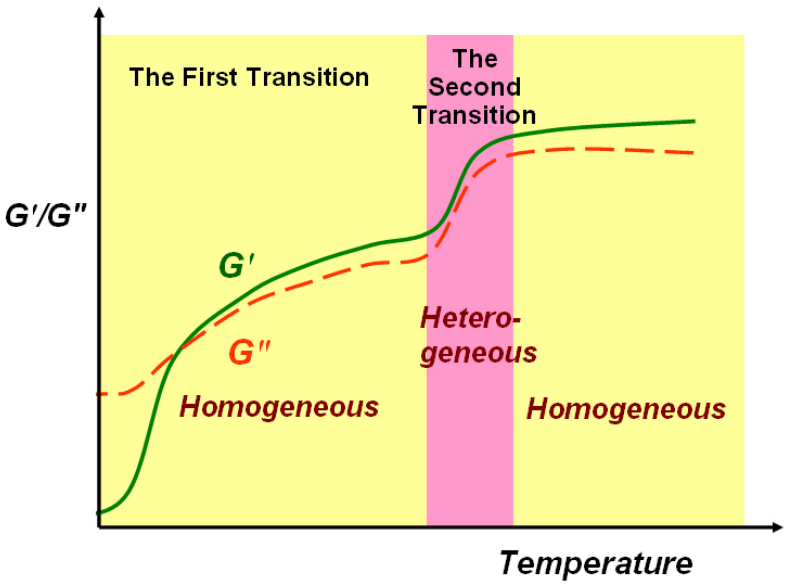

(b)

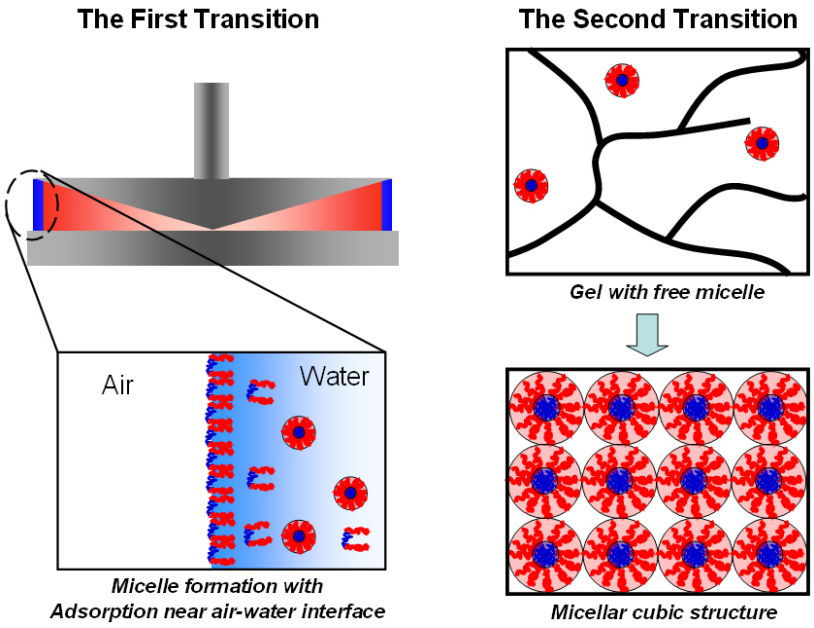

Figure 2.14 Hypothesis for a two-step gelation of PEO-PPO-PEO copolymer solution. (a) Schematic formation mechanism of temperature-induced gel. (b) Schematic observations from macro-rheology for temperature-induced two-step gelation at the molecular level with increasing micellar concentration.

2.4.3 Conclusion

We have investigated the changes in rheological properties of aqueous F-68 and F-127 PEO-PPO-PEO triblock copolymers during gelation with oscillatory macro-rheology and with micro-rheology via PTVM. For macro-rheology measurements, oscillatory shear measurements were conducted on the polymer solutions with varying concentrations. It was found that the gelation process is complex, with multiple distinct transitions, a broad primary transition and a sharp secondary transition. The gelation is shifted towards lower temperatures at higher triblock copolymer concentrations and the strength of the viscoelastic samples increases with increasing polymer concentration. The F-127 and F-68 solutions studied in this section show similar temperature-induced gelation behavior. Compared to macro-rheology which shows a two-step transition, micro-rheology was only able to detect the secondary transition, we attribute the changes in viscoelastic properties in the primary transition to the formation of micelles as well as the adsorption/surface layer formation of the copolymer at the air-water interface. Whereas, the secondary transition observed by both macro-rheology and micro-rheology is the result of micellar gel formation. While conventional macro-rheology enabled average measurement of bulk properties, micro-rheology provided localized microstructural information. The result shows that the combination of macro-rheology and micro-rheology via PTVM is a useful and powerful tool to investigate physical property of material at the molecular level.

REFERENCES

1. Gardel, M.L., J.H. Shin, F.C. MacKintosh, L. Mahadevan, P. Matsudaira, and D.A. Weitz, *Elastic Behavior of cross-linked and bundled actin networks.* Science, 2004. **304**(5675): p. 1301-1305.

2. Liu, J., G.H. Koenderink, K.E. Kasza, F.C. MacKintosh, and D.A. Weitz, *Visualizing the strain field in semiflexible polymer networks: Strain fluctuations and nonlinear rheology of F-actin gels.* Physical Review Letters, 2007. **98**(19): p. 198304.

3. Shin, J.H., M.L. Gardel, L. Mahadevan, P. Matsudaira, and D.A. Weitz, *Relating microstructure to rheology of a bundled and cross-linked F-actin network in vitro.* Proceedings of the National Academy of Sciences of the United States of America, 2004. **101**(26): p. 9636-9641.

4. Valentine, M.T., Z.E. Perlman, M.L. Gardel, J.H. Shin, P. Matsudaira, T.J. Mitchison, and D.A. Weitz, *Colloid surface chemistry critically affects multiple particle tracking measurements of biomaterials.* Biophysical Journal, 2004. **86**(6): p. 4004-4014.

5. Roberts, M.T., A. Mohraz, K.T. Christensen, and J.A. Lewis, *Direct flow visualization of colloidal gels in microfluidic channels.* Langmuir, 2007. **23**(17): p. 8726-8731.

6. Wang, P., C.M. Song, and H.A. Makse, *Dynamic particle tracking reveals the ageing temperature of a colloidal glass.* Nature Physics, 2006. **2**(8): p. 526-531.

7. Weeks, E.R., J.C. Crocker, A.C. Levitt, A. Schofield, and D.A. Weitz, *Three-dimensional direct imaging of structural relaxation near the colloidal glass transition.* Science, 2000. **287**(5453): p. 627-631.

8. Dasgupta, B.R. and D.A. Weitz, *Microrheology of cross-linked polyacrylamide networks.* Physical Review E, 2005. **71**(2): p. 021504.

9. Liu, J., M.L. Gardel, K. Kroy, E. Frey, B.D. Hoffman, J.C. Crocker, A.R. Bausch, and D.A. Weitz, *Microrheology probes length scale dependent rheology.* Physical Review Letters, 2006. **96**(11): p. 118104.

10. Crocker, J.C., M.T. Valentine, E.R. Weeks, T. Gisler, P.D. Kaplan, A.G. Yodh, and D.A. Weitz, *Two-point microrheology of inhomogeneous soft materials.* Physical Review Letters, 2000. **85**(4): p. 888-891.

11. Slopek, R.P., H.K. McKinley, C.L. Henderson, and V. Breedveld, *In situ monitoring of mechanical properties during photopolymerization with particle tracking microrheology.* Polymer, 2006. **47**(7): p. 2263-2268.

12. Goulian, M. and S.M. Simon, *Tracking single proteins within cells.* Biophysical Journal, 2000. **79**(4): p. 2188-2198.

13. Schmidt, T., G.J. Schutz, W. Baumgartner, H.J. Gruber, and H. Schindler, *Imaging of single molecule diffusion.* Proceedings of the National Academy of Sciences of the United States of America, 1996. **93**(7): p. 2926-2929.

14. Valentine, M.T., P.D. Kaplan, D. Thota, J.C. Crocker, T. Gisler, R.K. Prud'homme, M. Beck, and D.A. Weitz, *Investigating the microenvironments of inhomogeneous soft materials with multiple particle tracking.* Physical Review E, 2001. **6406**(6): p. 061506.

15. Wong, I.Y., M.L. Gardel, D.R. Reichman, E.R. Weeks, M.T. Valentine, A.R. Bausch, and D.A. Weitz, *Anomalous diffusion probes microstructure dynamics of entangled F-actin networks.* Physical Review Letters, 2004. **92**(17): p. 178101.

16. Crocker, J.C. and D.G. Grier, *Methods of digital video microscopy for colloidal studies.* Journal of Colloid and Interface Science, 1996. **179**(1): p. 298-310.

17. Cheezum, M.K., W.F. Walker, and W.H. Guilford, *Quantitative comparison of algorithms for tracking single fluorescent particles.* Biophysical Journal, 2001. **81**(4): p. 2378-2388.

18. Weeks, E.R. and J.C. Crocker. Available from: http://www.physics.emory.edu/~weeks/idl/.

19. Breedveld, V. and D.J. Pine, *Microrheology as a tool for high-throughput screening.* Journal of Materials Science, 2003. **38**(22): p. 4461-4470.

20. Mason, T.G., K. Ganesan, J.H. vanZanten, D. Wirtz, and S.C. Kuo, *Particle tracking microrheology of complex fluids.* Physical Review Letters, 1997. **79**(17): p. 3282-3285.

21. Butt, H.J., R. Berger, E. Bonaccurso, Y. Chen, and J. Wang, *Impact of atomic force microscopy on interface and colloid science.* Advances in Colloid and Interface Science, 2007. **133**(2): p. 91-104.

22. Panacek, A., L. Kvitek, R. Prucek, M. Kolar, R. Vecerova, N. Pizurova, V.K. Sharma, T. Nevecna, and R. Zboril, *Silver colloid nanoparticles: Synthesis,*

characterization, and their antibacterial activity. Journal of Physical Chemistry B, 2006. **110**(33): p. 16248-16253.

23. Matijevic, E., *Preparation and Properties of Uniform Size Colloids.* Chemistry of Materials, 1993. **5**(4): p. 412-426.

24. Park, S.H., D. Qin, and Y. Xia, *Crystallization of mesoscale particles over large areas.* Advanced Materials, 1998. **10**(13): p. 1028-1030.

25. Debord, J.D. and L.A. Lyon, *Synthesis and characterization of pH-responsive copolymer microgels with tunable volume phase transition temperatures.* Langmuir, 2003. **19**(18): p. 7662-7664.

26. Debord, S.B. and L.A. Lyon, *Influence of particle volume fraction on packing in responsive hydrogel colloidal crystals.* Journal of Physical Chemistry B, 2003. **107**(13): p. 2927-2932.

27. Sato, J. and V. Breedveld, *Transient rheology of solvent-responsive complex fluids by integrating microrheology and microfluidics.* Journal of Rheology, 2006. **50**(1): p. 1-19.

28. Invitrogen, *FluoSpheres Fluorescent Microspheres*, in *Product Information*. 2005.

29. Pelton, R., *Temperature-sensitive aqueous microgels.* Advances in Colloid and Interface Science, 2000. **85**(1): p. 1-33.

30. Morris, G.E., B. Vincent, and M.J. Snowden, *Adsorption of lead ions onto N-isopropylacrylamide and acrylic acid copolymer microgels.* Journal of Colloid and Interface Science, 1997. **190**(1): p. 198-205.

31. Weissman, J.M., H.B. Sunkara, A.S. Tse, and S.A. Asher, *Thermally switchable periodicities and diffraction from mesoscopically ordered materials.* Science, 1996. **274**(5289): p. 959-960.

32. Hirotsu, S., I. Yamamoto, A. Matsuo, T. Okajima, H. Furukawa, and T. Yamamoto, *Brillouin-Scattering Study of the Volume Phase-Transition in Poly-N-Isopropylacrylamide Gels.* Journal of the Physical Society of Japan, 1995. **64**(8): p. 2898-2907.

33. Lide D.R. *et al.*, *CRC HANDBOOK OF CHEMISTRY AND PHYSICS.* (CRC Press LLC, Boca Raton, 2003).

34. Murthy, N., M.C. Xu, S. Schuck, J. Kunisawa, N. Shastri, and J.M.J. Frechet, *A macromolecular delivery vehicle for protein-based vaccines: Acid-degradable protein-loaded microgels.* Proceedings of the National Academy of Sciences of the United States of America, 2003. **100**(9): p. 4995-5000.

35. Lee, K. and S.A. Asher, *Photonic crystal chemical sensors: pH and ionic strength.* Journal of the American Chemical Society, 2000. **122**(39): p. 9534-9537.

36. Holtz, J.H. and S.A. Asher, *Polymerized colloidal crystal hydrogel films as intelligent chemical sensing materials.* Nature, 1997. **389**(6653): p. 829-832.

37. Kim, J., M.J. Serpe, and L.A. Lyon, *Photoswitchable microlens arrays.* Angewandte Chemie-International Edition, 2005. **44**(9): p. 1333-1336.

38. Richter, A., S. Klatt, G. Paschew, and C. Klenke, *Micropumps operated by swelling and shrinking of temperature-sensitive hydrogels.* Lab on a Chip, 2009. **9**(4): p. 613-618.

39. Beebe, D.J., J.S. Moore, J.M. Bauer, Q. Yu, R.H. Liu, C. Devadoss, and B.H. Jo, *Functional hydrogel structures for autonomous flow control inside microfluidic channels.* Nature, 2000. **404**(6778): p. 588-590.

40. DeMello, A.J., *Microfluidics - DNA amplification moves on.* Nature, 2003. **422**(6927): p. 28-29.

41. Rush, R.S., A.S. Cohen, and B.L. Karger, *Influence of Column Temperature on the Electrophoretic Behavior of Myoglobin and Alpha-Lactalbumin in High-Performance Capillary Electrophoresis.* Analytical Chemistry, 1991. **63**(14): p. 1346-1350.

42. Pearce, T.M., J.A. Wilson, S.G. Oakes, S.Y. Chiu, and J.C. Williams, *Integrated microelectrode array and microfluidics for temperature clamp of sensory neurons in culture.* Lab on a Chip, 2005. **5**(1): p. 97-101.

43. Hoang, V.N., G.V. Kaigala, and C.J. Backhouse, *Dynamic temperature measurement in microfluidic devices using thermochromic liquid crystals.* Lab on a Chip, 2008. **8**(3): p. 484-487.

44. Ross, D., M. Gaitan, and L.E. Locascio, *Temperature measurement in microfluidic systems using a temperature-dependent fluorescent dye.* Analytical Chemistry, 2001. **73**(17): p. 4117-4123.

45. Chung, K., J.K. Cho, E.S. Park, V. Breedveld, and H. Lu, *Three-Dimensional in Situ Temperature Measurement in Microsystems Using Brownian Motion of Nanoparticles.* Analytical Chemistry, 2009. **81**(3): p. 991-999.

46. Grosso, D., G.J.D.A.A. Soler-Illia, F. Babonneau, C. Sanchez, P.A. Albouy, A. Brunet-Bruneau, and A.R. Balkenende, *Highly organized mesoporous titania thin films showing mono-oriented 2D hexagonal channels.* Advanced Materials, 2001. **13**(14): p. 1085-1089.

47. Frindell, K.L., M.H. Bartl, A. Popitsch, and G.D. Stucky, *Sensitized luminescence of trivalent europium by three-dimensionally arranged anatase nanocrystals in mesostructured titania thin films.* Angewandte Chemie-International Edition, 2002. **41**(6): p. 959-962.

48. Crepaldi, E.L., G.J.D.A. Soler-Illia, D. Grosso, F. Cagnol, F. Ribot, and C. Sanchez, *Controlled formation of highly organized mesoporous titania thin films: From mesostructured hybrids to mesoporous nanoanatase TiO2.* Journal of the American Chemical Society, 2003. **125**(32): p. 9770-9786.

49. Choi, S.Y., B. Lee, D.B. Carew, M. Mamak, F.C. Peiris, S. Speakman, N. Chopra, and G.A. Ozin, *3D hexagonal (R-3m) mesostructured nanocrystalline titania thin films: Synthesis and characterization.* Advanced Functional Materials, 2006. **16**(13): p. 1731-1738.

50. Jeon, J.H. and D.A. Puleo, *Alternating release of different bioactive molecules from a complexation polymer system.* Biomaterials, 2008. **29**(26): p. 3591-3598.

51. Luk, V.N., G.C.H. Mo, and A.R. Wheeler, *Pluronic additives: A solution to sticky problems in digital microfluidics.* Langmuir, 2008. **24**(12): p. 6382-6389.

52. Amiji, M. and K. Park, *Prevention of Protein Adsorption and Platelet-Adhesion on Surfaces By PEO-PPO-PEO Triblock Copolymers.* Biomaterials, 1992. **13**(10): p. 682-692.

53. Sun, K.S., R. Kumar, D.E. Falvey, and S.R. Raghavan, *Photogelling Colloidal Dispersions Based on Light-Activated Assembly of Nanoparticies.* Journal of the American Chemical Society, 2009. **131**(20): p. 7135-7141.

54. Tuzar, Z. and P. Kratochvil, *Block and Graft Copolymer Micelles in Solution.* Advances in Colloid and Interface Science, 1976. **6**(3): p. 201-232.

55. Malmsten, M. and B. Lindman, *Self-Assembly in Aqueous Block Copolymer Solutions.* Macromolecules, 1992. **25**(20): p. 5440-5445.

56. Mortensen, K., W. Brown, and E. Jorgensen, *Phase-Behavior of Poly(Propylene Oxide) Poly(Ethylene Oxide) Poly(Propylene Oxide) Triblock Copolymer Melt and Aqueous-Solutions.* Macromolecules, 1994. **27**(20): p. 5654-5666.

57. Brown, W., K. Schillen, M. Almgren, S. Hvidt, and P. Bahadur, *Micelle and Gel Formation in a Poly(Ethylene Oxide) Poly(Propylene Oxide) Poly(Ethylene Oxide) Triblock Copolymer in Water Solution - Dynamic and Static Light-Scattering and Oscillatory Shear Measurements.* Journal of Physical Chemistry, 1991. **95**(4): p. 1850-1858.

58. Nolan, S.L., R.J. Phillips, P.M. Cotts, and S.R. Dungan, *Light scattering study on the effect of polymer composition on the structural properties of PEO-PPO-PEO micelles.* Journal of Colloid and Interface Science, 1997. **191**(2): p. 291-302.

59. Goldmints, I., G.E. Yu, C. Booth, K.A. Smith, and T.A. Hatton, *Structure of (deuterated PEO) (PPO) (deuterated PEO) block copolymer micelles as determined by small angle neutron scattering.* Langmuir, 1999. **15**(5): p. 1651-1656.

60. Habas, J.P., E. Pavie, A. Lapp, and J. Peyrelasse, *Understanding the complex rheological behavior of PEO-PPO-PEO copolymers in aqueous solution.* Journal of Rheology, 2004. **48**(1): p. 1-21.

61. Prudhomme, R.K., G.W. Wu, and D.K. Schneider, *Structure and rheology studies of poly(oxyethylene-oxypropylene-oxyethylene) aqueous solution.* Langmuir, 1996. **12**(20): p. 4651-4659.

62. Nystrom, B., H. Walderhaug, and F.K. Hansen, *Dynamic light scattering and rheological studies of thermoreversible gelation of a poly(ethylene oxide)-poly(propylene oxide)-poly(ethylene oxide) triblock copolymer in aqueous solution.* Faraday Discussions, 1995(101): p. 335-344.

63. Walderhaug, H., *PFG NMR study of polymer and solubilizate dynamics in aqueous isotropic mesophases of some poloxamers.* Journal of Physical Chemistry B, 1999. **103**(17): p. 3352-3357.

64. Mortensen, K., W. Brown, and E. Jorgensen, *Lamellar Mesophase of Poly(Ethylene Oxide) Poly(Propylene Oxide) Poly(Ethylene Oxide) Melts and Water-Swollen Mixtures.* Macromolecules, 1995. **28**(5): p. 1458-1463.

65. Mortensen, K., *Phase-Behavior of Poly(Ethylene Oxide)-Poly(Propylene Oxide)-Poly(Ethylene Oxide) Triblock-Copolymer Dissolved in Water.* Europhysics Letters, 1992. **19**(7): p. 599-604.

66. Glatter, O., G. Scherf, K. Schillen, and W. Brown, *Characterization of a Poly(Ethylene Oxide) Poly(Propylene Oxide) Triblock Copolymer (Eo(27)-Po39-Eo(27)) in Aqueous-Solution.* Macromolecules, 1994. **27**(21): p. 6046-6054.

67. Linse, P., *Micellization of Poly(Ethylene Oxide)-Poly(Propylene Oxide) Block-Copolymers in Aqueous-Solution - Effect of Polymer Polydispersity.* Macromolecules, 1994. **27**(22): p. 6404-6417.

68. Hvidt, S., C. Trandum, and W. Batsberg, *Effects of poloxamer polydispersity on micellization in water.* Journal of Colloid and Interface Science, 2002. **250**(1): p. 243-250.

69. Kim, A.J., V.N. Manoharan, and J.C. Crocker, *Swelling-based method for preparing stable, functionalized polymer colloids.* Journal of the American Chemical Society, 2005. **127**(6): p. 1592-1593.

70. Stuart, M.A.C., T. Cosgrove, and B. Vincent, *Experimental Aspects of Polymer Adsorption at Solid-Solution Interfaces.* Advances in Colloid and Interface Science, 1986. **24**(2-3): p. 143-239.

71. Jiang, Q., Y.C. Chiew, and J.E. Valentini, *Adsorption of ethylene oxide propylene oxide ethylene oxide triblock copolymers at the air/water interface.* Colloids and Surfaces a-Physicochemical and Engineering Aspects, 1996. **113**(1-2): p. 127-134.

72. M. G. Munoz, F. Monroy, F. Ortega, R. G. Rubio, D. Langevin, *Monolayers of Symmetric Triblock Copolymers at the Air−Water Interface. 1. Equilibrium Properties.* Langmuir, 2000. **16**(3): p. 1083-1093.

CHAPTER 3

STUDY OF PHASE BEHAVIOR OF PH-RESPONSIVE MICROGELS WITH TUNABLE INTERACTIONS INSIDE MICROFLUIDIC DIALYSIS CELL[*]

We report investigations of the phase behavior of ionic microgel suspensions, which have emerged as an important model system for soft colloidal particles. The experiments were performed in a microfluidic dialysis cell that enables *in situ* manipulation of solvent composition. The effective particle volume fraction of suspensions of poly(*N*-isopropylacrylamide-*co*-acrylic acid) (pNIPAm-*co*-AAc) microgel particles was tuned by altering the degree of ionization of AAc copolymer via changes in pH, thus causing swelling/deswelling of the microgel. The microdialysis cell enables reversible changes in the composition of the suspending medium (*e.g.*, pH, ionic strength), while the dynamics of the microgel particles can be monitored simultaneously via video microscopy. With this device the phase behavior of these suspensions was probed efficiently over a wide range of pH conditions. Our study reveals that concentrated microgel suspensions exhibit the same equilibrium phases as hard sphere systems: liquid, crystal, and liquid-crystal coexistence, but with a much broader coexistence region than that found. A key difference is that the coexistence region was found to be much broader than for hard spheres. Additionally, non-equilibrium jammed

---

[*] This chapter has been submitted as "Study of Phase Behavior of pH-responsive Microgels with Tunable Interactions inside Microfluidic Dialysis Cell" by J.K. Cho, Z. Meng, L.A. Lyon, and V. Breedveld (2009).

states were observed upon rapid volumetric expansion of the microgels. The resulting phase diagram shows the importance of microgel deformability and illustrates the existence of complex interparticle interactions with interplay between a weak attractive force and soft repulsive interaction.

3.1 Introduction

Over the past decades, phase behavior of colloidal suspensions has been extensively studied as a valuable model system [1-4], as they exhibit rich phase behavior ranging from gas to crystal, similar to atomic system. The interactions between colloids and between atoms show remarkable similarity and the larger size of colloids makes the time and length scales of their dynamics much more readily accessible experimentally. As discussed in Ch. 1, for the simplest colloidal system, a suspension of hard-spheres with a strongly repulsive interaction on direct contact, the effective particle volume fraction (ϕ_{eff}) determines phase behavior, which is characterized by a transition from a liquid-like to crystalline or glassy state with increasing particle concentration. As experimental hard-sphere systems researchers have been using sterically stabilized poly (methyl methacrylate) (PMMA) [1, 5]. More recently, mesoscopic covalently cross-linked microgels have attracted attention as soft-sphere model systems. The most widely used model colloidal microgel systems are those composed mainly of poly(*N*-isopropylacrylamide) (pNIPAm) [6, 7]. In aqueous media, pNIPAm undergoes a reversible and continuous volume phase transition as a function of temperature [8], which provides temperature-tunability of ϕ_{eff} [9, 10]. By introducing ionizable groups via copolymerization into the microgel network, additional tunability of particle size via pH and ionic strength change can be achieved [11]. The deformability of these soft colloidal microgels adds significant complexity to the interparticle potential and resulting phase behavior. Compared to hard sphere colloids, the combination of softness of the polymer

network and delicate balance between polymer-solvent/polymer-polymer interaction exhibit a much richer phase behavior [12].

In this chapter, we investigated the phase behavior of suspensions of stimuli-responsive ionic colloidal microgels. By using the microdialysis cell with PTVM, we can observe the dynamics and phase behavior of the colloidal suspensions *in situ* with high temporal resolution. By changing the composition of the buffer solution, we have investigated phase transitions in two types of experiments. First, gradual stepwise changes in pH (ΔpH = ± 0.1) were used to investigate the equilibrium phase behavior of the colloidal microgels. In a second set of experiments, large jumps in pH (and ϕ_{eff}) were imposed, which result in non-equilibrium jammed phases, similar to glasses in colloidal hard sphere suspensions.

3.2 Experimental Section

To control the solvent composition in a microgel suspension without affecting the particle number density, we utilized the microdialysis cell that is discussed in detail in Ch. 2. Because the microgels are about 50 times bigger than the pore size of the membrane (20 nm), the number density of microgels in the sample chamber remains constant during the experiments. Synthesis of pNIPAm-*co*-AAc microgels cross-linked with *N*, *N*'-methylene bis (acrylamide) (BIS) was carried out via free radical precipitation polymerization (NIPAm : AAc : BIS = 84.3 : 14.7 : 1.0 in mol %) as reported elsewhere [11, 13, 14]. After freeze-drying, the particles were resuspended in aqueous media as needed. All experiments were performed at 23 °C to prevent temperature-induced deswelling and the ionic strength of the pH buffers was kept constant at 15 mM with NaCl in order to minimize electrostatic interactions. We used an inverted optical

microscope (DM-IRB, Leica) in DIC mode and 100 × N.A. 1.3 oil immersion objective. To avoid wall effects, measurements were made at least 40 μm from the wall.

3.3 Results and Discussion

For our pNIPAm-*co*-AAc microgels, the normalized radius is plotted in Fig. 3(a) as a function of pH. The data can be described empirically with the following equation:

$$R_H / R_{H,\,pH=3} = 0.9235 + \frac{0.9072}{1 + \left(\frac{pH}{4.3543}\right)^{-7.389}} \tag{3.1}$$

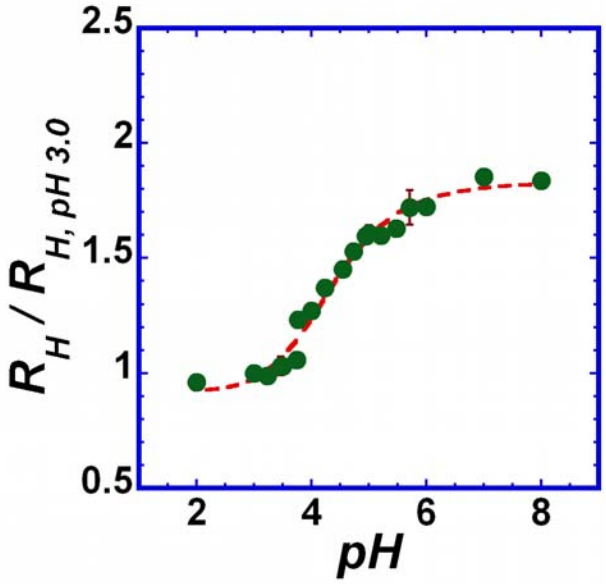

Figure 3.1 Normalized hydrodynamic radius of pNIPAm-*co*-AAc in dilute suspensions at 23 °C via PTVM; radii are normalized to the value at pH = 3.0, 0.88 μm and the dashed line represents Eq. (3.1).

As pH increases, R_H shows strong swelling between pH ≈ 4 and pH ≈ 6 and a plateau is reached at higher pH values. Although Eq. (3.1) can be used to calculate changes in effective volume fraction (ϕ_{eff}) as a function of pH, additional information is required to determine the absolute value of ϕ_{eff} for microgels in suspension. In order to relate the mass concentration of microgels in the dispersion, *c* (weight of microgels per solution weight), to the volume fraction ϕ_{eff}, the shift factor *k* is used: $\phi_{eff} = kc$. To determine *k*, one can use Batchelor's model for the shear viscosity of dilute hard-sphere suspensions: $\eta_r = \eta / \eta_s = 1 + 2.5\phi_{eff} + 6.2\phi_{eff}^2$ where η_r, η, and η_s are the relative viscosity, suspension viscosity, and solvent viscosity, respectively [8, 15, 16]. For this study, the viscosity of dilute microgel dispersions was investigated with a stress controlled MCR 300 rheometer (Anton Paar) in 50 mm-1° cone and plate geometry with Peltier temperature control. At 23 °C and at pH = 4.37, we found $k = 15.784 \pm 0.323$ for pNIPAm-*co*-AAc microgels by fitting experimental η data at different mass concentrations to Batchelor's equation. By combining this *k* value with Eq. (3.1), we can calculate ϕ_{eff} at all mass concentrations *c* and pH values.

Equilibrium phase behavior studies of concentrated pNIPAm-*co*-AAc microgel dispersions were then carried out in the microdialysis cell by changing pH of the solution reversibly. It is important to point out that the solution composition within the sample chamber changes fully within less than 5 min [17]. To ensure equilibrium states in the suspension, we used gradual stepwise changes of less than 4 % in microgel volume (ΔpH ≈ 0.1). More than 90 % volume of pNIPAm-*co*-AAc microgel is water, so that density differences between microgels and medium are small and sedimentation can be neglected. In addition to its short response time, miniaturization of the system facilitates crystal growth in the microdialysis cell in comparison with other methods for assembly of

colloidal crystals, such as those based on sedimentation [18], evaporation of solvent [19], or centrifugation [11].

PTVM yields trajectories of individual microgels, which can be used to extract information about the colloidal dynamics of the suspension; in particular, it is useful to calculate both the ensemble-averaged mobility and the spatial distribution of microgel mobility to study phase transitions. In addition, the static structure of the suspension can be investigated by determining the pair distribution function ($g(r)$) from the particle positions, or by directly applying a Fourier Transformation (FT) to the image. Figure 3.2 shows how a 2.8 wt% pNIPAm-*co*-AAc microgel suspension evolves as ϕ_{eff} is increased via pH. Like hard-sphere systems, microgel suspensions undergo phase transitions from liquid to crystal [20, 21]. At low effective volume fractions, ϕ_{eff} = 43.5 %, the system is liquid-like: there is no obvious structure in the trajectories (Fig. 3.2(a)), the MSD contour plot shows that the mobility is high and homogeneous; and the image FT yields a vague ring-like structure, indicating isotropy and weak translational correlations. As ϕ_{eff} is increased to 57.3 % and then 73.1 %, the colloidal suspension displays nucleation and crystal growth in liquid/crystal coexistence (Fig. 3.2(b) ~ 3.2(c)). Specifically, at ϕ_{eff} = 57.3 %, the particle trajectories and MSD contour plot show that nucleation occurs near the left bottom, where an area with hexagonal structure and low mobility develops. At ϕ_{eff} = 73.1 %, most particles in the field of view have slowed down, although the right hand side still lacks structure and is more mobile. Eventually, the suspensions becomes fully crystalline, as clearly shown by the trajectories and the six-fold hexagonal pattern in the FT for ϕ_{eff} = 83.5 %. The coexistence of disordered, mobile liquid domains and less mobile crystalline domains at the intermediate volume fractions is an equilibrium state of the suspension.

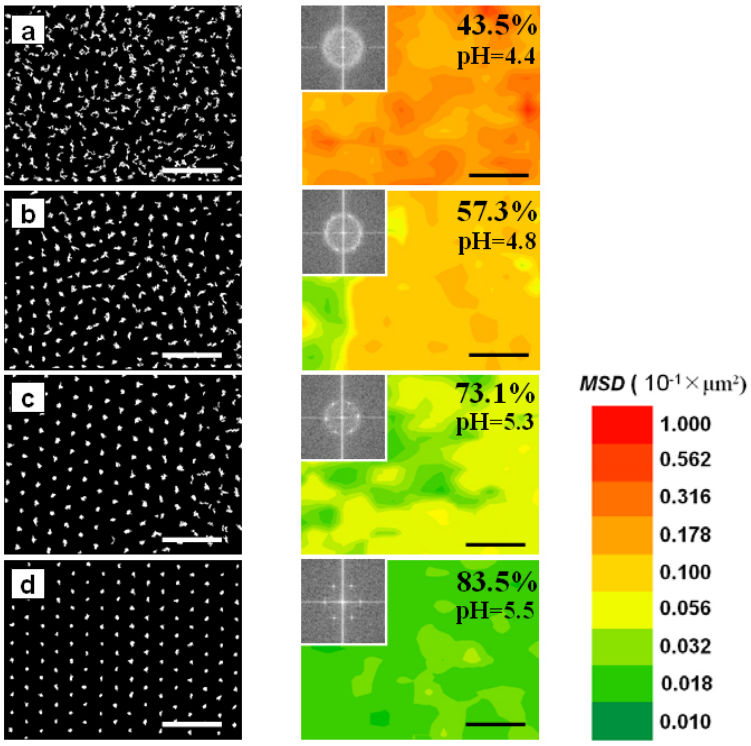

Figure 3.2 Structural evolution of pNIPAm-*co*-AAc suspensions at 2.8 wt% as a function of pH. The left figures show particle trajectories (duration 10 seconds) and the right figures are MSD contour plots (correlation time τ = 0.133 s) with consistent color-coding for all four concentrations. Insets and numbers in the right figures are direct FTs and ϕ_{eff}, respectively. All scale bars are 5 μm.

Figure 3.3 presents ensemble averaged dynamic and static characteristics of the samples introduced in Fig. 3.2. The average mobility is shown in a double logarithmic plot of MSD vs. correlation time τ (Fig. 3.3(a)). At low effective volume fractions (e.g., ϕ_{eff} = 43.5 %), the slope of log(MSD) vs. log(τ) is close to 1, which indicates diffusive particle motion, while at ϕ_{eff} = 83.5 %, the plateau indicates that microgel particles are caged. We also calculated the $g(r)$ and the results are displayed in Fig. 3.3(b) [22]. For low ϕ_{eff}, we observe a typical liquid-like structure without long-range correlations. With increasing ϕ_{eff}, one can clearly observe that the peaks in $g(r)$ become more pronounced and that a typical hexagonal long-range correlation develops. One interesting phenomenon is a shift of the nearest-neighbor peak from ~1.2 μm to ~1.4 μm, which

reflects the fact that ϕ_{eff} is increased via particle swelling due to deprotonation of AAc groups with increasing pH.

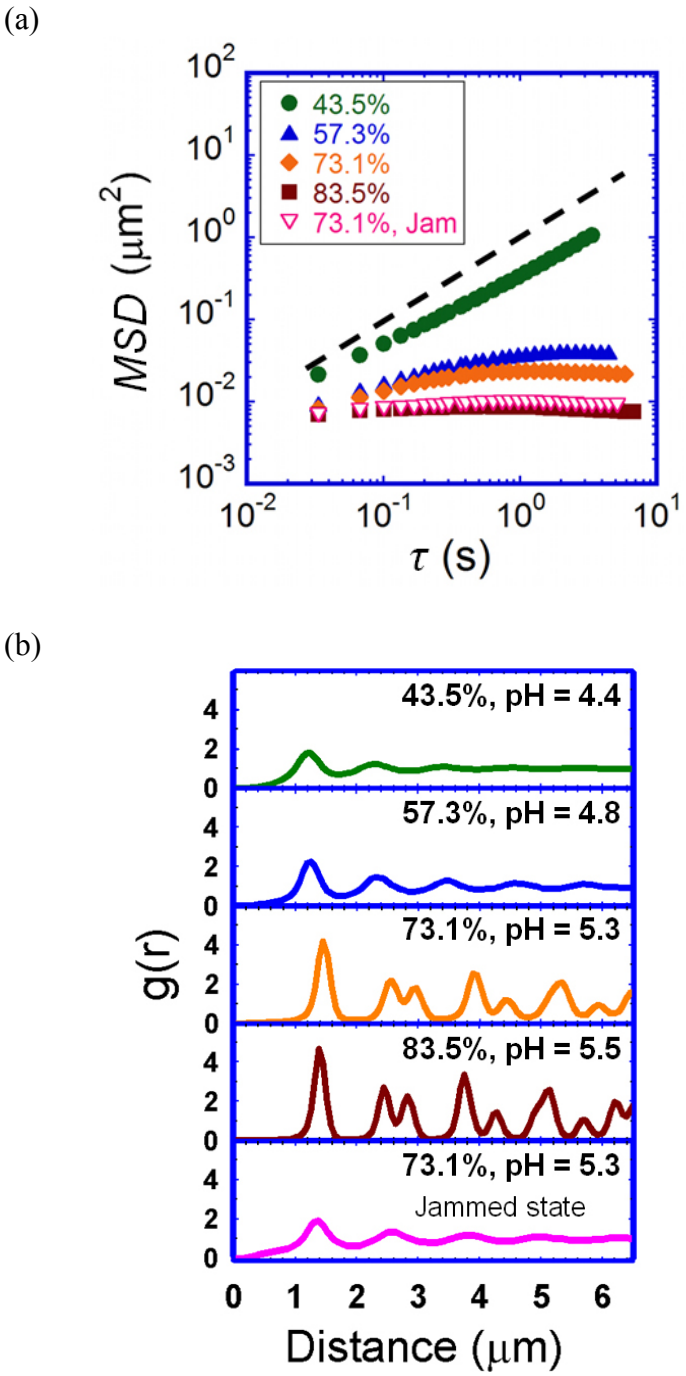

Figure 3.3 (a) MSD and (b) $g(r)$ for pNIPAm-*co*-AAc suspensions of 2.8 wt% at various ϕ_{eff} / pH values. The dashed line with slope = 1 represents diffusive motion.

In addition to our equilibrium studies with gradual pH changes, non-equilibrium states can also be investigated with the microdialysis cell by imposing sudden large pH increase ($\Delta pH \geq 1$, $\Delta \phi_{eff} >> 20$ %). In Figure 3.3, we also present data for a 2.8 wt% suspension that underwent a large pH jump from 3.0 to 5.3. Although the final ϕ_{eff} of 73.1 % is commensurate with liquid-crystal coexistence in case of gradual pH changes, the rapid microgel expansion instead results in an unordered, jammed state. The mobility (MSD) of this jammed state is close to the values found for the equilibrium crystalline state at 83.5 %, but $g(r)$ is liquid-like with very weak long-range correlation. The jammed state did not show any signs of relaxation towards the equilibrium coexistence even after waiting for 24 hours. Jammed, glassy states have also been observed for hard sphere systems [23, 24] and they were always found in the pure crystalline region. In contrast, jammed disordered states for our pH-responsive microgel suspensions are found at volume fractions in the middle of the equilibrium liquid-crystal coexistence region.

The experiments described above were repeated at different microgel weight fractions in order to construct a full experimental phase diagram; the results are summarized in Fig. 3.4. All experiments were carried out at 23 °C (below the lower critical solution temperature (LCST) of NIPAm) with I = 15 mM. Under our experimental conditions, the Debye screening length is about 2.5 nm and van der Waals attractions can be ignored due to marginal differences in the refractive index. Gradual pH changes with equilibration times of more than an hour were used to achieve equilibrium phases. In these studies, large parts of the sample chamber were scanned to distinguish between pure phases (liquid or crystalline) and coexistence phase. Reversibility tests (alternatingly increasing and decreasing pH) were also performed to confirm the location of phase boundaries. Along the horizontal axis of Fig. 3.4 we have plotted the effective volume fraction, calculated based on the hydrodynamic radius of microgels in dilute suspension. One should be careful in interpreting this data: monodisperse hard spheres

are limited to volume fractions below 74 % due to maximum packing constraints, but microgels are both deformable and compressible, so that values of ϕ_{eff} above 100 % can be obtained [25]. Obviously, compression/deswelling of the microgels would affect the physical meaning of ϕ_{eff}. In spite of this caveat, it is clear that the coexistence region of the microgel system is very broad in comparison with hard spheres, for which the coexistence domain ranges from ϕ_{eff} = 49.4 % to ϕ_{eff} = 54.5 % [2]. Also, the microgels start to crystallize at lower ϕ_{eff} than hard spheres. Another interesting result is the coexistence regime which shifts to higher volume fractions and widens for higher pH; ultimately, the crystal boundary converges toward ϕ_{eff} = 74 % which is reminiscent of the maximum packing fraction for hard spheres. The jamming transition was determined by systematically performing experiments starting at initial pH 3.0 and jumping directly to varying final pH values. The jamming transition (solid lines in Fig. 3.4) marks the final pH above which unordered jammed states were observed that did not relax to liquid-crystal coexistence after 24 hours. Below the jamming transition, the behavior in rapid expansion experiments was the same as from the equilibrium measurements with small pH jumps at the same pH, *i.e.* with liquid-like and liquid/crystalline coexistence regions.

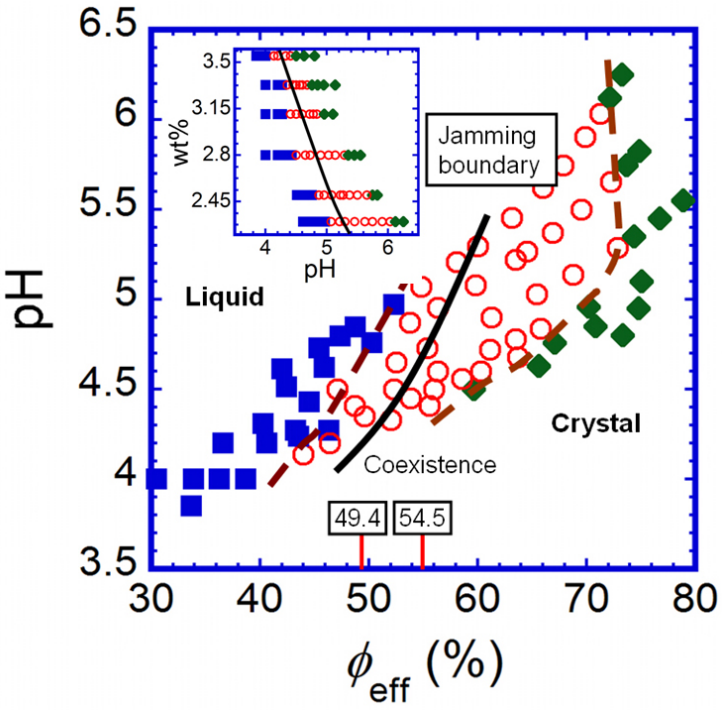

Figure 3. 4 Phase diagram of microgel suspensions within the microdialysis cell as a function of pH. ■, ○, and ◆ represent liquid, liquid/crystal coexistence, and crystal region, from equilibrium experiments, with the dashed lines indicating the phase boundaries. On the horizontal axis, the liquid/crystal coexistence region for hard sphere is marked. The inset displays the raw phase diagram, as function of pH for different weight fractions. The solid lines represent the jamming transition observed in rapid expansion experiments.

The unusual phase diagram in Fig. 3.4 is the result of interplay between deformability/compressibility of particles and tunable attractive and repulsive interactions [26]. Crystallization at low ϕ_{eff} with pH < pKa of AAc can be explained by weakly attractive forces due to hydrogen bonding between protonated AAc groups and amide groups, as described in previous studies [11, 12, 14, 26]. Increases in pH cause microgel swelling. Under these conditions crystallization seems to be frustrated by the deformability and compressibility of microgels, as indicated by unusual broad coexistence regime. For hard spheres, crystallization is driven solely by the increase in local entropy, since the interparticle potential renders energetic effects irrelevant. In the

microgel suspensions, on the other hand, particles can adjust their size by deswelling; although deswelling comes at an enthalpic cost, the higher global entropy of a liquid phase can off-set this. Our experiments show that crystallization of the swollen microgels (at high pH) requires much higher volume fractions than hard spheres and that the melting transition increases with pH. The crystallization also can be hindered because of intricate steric interactions between polymer chains on the surface as microgels have higher monomer density in the center and decays exponentially toward the surface with dangling polymer segments [27, 28]. This effect is more pronounced with pH increase. At the same time, when large particle volume changes are suddenly induced, microgel particles are kinetically trapped in concentrated unordered phases. Dangling polymer segments at the microgel surface [27, 28] can become entangled, which contributes to the inability of the jammed phase to relax towards the equilibrium structure. It is important to realize the difference between the current study and our previously reported studies of the phase behavior of microgel suspensions in closed capillaries; for those experiments heating and subsequent quenching to 20 °C were used to prepare samples, analogous to the large pH jumps in the current work. Those earlier studies studied microgel dynamics over many days, revealing remarkable aging of microgel suspensions [12]. One key observation was slow crystallization over periods of many weeks, with slowly swelling particles; this phenomenon was attributed to the delicate balance between energetic and entropic effects that are unique to microgels. Since these timescales can not be probed with our microdialysis cell, the current study focuses on the equilibrium behavior at relatively short time scales, which are made possible by the fast solvent response of our apparatus.

Crystal growth in colloidal suspension is the result of competition between thermodynamics and kinetics. For typical hard sphere systems, simulation results indicate that the face-centered cubic (FCC) structure has a higher entropy than hexagonal close-packed (HCP) and is thus the most stable state [29]. However, the entropy difference

between FCC and HCP is minute and has been controversial. Under normal gravity conditions, hard sphere suspensions have been found to form a mixture of random hexagonal close-packed (RHCP) and FCC crystals [2]. In microgravity, on the other hand, FCC packing was never found, suggesting that a bias towards FCC is induced by gravity [30]. Interestingly, as shown in Fig. 3.5, the stacking sequence in our microdialysis cell experiments, where gravity is also negligible, was exclusively RHCP; crystal structures were determined by reconstructing stacking sequences of hexagonal layers from image sequences at different sample depths.

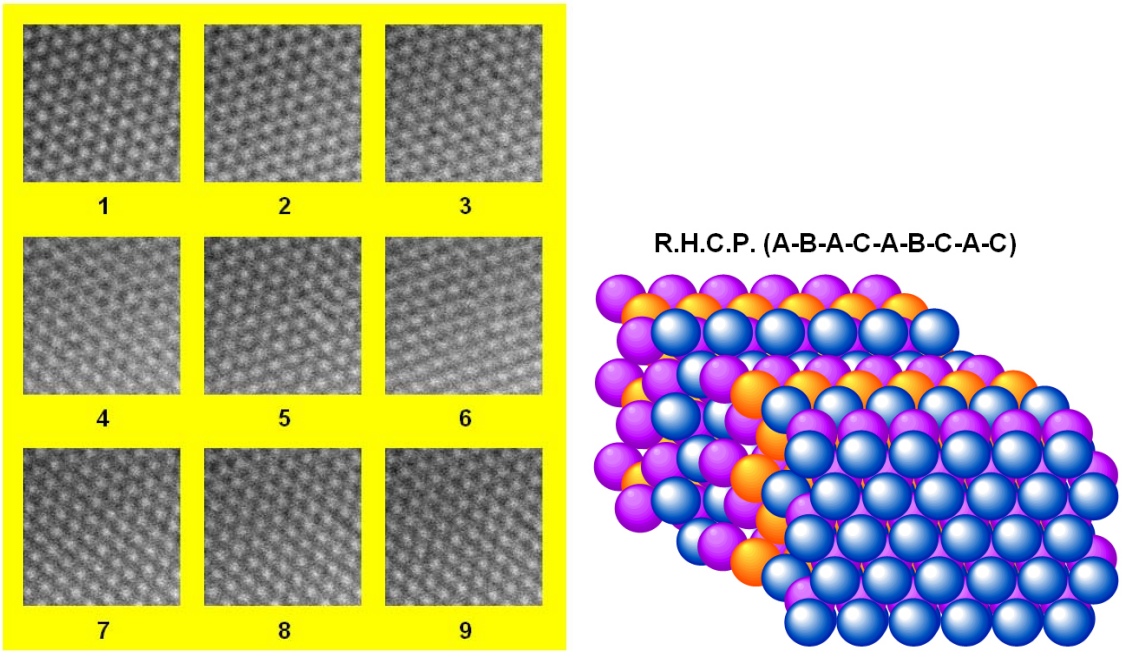

Figure 3.5 Series of optical sections of optical microscopy images of pNIPAm-*co*-AAc microgel colloidal crystal. The image sizes are 8 μm × 8 μm.

3.4 Conclusion

In conclusion, we fabricated a microfluidic device with which we can control the solvent composition in colloidal suspensions rapidly and reversibly. By integrating the microfluidic device with particle tracking video-microscopy, we were able to investigate the phase behavior of soft pH-responsive pNIPAm-*co*-AAc microgels. Like hard-sphere systems, microgels undergo liquid/crystal phase transitions. However, due to the deformability, compressibility and complex interparticle interactions, a broad liquid/crystal coexistence region was observed that shifts and expands to higher effective volume fractions with increased degree of microgel swelling (pH). We also determined the location of non-equilibrium, jammed states in the phase diagram, which were generated by rapidly expanding the volume of the microgels and stable for at least 24 hours. Surprisingly, the boundary between non-jammed and jammed states is located in the middle of the equilibrium liquid/crystal coexistence domain. Finally, all crystals grown in the microdialysis cell exhibited RHCP structures.

REFERENCES

1. Pusey, P.N. and W. Vanmegen, *Phase-Behavior of Concentrated Suspensions of Nearly Hard Colloidal Spheres.* Nature, 1986. **320**(6060): p. 340-342.

2. Pusey, P.N., W. Vanmegen, P. Bartlett, B.J. Ackerson, J.G. Rarity, and S.M. Underwood, *Structure of Crystals of Hard Colloidal Spheres.* Physical Review Letters, 1989. **63**(25): p. 2753-2756.

3. Anderson, V.J. and H.N.W. Lekkerkerker, *Insights into phase transition kinetics from colloid science.* Nature, 2002. **416**(6883): p. 811-815.

4. Gasser, U., E.R. Weeks, A. Schofield, P.N. Pusey, and D.A. Weitz, *Real-space imaging of nucleation and growth in colloidal crystallization.* Science, 2001. **292**(5515): p. 258-262.

5. Oxtoby, D.W., *New Perspectives on Freezing and Melting.* Nature, 1990. **347**(6295): p. 725-730.

6. Pelton, R., *Temperature-sensitive aqueous microgels.* Advances in Colloid and Interface Science, 2000. **85**(1): p. 1-33.

7. Das, M., H. Zhang, and E. Kumacheva, *Microgels: Old materials with new applications.* Annual Review of Materials Research, 2006. **36**: p. 117-142.

8. Senff, H. and W. Richtering, *Temperature sensitive microgel suspensions: Colloidal phase behavior and rheology of soft spheres.* Journal of Chemical Physics, 1999. **111**(4): p. 1705-1711.

9. Wu, J.Z., B. Zhou, and Z.B. Hu, *Phase behavior of thermally responsive microgel colloids.* Physical Review Letters, 2003. **90**(4): p. 048304.

10. Alsayed, A.M., M.F. Islam, J. Zhang, P.J. Collings, and A.G. Yodh, *Premelting at defects within bulk colloidal crystals.* Science, 2005. **309**(5738): p. 1207-1210.

11. Debord, S.B. and L.A. Lyon, *Influence of particle volume fraction on packing in responsive hydrogel colloidal crystals.* Journal of Physical Chemistry B, 2003. **107**(13): p. 2927-2932.

12. Meng, Z., J.K. Cho, V. Breedveld, and L.A. Lyon, *Physical Aging and Phase Behavior of Multiresponsive Microgel Colloidal Dispersions.* Journal of Physical Chemistry B, 2009. **113**(14): p. 4590-4599.

13. Debord, J.D. and L.A. Lyon, *Synthesis and characterization of pH-responsive copolymer microgels with tunable volume phase transition temperatures.* Langmuir, 2003. **19**(18): p. 7662-7664.

14. Meng, Z.Y., J.K. Cho, S. Debord, V. Breedveld, and L.A. Lyon, *Crystallization behavior of soft, attractive microgels.* Journal of Physical Chemistry B, 2007. **111**(25): p. 6992-6997.

15. Senff, H., W. Richtering, C. Norhausen, A. Weiss, and M. Ballauff, *Rheology of a temperature sensitive core-shell latex.* Langmuir, 1999. **15**(1): p. 102-106.

16. Batchelor, G.K., *Brownian Diffusion of Particles with Hydrodynamic Interaction.* Journal of Fluid Mechanics, 1976. **74**(9): p. 1-29.

17. Sato, J. and V. Breedveld, *Transient rheology of solvent-responsive complex fluids by integrating microrheology and microfluidics.* Journal of Rheology, 2006. **50**(1): p. 1-19.

18. Ackerson, B.J., S.E. Paulin, B. Johnson, W. van Megen, and S. Underwood, *Crystallization by settling in suspensions of hard spheres.* Physical Review E, 1999. **59**(6): p. 6903-6913.

19. Jiang, P., J.F. Bertone, K.S. Hwang, and V.L. Colvin, *Single-crystal colloidal multilayers of controlled thickness.* Chemistry of Materials, 1999. **11**(8): p. 2132-2140.

20. Cheng, Z.D., P.M. Chaikin, J.X. Zhu, W.B. Russel, and W.V. Meyer, *Crystallization kinetics of hard spheres in microgravity in the coexistence regime: Interactions between growing crystallites.* Physical Review Letters, 2002. **88**(1): p. 015501.

21. Cheng, Z.D., J.X. Zhu, W.B. Russel, W.V. Meyer, and P.M. Chaikin, *Colloidal hard-sphere crystallization kinetics in microgravity and normal gravity.* Applied Optics, 2001. **40**(24): p. 4146-4151.

22. Chaikin, P.M., *Principles of Condensed Matter Physics*. (Cambridge University Press, Cambridge, England, 1995).

23. Vanmegen, W. and S.M. Underwood, *Change in Crystallization Mechanism at the Glass-transition of Colloidal Spheres.* Nature, 1993. **362**(6421): p. 616-618.

24. Harland, J.L., S.I. Henderson, S.M. Underwood, and W. Vanmegen, *Observation of Accelerated Nucleation in Dense Colloidal Fluids of Hard-sphere Particles.* Physical Review Letters, 1995. **75**(19): p. 3572-3575.

25. St John, A.N., V. Breedveld, and L.A. Lyon, *Phase behavior in highly concentrated assemblies of microgels with soft repulsive interaction potentials.* Journal of Physical Chemistry B, 2007. **111**(27): p. 7796-7801.

26. Cho, J.K., Z. Meng, L.A. Lyon, and V. Breedveld, *Tunable attractive and repulsive interactions between pH-responsive microgels.* Soft Matter, 2009. p. DOI:10.1039/<B912105F>.

27. Stieger, M., W. Richtering, J.S. Pedersen, and P. Lindner, *Small-angle neutron scattering study of structural changes in temperature sensitive microgel colloids.* Journal of Chemical Physics, 2004. **120**(13): p. 6197-6206.

28. Eckert, T. and W. Richtering, *Thermodynamic and hydrodynamic interaction in concentrated microgel suspensions: Hard or soft sphere behavior?.* Journal of Chemical Physics, 2008. **129**(4): p. 124902.

29. Mau, S.C. and D.A. Huse, *Stacking entropy of hard-sphere crystals.* Physical Review E, 1999. **59**(4): p. 4396-4401.

30. Zhu, J.X., M. Li, R. Rogers, W. Meyer, R.H. Ottewill, W.B. Russell, and P.M. Chaikin, *Crystallization of hard-sphere colloids in microgravity.* Nature, 1997. **387**(6636): p. 883-885.

CHAPTER 4

TUNABLE ATTRACTIVE AND REPULSIVE INTERACTIONS BETWEEN PH-RESPONSIVE MICROGELS*

We investigated direct measurements of the pairwise interparticle potential between poly(*N*-isopropylacrylamide-*co*-acrylic acid) (pNIPAm-*co*-AAc) colloidal microgels as a function of pH, as determined through Ornstein-Zernike analysis of the pair distribution function of quasi-2D dilute colloidal suspensions. The interaction potential ranges from purely repulsive at high pH due to electrosteric interactions to weakly attractive at low pH due to hydrogen bonding, which explains previous observations on the unique phase behavior of these particles in concentrated suspensions.

4.1 Introduction

As discussed in Ch. 1, Colloidal suspensions display various phases and microscopic structures, ranging from random disordered to self-assembled ordered structures [1-4]. The phase behavior is determined by the effective volume fraction of the suspension and interparticle forces, such as van der Waals attractions, Coulombic interactions, steric repulsions and hydrogen-bonding. Understanding the interplay between these intermolecular forces is essential to control colloidal phase behavior, for

---

* This chapter has been accepted to soft matter as "Tunable attractive and repulsive interactions between pH-responsive microgel" by J. Cho, Z. Meng, L.A. Lyon, and V. Breedveld (2009), DOI:10.1039/<B912105F>.

example to fabricate ordered colloidal structures for specific applications. The majority of studies to date have been devoted to hard-sphere systems, which have simple intermolecular forces dominated by entropic excluded volume effects [5] and to other colloidal systems with relatively well-understood additional interactions, such as Coulombic repulsion and depletion attractions [6, 7]. Only fairly recently, soft and deformable particles, in particular star polymers and microgels, have attracted significant attention under the impulse of improved synthesis techniques. These soft colloidal systems are characterized by tunability of their softness and complex interparticle interactions, which result in rich phase diagrams and unique hydrodynamic behavior [8, 9].

In spite of several studies on the phase behavior of colloidal microgels as a model system for soft spheres, both from our groups and from other researchers [10-14], direct measurements of the underlying interparticle interactions have not been reported. However, previous experimental observations in our groups have indicated that these interactions are non-trivial, especially in pNIPAm-*co*-AAc microgels. While the phase behavior of pure pNIPAm microgels can be explained relatively well by defining an effective volume fraction of particles and using hard-sphere-like interactions, the incorporation of AAc adds significant complexity to the system. Hard sphere theory is not sufficient to explain the dynamics of these pH-responsive microgels, as illustrated by the following examples from our own research. First, pNIPAm microgel suspensions are liquid-like below the hard sphere freezing volume fraction of 0.494, but pNIPAm-*co*-AAc microgels were found to exhibit close-packed crystalline structures under experimental conditions that yield effective volume fractions below 0.40 [10]. In another study, we observed two unexpected phenomena: irreversible adhesion of pNIPAm-*co*-AAc microgels to glass substrates in very dilute suspensions, and enhanced thermal stability of pNIPAm-*co*-AAc colloidal crystals at temperatures well above the volume phase transition temperature [11]. These observations were specific for low pH

conditions, where AAc groups are protonated and Coulombic repulsions are minimized, and strongly suggest the existence of an attractive interparticle potential. A third set of experiments provides further clues about the interparticle interactions: the microstructure of concentrated pNIPAm-*co*-AAc microgels was found to slowly evolve from diffusive to sub-diffusive liquid and ultimately to crystalline over several weeks of aging [13]. This last set of experiments suggests that the attractive interaction must be weak ($< k_B T$); otherwise microgels should have formed aggregates or crystals on much shorter timescales [15]. On the other hand, if the attractive potential is only a fraction of $k_B T$, multi-particle interactions are required to form stable structures. The coordination of multiple particles into specific organized structures is statistically unlikely, which significantly slows the kinetics of formation. Based on all of these experimental results and for lack of other explanations, we have hypothesized previously that the interaction between pNIPAm-*co*-AAc microgels is pH-dependent: weakly attractive at low pH due to hydrogen bonding and repulsive at high pH due to electrosteric forces [13]. In particular the hypothesized existence of weakly attractive forces has been somewhat controversial, because there is no other colloidal system in which these forces are known to play a dominant role. We therefore aimed to measure the interparticle potentials experimentally to clarify this sticky issue. In this communication, we present measurements of the pairwise interparticle potential between colloidal pNIPAm-*co*-AAc microgels as a function of pH. The results were obtained from optical videomicroscopy of core/shell (C/S) microgel particles under quasi-2D confinement. To the best of our knowledge, no previous study has attempted to measure the interactions between stimuli-responsive microgels as a function of environmental conditions.

Direct measurements of intermolecular forces have been achieved by a variety of methods, for example, surface force apparatus (SFA) [16], total internal reflection microscopy (TIRM) [17], atomic force microscopy (AFM) [18], and optical tweezers

(OT) [19]. However, each of these techniques has specific limitations that make it difficult to apply them to colloidal microgels. For example, AFM and SFA are well suited for interactions that are stronger than several $k_B T$. TIRM measures the equilibrium probability distribution of particles relative to a wall under the influence of gravity and thus requires density contrast between particle and fluid, which is not present in microgel systems. Furthermore, TIRM yields particle-wall interaction rather than particle-particle interactions. OT require a minimum refractive index difference between particles and suspending medium in order to trap them in the laser beam, which highly swollen microgels do not offer. An alternative method is to extract the equilibrium pair interparticle potential between colloidal particles from measurements of the spatial particle distributions in suspension, based on liquid structure theory [20-22]. Key advantages of this method are its high sensitivity and the ability to measure particle-particle interactions without external perturbations, which is important for soft materials like pNIPAm-*co*-AAc microgels that easily deform and compress upon external forces and are hypothesized to have weak interactions. The pair distribution function can be determined via optical microscopy, but this technique provides two important challenges. First of all, accurate detection of particle positions requires good imaging contrast, even though the demands are less stringent than for OT. Individual pNIPAm-*co*-AAC microgel particle can be tracked in differential interference contrast (DIC) mode, but the optical contrast is insufficient to accurately determine the positions of microgel particles at close separation, which is crucial to achieve pair distribution measurements that are suitable for potential calculations. In order to solve this problem, we synthesized core/shell (C/S) microgel particles with a fluorescent polystyrene (PS) core and pNIPAm-*co*-AAc shell. These C/S particles can be tracked individually even at interparticle contact. Secondly, it is desirable to confine the colloidal particles to a quasi-2D geometry in order to prevent artifacts due to the projection of the actual particle positions in three dimensions to a two-dimension video-microscopy image [23]. We achieve this by utilizing mono-disperse

colloids as spacers between glass slides to create a quasi-2D geometry with precisely controlled separation between the glass slides across a large sample area.

4.2 Experimental Section

Synthesis of core/shell microgels

The C/S colloidal microgels were synthesized via aqueous precipitation polymerization, using fluorescently labeled carboxylate-modified polystyrene (PS) microspheres (FluoSphere®, 0.50 μm diameter, Invitrogen) as seeds and creating a layer of poly(*N*-isopropylacrylamide-*co*-acrylic acid) (pNIPAm-*co*-AAc) hydrogel as shell. NIPAm (Sigma-Aldrich) was purified by recrystallization from hexane (J.T. Baker) before use. AAc (Sigma-Aldrich), cross-linker (*N*,*N*'-methylene bis(acrylamide) (BIS); Fluka) and initiator (ammonium persulfate (APS); Sigma-Aldrich) were used as received. NIPAm (0.1333g; 81.3 mol%) / AAc (0.0148g; 14.2 mol%) / BIS (0.0100g; 4.5 mol%) were dissolved in 30 *mL* DI water containing purified microspheres. The colloidal suspension with reaction mixture was pre-heated to 60 ºC and purged with N_2, followed by initiation by adding APS after 30 minutes. The reaction was performed at 60 ºC for 4 hours and the synthesized C/S microgels were purified extensively by dialysis against DI water over 3 weeks to remove unreacted components. The polydispersity of the C/S microgels was determined to be less than 8 % by PCS measurements (Protein Solutions).

Characterization hydrodynamic radius of core/shell microgels

The hydrodynamic radius R_H of the C/S microgels as a function of pH was characterized by PTVM. We selected PTVM over DLS to determine R_H, because the latter is highly sensitive to the presence of impurities and small aggregates, which can explicitly be ignored during image analysis. The results are shown in Fig. 4.1, where R_H has been plotted as a function of pH. Like pure pNIPAm-*co*-AAc microgel, ionization of AAc in the C/S microgels, induced by pH increase, results in reversible volumetric

swelling of the hydrogel shell as a result of the Coulombic repulsion between deprotonated AAc groups, ingress of cations from the medium, and a resultant osmotic pressure difference between the microgel and medium [24].

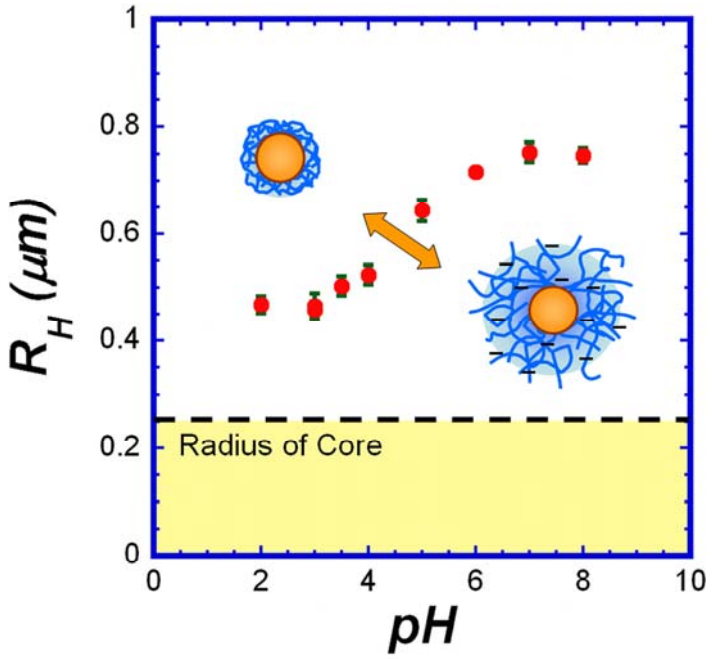

Figure 4.1 Hydrodynamic radius of stimuli-responsive C/S microgel particles as a function of pH at a concentration of ~ 0.01 wt%. The dashed line represents the radius of the fluorescent core, 0.25 μm.

Fabrication of 2D confined cell

A uniform quasi-2D suspension in a confinement cell was created by using monodisperse hard colloidal particles as spacers between two glass slides, as previously described by our group [8] (see figure 4.2(a)). A dilute suspension of core/shell colloidal particles and 2.0 μm diameter polystyrene (Invitrogen) spacer particles was prepared in various pH buffers from pH 2 ~ 8 at constant ionic strength I = 15 mM. Prior to mixing, both species of particles were extensively purified with DI water by repeated centrifugation and washing steps. To ensure efficient and robust convergence of numerical calculations during data analysis, concentrations of the particle suspensions

were chosen so that all samples had a projected area coverage of ca. 10 % for each pH. A drop of the suspension was placed between a glass coverslip and microscope slide, excess fluid was removed to reduce the spacing between slides to the diameter of the spacer particles, and the cell was sealed with fast curing epoxy resin. To prevent adhesion between the C/S particles and glass walls, we gently sonicated the confinement cell and all measurements were made within 1 hr of sonication. An inverted optical microscope (Leica DM-IRB) with 100× N.A. 1.30 oil immersion objective and Peltier-cooled CCD camera (Cohu, Poway, CA) was used to record movies of the suspension and every measurement was performed at 23 °C. Typically, images of particles within a ~ 64 × 48 μm field of view were captured for 10 min at 30 frame/sec and analyzed using image analysis routines in IDL software [25]. As explained above, imaging of the fluorescent PS cores is not affected by swelling-deswelling of the microgel shell and one can locate the position of particles accurately at all pH values; a representative image from videomicroscopy is shown in figure 4.2(b). The absence of out-of plane motion of the particles confirmed that the colloidal particle suspensions are quasi-2D.

(a)

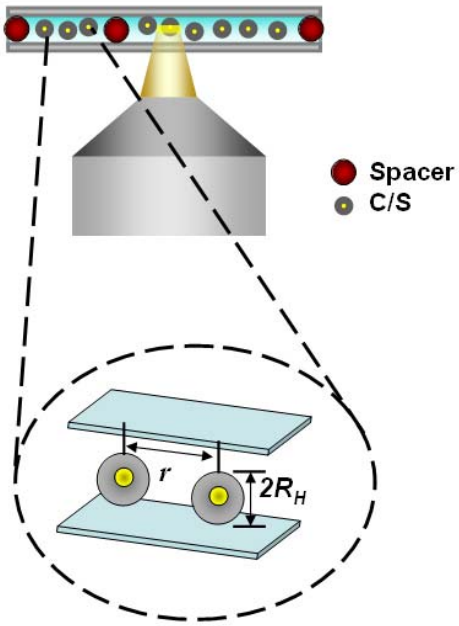

(b)

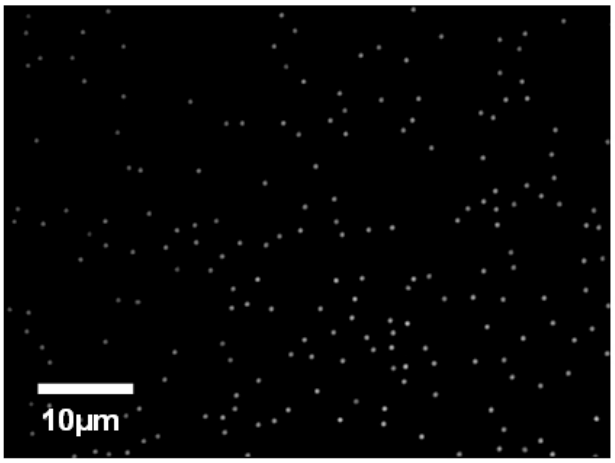

Figure 4.2 (a) Schematic of experimental set-up in quasi-2D where *r* is the center-to-center separation between C/S particles. (b) Representative image from fluorescence microscopy of C/S colloidal suspension in quasi-2D confinement cell at pH 6.0 and *I* = 15 mM. For all pH conditions, C/S colloidal suspensions of ~ 10 % area density were used; only the PS core is visible in fluorescence microscopy.

4.3 Results and Discussion

The pairwise interaction potential between colloidal particles in a medium can be determined from the equilibrium structure of particle suspensions [20-22]. In our case, this is quantified via the two-dimensional radial distribution function $g(r)$, which provides the probability of finding neighboring particles at specific separation distances as shown in figure 4.3(a). Since single images only contain a moderate number of particles (ca. 200 within field of view), $g(r)$ was obtained by averaging over 20,000 frames to get meaningful statistics. Theoretically, in the infinitely dilute regime $g(r)$ can be related directly to the pairwise interparticle potential $u(r)$ via the Boltzmann distribution as $\lim_{n\to 0} g(r) = \exp\left[-u(r)/k_B T\right]$ where n is the areal number density of particles. However, in reality, under the experimental conditions that are required to

measure $g(r)$ accurately, multi-body interactions play a role and the multi-particle potential $w(r)$ is found rather than $u(r)$: $g(r) \approx \exp\left[-w(r)/k_B T\right]$. It is possible to extract $u(r)$ from $w(r)$ using the Ornstein-Zernike convolution integral equation in combination with a suitable approximate closure relation. The hypernetted chain (HNC) approximation (Eq. (1)) is known to be appropriate for soft spheres: [26]

$$u(r) = w(r) + nk_B T\, I(r) \tag{4.1}$$

The convolution integral can be solved iteratively from the experimental $g(r)$ data:

$$I(r) = \int_A \left[g(r') - 1 - nI(r)\right]\left[g(|r' - r|) - 1\right] d^2 r' \tag{4.2}$$

Our experimental results of $g(r)$ for C/S colloidal microgels as a function of pH appear in figure 4.3(a). It is important to note that the microgels change their size as a function of pH. As expected, the position of the nearest-neighbor peak, therefore, shifts towards larger separation r as the microgels swell at higher pH. It is also apparent from the lack of structure of $g(r)$ that the quasi-2D C/S colloidal suspensions are liquid-like. Equations (4.1) and (4.2) were applied iteratively until convergence was achieved. We also confirmed that $u(r)$ is independent of areal density *n* by performing experiments at slightly different areal coverages. The final results for $u(r)$ as a function pH appear in figure 4.3(b). It is reasonable to assume that $u(r)$ accurately reflects the interparticle potential between pNIPAm-*co*-AAc microgels, since the core (PS) is covered by a thick pNIPAM-*co*-AAc hydrogel layer. Clearly, $u(r)$ is pH-sensitive and changes from attractive to repulsive as the pH increases.

(a)

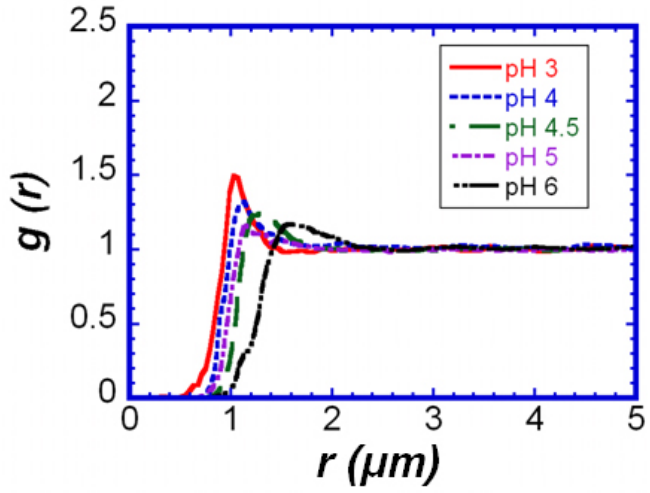

(b)

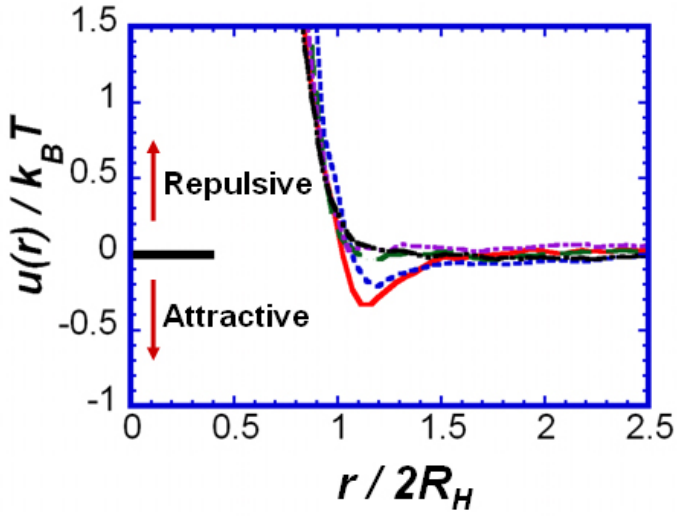

Figure 4.3 (a) Pair distribution function $g(r)$ of C/S colloidal suspensions as a function of r and pH. (b) Pairwise interaction potential between C/S colloidal suspensions as a function of normalized separation and pH.

Although pNIPAm microgels have soft repulsive interactions, our experiments confirm that the incorporation of AAc to the polymer network alters not only the chemistry of the material, but also the physical behavior of microgels. At low pH values, the potential is attractive, but weakly, as we hypothesized; this is indicated by the depth of the potential well of less than $k_B T$ for pH 3.0 and 4.0. The attractive interaction is observed only below the pKa (~ 4.15) of the AAc moieties, where the C/S particles have negligible surface charge. Additionally, the ionic strength of our buffers is 15 mM, so that the Debye screening length $\kappa^{-1} \approx 3\,\text{nm}$ and Coulombic interactions should not play a major role in $u(r)$ on the lengths scales shown in Fig. 4.3(b) and the attractions in our system therefore differ from the attractions between like-charged particles previously reported by Grier group [21, 27].

Attractive interactions in our system can be attributed to three forces: van der Waals attraction, hydrogen bonding between protonated AAc groups and amide groups, and hydrophobic interactions between isopropyl groups. The fact that the attractions are most pronounced at low pH leads to the conclusion that the major contribution comes from hydrogen bonding between AAc groups (e.g. salt-bridges) and acid-amide interactions. Another interesting feature is that the interactions are apparently long-range (~ 50 nm), which can be explained with two phenomena: (1) the ambiguity between the physical size of the microgel particle, as defined by the outer dimensions of the fuzzy microgel interface, and the particle hydrodynamic radius and (2) the presence of dangling polymer chains at the microgel surface, which can be extended if the enthalpic gain of multiple hydrogen bonds overcomes the entropy penalty of stretching. At high pH (above the pKa of AAc) where most of AAc moieties are deprotonated, the interaction between microgels is purely repulsive. This repulsive behavior is expected in the presence of charged, dangling chains protruding from the surface, providing electrosteric repulsion between C/S microgels. The current results are in excellent agreement with our previous

observations that were discussed above: Fig. 4.3(b) clearly shows that attractive interparticle interactions of magnitudes less than $k_B T$ exist in pNIPAm-*co*-AAc microgel systems and that these attractions can be attributed to hydrogen bonding.

4.4 Conclusion

In this chapter, we have directly measured pairwise interparticle potentials $u(r)$ between pNIPAm-*co*-AAc microgel colloids in quasi-2D. We confirmed the existence of weak attractive potential below the *pKa* of AAc, which is consistent with our previous observations and the interparticle potential changed to repulsive beyond the *pKa* . This pH-dependent long-range interaction implies that the origin of attractive interaction arises mainly from rearrangement/reorientation of multiple weak hydrogen bondings between acid/amide groups on dangling polymer chains. Our result clearly demonstrates that by incorporating additional functional groups in the network one can enhance tunability of interactions between colloidal microgels. It is likely that this tunable potential will open up new avenues for self-assembly of soft building blocks for advanced materials by tuning colloidal interactions.

REFERENCES

1. Savage, J.R., D.W. Blair, A.J. Levine, R.A. Guyer, and A.D. Dinsmore, *Imaging the sublimation dynamics of colloidal crystallites.* Science, 2006. **314**(5800): p. 795-798.

2. Yethiraj, A. and A. van Blaaderen, *A colloidal model system with an interaction tunable from hard sphere to soft and dipolar.* Nature, 2003. **421**(6922): p. 513-517.

3. Zahn, K., R. Lenke, and G. Maret, *Two-stage melting of paramagnetic colloidal crystals in two dimensions.* Physical Review Letters, 1999. **82**(13): p. 2721-2724.

4. Anderson, V.J. and H.N.W. Lekkerkerker, *Insights into phase transition kinetics from colloid science.* Nature, 2002. **416**(6883): p. 811-815.

5. Pusey, P.N. and W. Vanmegen, *Phase-Behavior of Concentrated Suspensions of Nearly Hard Colloidal Spheres.* Nature, 1986. **320**(6060): p. 340-342.

6. Monovoukas, Y. and A.P. Gast, *The Experimental Phase-Diagram of Charged Colloidal Shspensions.* Journal of Colloid and Interface Science, 1989. **128**(2): p. 533-548.

7. Shah, S.A., Y.L. Chen, K.S. Schweizer, and C.F. Zukoski, *Phase behavior and concentration fluctuations in suspensions of hard spheres and nearly ideal polymers.* Journal of Chemical Physics, 2003. **118**(7): p. 3350-3361.

8. Cho, J.K., L.A. Lyon, and V. Breedveld, *Hindered diffusion of hard and soft colloids under geometric confinement.* 2009 (Submitted).

9. Watzlawek, M., C.N. Likos, and H. Lowen, *Phase diagram of star polymer solutions.* Physical Review Letters, 1999. **82**(26): p. 5289-5292.

10. Debord, S.B. and L.A. Lyon, *Influence of particle volume fraction on packing in responsive hydrogel colloidal crystals.* Journal of Physical Chemistry B, 2003. **107**(13): p. 2927-2932.

11. Meng, Z.Y., J.K. Cho, S. Debord, V. Breedveld, and L.A. Lyon, *Crystallization behavior of soft, attractive microgels.* Journal of Physical Chemistry B, 2007. **111**(25): p. 6992-6997.

12. Wu, J.Z., B. Zhou, and Z.B. Hu, *Phase behavior of thermally responsive microgel colloids.* Physical Review Letters, 2003. **90**(4): p. 048304.

13. Meng, Z., J.K. Cho, V. Breedveld, and L.A. Lyon, *Physical Aging and Phase Behavior of Multiresponsive Microgel Colloidal Dispersions.* Journal of Physical Chemistry B, 2009. **113**(14): p. 4590-4599.

14. Han, Y., N.Y. Ha, A.M. Alsayed, and A.G. Yodh, *Melting of two-dimensional tunable-diameter colloidal crystals.* Physical Review E, 2008. **77**(4): p. 041406.

15. Lu, P.J., E. Zaccarelli, F. Ciulla, A.B. Schofield, F. Sciortino, and D.A. Weitz, *Gelation of particles with short-range attraction.* Nature, 2008. **453**(7194): p. 499-U4.

16. Israelachvili, J.N., R.K. Tandon, and L.R. White, *Measurement of Forces between 2 Mica Surfaces in Aqueous Poly(Ethylene Oxide) Solutions.* Nature, 1979. **277**(5692): p. 120-121.

17. Prieve, D.C., *Measurement of colloidal forces with TIRM.* Advances in Colloid and Interface Science, 1999. **82**(1-3): p. 93-125.

18. Li, Y.Q., N.J. Tao, J. Pan, A.A. Garcia, and S.M. Lindsay, *Direct Measurement of Interaction Forces betwee nColloidal Particles using the Scanning Force Microscope.* Langmuir, 1993. **9**(3): p. 637-641.

19. Sainis, S.K., V. Germain, and E.R. Dufresne, *Statistics of particle trajectories at short time intervals reveal fN-scale colloidal forces.* Physical Review Letters, 2007. **99**(1): p. 018303.

20. Behrens, S.H. and D.G. Grier, *Pair interaction of charged colloidal spheres near a charged wall.* Physical Review E, 2001. **6405**(5): p. 050401.

21. Han, Y.L. and D.G. Grier, *Confinement-induced colloidal attractions in equilibrium.* Physical Review Letters, 2003. **91**(3): p. 038302.

22. Wu, H.J., T.O. Pangburn, R.E. Beckham, and M.A. Bevan, *Measurement and interpretation of particle-particle and particle-wall interactions in levitated colloidal ensembles.* Langmuir, 2005. **21**(22): p. 9879-9888.

23. Ramirez-Saito, A., C. Bechinger, and J.L. Arauz-Lara, *Optical microscopy measurement of pair correlation functions.* Physical Review E, 2006. **74**(3): p. 030401.

24. Das, M., H. Zhang, and E. Kumacheva, *Microgels: Old materials with new applications.* Annual Review of Materials Research, 2006. **36**: p. 117-142.

25. Crocker, J.C. and D.G. Grier, *Methods of digital video microscopy for colloidal studies.* Journal of Colloid and Interface Science, 1996. **179**(1): p. 298-310.

26. Hansen, J.P. and I. R. McDonald, *Theory of simple liquids*. 2nd ed. (Academic Press, London, 1986).

27. Crocker, J.C. and D.G. Grier, *When like charges attract: The effects of geometrical confinement on long-range colloidal interactions.* Physical Review Letters, 1996. **77**(9): p. 1897-1900.

CHAPTER 5

HINDERED DIFFUSION OF HARD AND SOFT COLLOIDS UNDER GEOMETRIC CONFINEMENT*

We have investigated Brownian diffusion of fluorescent colloidal particles under geometric confinement between parallel walls via particle tracking video microscopy. The hydrodynamic coupling between particle and confining walls hinders the diffusion of particles. Hard (polystyrene) and soft (polystyrene core with microgel shell) colloids were used to determine the effect of softness on hindered diffusion. Hindrance coefficients were obtained as a function of degree of confinement, *i.e.* spacing between walls. Whereas the hindered diffusion for hard spheres was found to be in excellent agreement with numerical model predictions, soft microgels exhibited unusually high mobility even when the wall spacing was smaller than the unperturbed particle diameter, due to the deformable and compressible structure of the soft microgel shell.

5.1 Introduction

Hydrodynamic interaction of colloidal particles with stationary walls has been of interest because of numerous technological and scientific applications, for example, nano/micro-fluidic devices, molecular transport in porous media, membrane separations, and chromatography [1-6]. The presence of a solid wall imposes constraints on the flow

---

* This chapter has been submitted as "Hindered diffusion of hard and soft colloids under geometric confinement" by J. Cho, Z. Meng, L.A. Lyon, and V. Breedveld (2009).

field and affects the mobility of a particle by hydrodynamic coupling or drag. As a result, Brownian diffusion of colloids is suppressed significantly near walls. Starting with Faxen's pioneering work, which provided asymptotic solutions for hydrodynamic interactions between a rigid, flat wall and a rigid single sphere [7], the Brownian motion of a hard sphere confined between two hard walls has been studied experimentally and numerically [8-13]. Early experimental studies investigated the Brownian motion of particles trapped between two walls via light scattering [12, 14], which provides ensemble-averaged results for all particles in the scattering volume and, as a result, cannot give direct insight into the mobility of particles as a function distance to the walls. Recent microscopy-based studies using particle tracking video-microscopy (PTVM) coupled with optical tweezers [10] and total internal reflection microscopy (TIRM) [15], have provided direct measurements of hindered Brownian diffusion near solid walls. However, most of these experiments were performed under "mild" confinement, *i.e.* the distance between confining hard walls is larger than twice the diameter of the confined sphere [11, 12, 14, 16] or measured hydrodynamic coupling between particles rather than between particle and wall [10, 17]. In this letter we report a systematic experimental study of confined colloidal diffusion over a wide range of wall spacings. For hard spheres, we present data down to gap sizes that are only slightly larger than the sphere diameter, which enables a rigorous comparison with theoretical predictions. For soft spheres, we explored Brownian diffusion all the way into the compressed regime, with wall spacings smaller than the unperturbed hydrodynamic particle diameter.

While several experimental and numerical studies have been devoted to the hydrodynamic coupling between hard spheres and hard walls, the effects of confinement on the mobility of soft spheres are poorly understood, in spite of the importance of soft colloids for various applications, such as biomolecular transport through nanopores [18, 19] and emulsion and microspheres in microfluidic devices [20-22]. In a recent study, silica particles near a planar silica surface covered with thermally responsive polymer

brushes showed significantly reduced hydrodynamic coupling in comparison with numerical predictions for hard walls [23]. This experimental observation clearly indicates that softness can dramatically alter hydrodynamic interactions, but it leaves questions regarding the hindered diffusion of soft sphere under strong confinement between solid walls. In this letter, we use core/shell polystyrene/microgel particles to investigate the hindered diffusion of soft spheres and compare the results with hard polystyrene particles.

5.2 Experimental Section

We use PTVM to measure the hindrance effect for colloidal spheres between parallel solid walls [24]. The fabrication of the cells is described in detail in Ch. 4: dilute suspension mixtures of colloids of interest and silica spacer particles are loaded between glass slides and excess liquid is removed to create a confined cell in which the spacing between walls is defined by the monodisperse silica spacers, as shown in Fig. 5.1. The volumetric ratio of spacers and sample particles was 1:100 and the total particle concentration was kept below 0.01 wt% to avoid hydrodynamic coupling among the diffusing particles and with the silica spacers (diameters 1.61, 1.85, 2.06, 2.28, 3.01 and 4.63 μm; Bangs Laboratories). As hard spheres, fluorescent carboxylate-modified polystyrene (PS) microspheres of three different sizes were used (diameters 0.50, 1.1 and 2.0 μm; Invitrogen). For soft spheres, we used C/S pNIPAm-*co*-AAc microgels, as described in Ch. 4. All particle suspensions were sonicated and extensively dialyzed against deionized (DI) water before use to remove impurities. To evaluate the effect of electrostatic interactions, the PS and core/shell particles were studied in DI water and in 2 mM sodium chloride (NaCl) solutions.

A key advantage of using with multiple mono-disperse silica spacers between the glass slide is the ability to create a well-defined wall spacing over a large sample area. In

our experiments, the average distance between silica spacers was ~ 200 μm, which prevents buckling of the cover slip. Precise control over the wall spacing is critical, because the hindrance is a strong function of the degree of confinement, with particles further away from the walls moving faster than particles that are closer; this generates a diffusion coefficient gradient and can even result in particle drift [25]. As illustrated in figure 5.1, the spacing of our confined cell (H) can simply be tuned by using different sizes of silica spacers. The experimental cell is then placed on an optical microscope (Leica DM-IRB). In differential interference contrast (DIC) mode, the focal plane of the 100× immersion oil objective was set at the mid-plane of the cell ($h = H / 2$), where the motion of colloids (both hard and soft) was recorded in fluorescent mode with a CCD camera at 30 frame/sec at 20 °C.

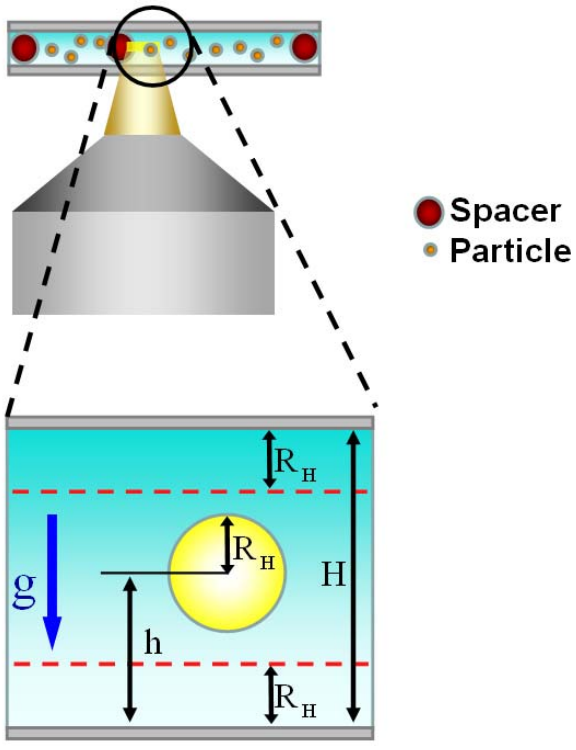

Figure 5.1 Schematic of confinement cell mounted on optical microscope. H represents the spacer diameter, h the particle height, and R_H the hydrodynamic radius, respectively. Two dashed lines indicate the excluded volume inaccessible to particles.

5.3 Results and Discussion

Theoretical predictions for hindered diffusion are all benchmarked to the diffusion coefficient for free diffusion of a sphere far from any restrictions as given by the well-known Stokes-Einstein relation $D_0 = k_B T / 6\pi\eta R_H$, where k_B is the Boltzmann constant, T the absolute temperature, η the fluid viscosity, and R_H the hydrodynamic sphere radius. For a single sphere near a rigid wall, the lateral diffusion is defined as $D_{//} = f_{//,1} D_0$, where $f_{//,1}$ is the hindrance coefficient that is commonly approximated as a power series [7]:

$$f_{//,1}(R_H, h) = \frac{D_{//}}{D_0} \approx 1 - \frac{9}{16}\left(\frac{R_H}{h}\right) + \frac{1}{8}\left(\frac{R_H}{h}\right)^3 - \frac{45}{256}\left(\frac{R_H}{h}\right)^4 - \frac{1}{16}\left(\frac{R_H}{h}\right)^5 \qquad (5.1)$$

For a hard sphere confined between two parallel walls, the total hindrance effect of the walls $f_{//,2}$ can be calculated via the linear superposition approximation (LSA) suggested by Oseen [7]:

$$f_{//,2}(R_H, h) = \left[f_{//,1}(R_H, h)^{-1} + f_{//,1}(R_H, H-h)^{-1} - 1 \right]^{-1} \qquad (5.2)$$

Various alternative methods have been proposed to account for the combined hindrance of the two walls, but LSA is mathematically simple and has been shown to agree quite well with experimental results from prior studies [11, 12, 26-28]. Equation (5.1) technically applies only to cases with $R_H/h < 0.91$; for smaller gaps, lubrication corrections are needed. However, for all experimental cases studied in this paper (R_H/h up

to 0.97), the simplified expression of Eq. (5.1) causes deviations of less than a few percent, well within experimental errors.

Equations (5.1) and (5.2) pose an experimental challenge: because of the strong dependence of the hindrance coefficient on the distance between particles and walls, the position of particles – or their spatial distribution – must be known exactly to enable direct comparison with model predictions. For our particle tracking microscopy experiments in the confinement cell, there are two experimental concerns: sedimentation and the finite depth of focus of the optical detection system. In the horizontally mounted cell, gravity introduces a slightly asymmetric distribution of particles with a higher particle concentration near the bottom wall, which can be described by the Boltzmann distribution P_B [16]. The average height of particles in the confined geometry can then be calculated as:

$$\overline{h} = \frac{\int_{R_H}^{H-R_H} hP_B(h)\,dh}{\int_{R_H}^{H-R_H} P_B(h)\,dh} \tag{5.3}$$

Because the centers of mass of the particles cannot get closer to the wall than their radius R_H, the integration limits in Eq. (5.3) are R_H and $H - R_H$, respectively. Figure 5.2 (a) clearly shows that the effect of gravity cannot be ignored for 2 μm PS spheres. Nevertheless, the average particle height in the sample is close to mid-plane ($h = H / 2 =$ 2.315 μm) under all experimental conditions. We can also calculate the number-averaged hindrance coefficient ($\overline{f_{//,2}}$) in the sample:

$$\overline{f_{//,2}}\left(R_H, H\right) = \frac{\int_{R_H}^{H-R_H} f_{//,2}\left(R_H, h\right) P_B\left(h\right) dh}{\int_{R_H}^{H-R_H} P_B\left(h\right) dh} \tag{5.4}$$

Numerical results for $\overline{f_{//,2}}$ as a function of degree of confinement ($2R_H / H$) are summarized in Fig. 5.2 (b) for the particle sizes in this study. As expected, under strong confinement ($2R_H / H \approx 1$), $\overline{f_{//,2}}$ drops to 0, indicating that the walls arrest Brownian diffusion, whereas in bulk ($2R_H / H \approx 0$) particles experience minimal hindrance and $\overline{f_{//,2}}$ =1. For comparison, the solid line represents the value of $f_{//,2}$ at the mid-plane of the cell ($h = H / 2$) without integrating over the particle distribution. Deviations between the averaged and mid-plane values of the hindrance function are obvious. The averaged hindrance factor is always lower than the mid-plane value; for off-center particles the enhanced hindrance by the closest wall outweighs the decreased hindrance by the more distant opposite wall. For large particles (2.0 μm) gravitation towards the bottom wall causes hindrance effects even if $R_H \ll H$.

(a)

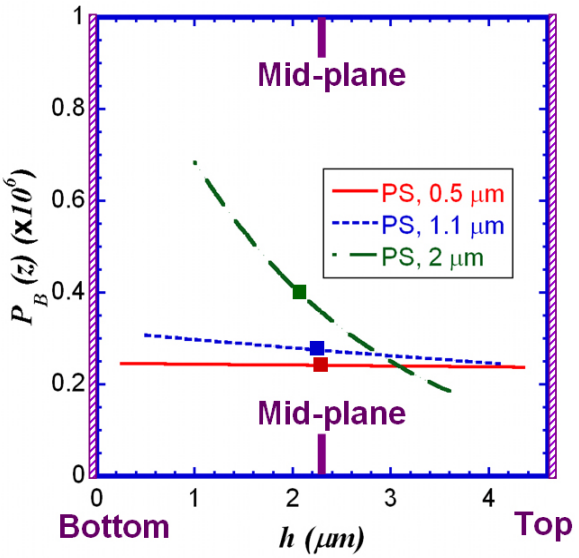

(b)

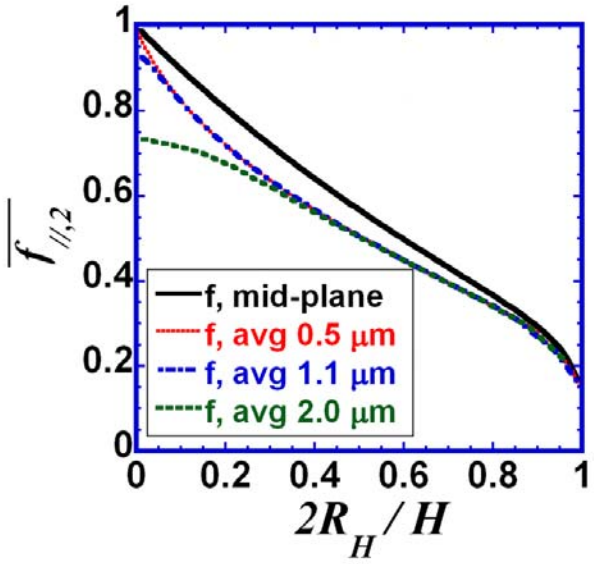

Figure 5.2 (a) Particle height distributions of polystyrene particles for H = 4.63 μm with three particle sizes: 0.50 (solid), 1.1 (dotted) and 2.0 μm (dashed). Square symbols indicate the average particle height. (b) Numerical prediction of hindrance coefficient averaged over the entire sample volume as a function of wall spacing for three different particle sizes: 0.50 (dotted), 1.1 (dash-dotted), and 2.0 μm (dashed). The solid black line represents the hindrance factor at the mid-plane (Eq. (5.2)).

The second effect that is important for the interpretation of our experimental results is the finite depth of focus (*DOF*) of the optical microscope. *DOF* is a function of wavelength, magnification, numerical aperture, and refractive index of medium between coverslip and objective and marks the distance above and below the focal plane where particles can be detected. Only particles that reside within the *DOF* can be tracked and contribute to the hindrance factor measured via PTVM, so that the integration in Eq. (5.4) should be restricted to the *DOF*. If measurements are taken at the mid plane of the cell ($h = H/2$), Eq. (5.4) must be modified to:

$$\overline{f_{//,2}^{DOF}}\left(R_H, H\right) = \frac{\int_{H/2-DOF/2}^{H/2+DOF/2} f_{//,2}\left(R_H, h\right) P_B\left(h\right) dh}{\int_{H/2-DOF/2}^{H/2+DOF/2} P_B\left(h\right) dh} \tag{5.5}$$

For a 100× oil immersion objective, the detection efficiency for 0.50 μm diameter particles decays to 50 % within ± 0.5 μm from the focal plane, corresponding to about 1 μm vertical resolution [29]. Results for $\overline{f_{//,2}^{DOF}}$ as a function of $2R_H / H$ are presented in Fig. 5.3. We can identify two important regimes: (i) $H \gg DOF$ and (ii) $H - 2R_H < DOF$. In regime (i), the cell height is much larger than the focal depth; as a result, none of the particles within the *DOF* experience significant wall effects and the experimentally determined hindrance factor equals the mid-plane value. As the cell height decreases, some particles within the *DOF* experience enhanced hindrance from the walls and the average hindrance factor gradually deviates from the mid-point prediction. Once the *DOF* becomes larger than $H - 2R_H$, all particles in the cell are detected optically and Eq. (5.5) becomes identical to Eq. (5.4). It is useful to point out that the three curves in Fig. 5.3 represent anticipated results from three classes of experimental techniques. Methods that average over the entire cell volume, *e.g.* light scattering [30],

should follow Eq. (5.4). On the other hand, methods that actively restrict particles to the mid-plane, *e.g.* optical tweezers [10], follow Eq. (5.2) (with $h = H/2$). Finally, PTVM experiments provide hindrance values that are in between these extremes (Eq. (5.5)).

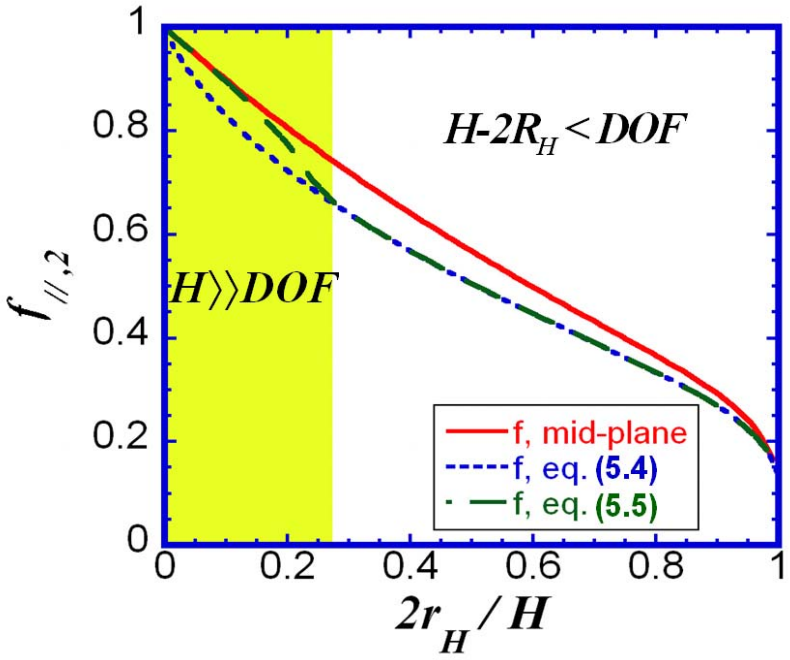

Figure 5.3 The hindrance coefficient as a function of degree of confinement ($2R_H / H$) for PTVM (averaged over *DOF*, Eq. (5.5)), in comparison with mid-plane value and value averaged over the entire sample volume (Eq. (5.4)).

In Fig. 5.4, we compare the results from our experiments with the numerical predictions. The error bar in x-axis represents standard deviation from five repeatative experiments and the error bar in y-axis is the result of polydispersity of particles as well as spacers. There is excellent agreement between model predictions and experimental results for hard-polystyrene spheres measured by PTVM over the entire range of wall spacings that were probed. It must be reiterated that previous experiments explored a much more limited range of confinement, with $2R_H/H$ less than 0.50. In contrast, our experiments systematically cover a much wider range of confinement, with $2R_H/H$

between 0.11 and 0.97. This improvement is made possible by the excellent control that we have over the wall spacing in our confinement cell through the use of monodisperse silica spacers. As predicted by models, Brownian diffusion under geometric confinement becomes more hindered as the separation between walls (H) approaches the size of particles, and the hindrance coefficient converges to zero. To the best of our knowledge, experimental observations of diffusion under such strong confinement ($2R_H \approx H$) have not been reported before. The agreement between experimental results and model Eq. (5.5) is within experimental errors across the entire range of confinement. Deviations between experimental data and Eqs. (5.4) and (5.2), the mid-plane and sample-averaged values, respectively, are somewhat inconclusive due to experimental uncertainties, but Eq. (5.5) seems to agree best with data. Electrostatic interactions between particles and walls do not play a significant role, as is proven by the overlapping results for experiments in low-salt DI water and 2 mM NaCl solutions.

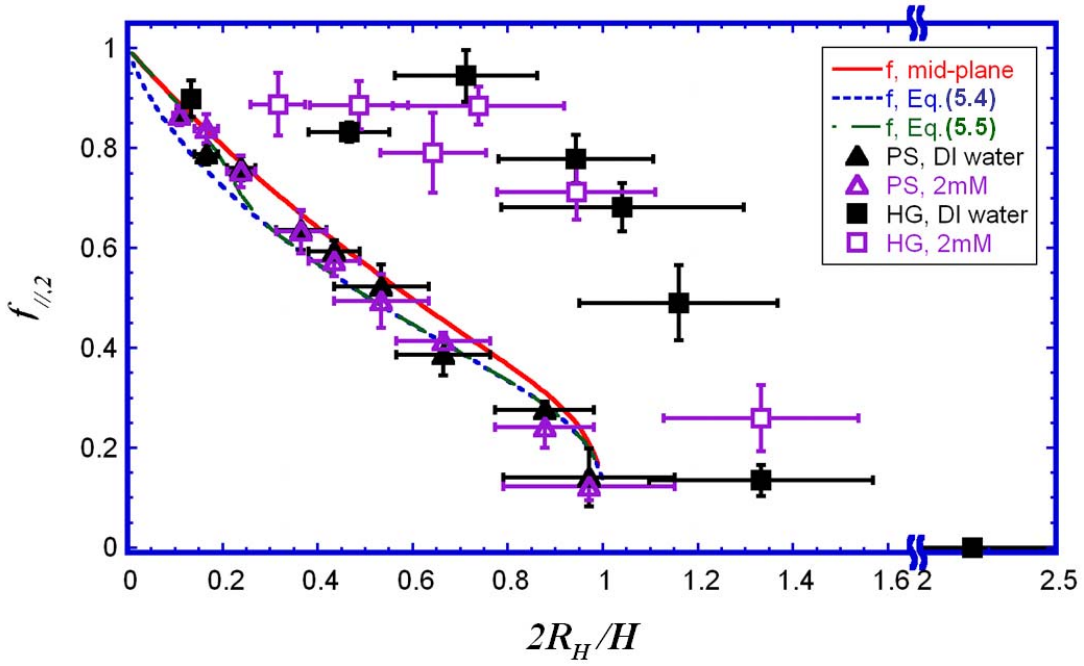

Figure 5.4 Experimental hindrance coefficients for hard spheres (triangles) and soft spheres (squares) as a function of confinement, $2R_H / H$. Both types of particles were

measured in DI water (solid symbols) and in 2 mM NaCl solution (open symbols). The lines represent the numerical predictions from Fig. 5.3.

Experimental confirmation of the predicted hindrance between hard walls and hard spheres is a strong result, but even more interesting are our experimental observations of hindered diffusion of soft spheres, also shown in Fig. 5.4. Like for hard spheres, the hindrance coefficient for soft core/shell particles decays with increasing degrees of confinement. However, the hydrodynamic hindrance of soft core/shell spheres is suppressed dramatically: at $2R_H / H \approx 0.8$, the soft spheres diffuse roughly four times faster than their hard sphere equivalents. It is suspected that the porous structure of the microgel shell allows water to penetrate, thus reducing the hydrodynamic coupling between sphere and wall. Even more striking is the observation that our core/shell particles exhibit significant mobility even under extreme confinement that requires particle deformation, for $2R_H / H > 1$, a regime inaccessible with hard spheres. Under these conditions the soft particles must deform and/or shrink. When the wall spacing is further decreased, the core/shell particles slow down and eventually become fully arrested (see data point for $2R_H / H = 2.16$). It is clear from Fig. 5.4 that numerical predictions for hard spheres do a very poor job of describing the hindered diffusion of soft spheres, even under relatively mild confinement conditions, where a hard sphere approximation might have been expected to be valid. The soft particles have a solid polystyrene core (~250 nm radius) covered with a soft pNIPAm-*co*-AAc microgel shell (~700 nm thick in DI water and ~400 nm thick in 2 mM NaCl solution). Although the microgel layer is polyelectrolytic (due to the AAc co-monomers), Coulombic interactions do not affect the hindrance significantly. After changes in hydrodynamic radius are taken into account, hindered diffusion is the same in DI water and 2 mM NaCl solution.

5.4 Conclusion

Our study is the first direct observation of hindered Brownian diffusion of hard and soft spheres between parallel walls over a wide range of degrees of confinement. Lateral diffusion of colloidal particles was measured parallel to the walls and, as expected, hydrodynamic coupling with confining walls was found to suppress Brownian diffusion. Experimental results for hard spheres are in excellent agreement with numerical prediction from the LSA model across the entire experimental range. On the other hand, soft core/shell particles, which are porous, compressible and deformable, can dissipate hydrodynamic coupling effectively, resulting in enhanced mobility under confinement. Even when the wall spacing is smaller than the unperturbed diameter of soft spheres, they still exhibit Brownian diffusion; this anomalous behavior cannot be explained with current numerical predictions.

REFERENCES

1. Sexton, L.T., L.P. Horne, S.A. Sherrill, G.W. Bishop, L.A. Baker, and C.R. Martin, *Resistive-pulse studies of proteins and protein/antibody complexes using a conical nanotube sensor.* Journal of the American Chemical Society, 2007. **129**(43): p. 13144-13152.

2. Susanto, A., T. Herrmann, E. von Lieres, and J. Hubbuch, *Investigation of pore diffusion hindrance of monoclonal antibody in hydrophobic interaction chromatography using confocal laser scanning microscopy.* Journal of Chromatography A, 2007. **1149**(2): p. 178-188.

3. Dziennik, S.R., E.B. Belcher, G.A. Barker, M.J. DeBergalis, S.E. Fernandez, and A.M. Lenhoff, *Nondiffusive mechanisms enhance protein uptake rates in ion exchange particles.* Proceedings of the National Academy of Sciences of the United States of America, 2003. **100**(2): p. 420-425.

4. Deen, W.M., *Hindered Transport of Large Molecules in Liquid-Filled Pores.* AIChE Journal, 1987. **33**(9): p. 1409-1425.

5. Wind, J.D., D.R. Paul, and W.J. Koros, *Natural gas permeation in polyimide membranes.* Journal of Membrane Science, 2004. **228**(2): p. 227-236.

6. Schoch, R.B., J.Y. Han, and P. Renaud, *Transport phenomena in nanofluidics.* Reviews of Modern Physics, 2008. **80**(3): p. 839-883.

7. Happel, J. and H. Brenner, *Low Reynolds number hydrodynamics.* 2nd ed. (Noordhoff International press, Leiden, 1973).

8. Goldman, A.J., R.G. Cox, and H. Brenner, *Slow Viscous Motion of a Sphere Parallel to a Plane Wall .I. Motion through a Quiescent Fluid.* Chemical Engineering Science, 1967. **22**(4): p. 637-&.

9. Dufresne, E.R., D. Altman, and D.G. Grier, *Brownian dynamics of a sphere between parallel walls.* Europhysics Letters, 2001. **53**(2): p. 264-270.

10. Dufresne, E.R., T.M. Squires, M.P. Brenner, and D.G. Grier, *Hydrodynamic coupling of two Brownian spheres to a planar surface.* Physical Review Letters, 2000. **85**(15): p. 3317-3320.

11. Lin, B.H., J. Yu, and S.A. Rice, *Direct measurements of constrained Brownian motion of an isolated sphere between two walls.* Physical Review E, 2000. **62**(3): p. 3909-3919.

12. Lobry, L. and N. Ostrowsky, *Diffusion of Brownian particles trapped between two walls: Theory and dynamic-light-scattering measurements.* Physical Review B, 1996. **53**(18): p. 12050-12056.

13. Lauga, E. and T.M. Squires, *Brownian motion near a partial-slip boundary: A local probe of the no-slip condition.* Physics of Fluids, 2005. **17**(10): p. 103102.

14. Feitosa, M.I.M. and O.N. Mesquita, *Wall-Drag Effect on Diffusion of Colloidal Particles near Surfaces - a Photon-Correlation Study.* Physical Review A, 1991. **44**(10): p. 6677-6685.

15. Eichmann, S.L., S.G. Anekal, and M.A. Bevan, *Electrostatically confined nanoparticle interactions and dynamics.* Langmuir, 2008. **24**(3): p. 714-721.

16. Faucheux, L.P. and A.J. Libchaber, *Confined Brownian-Motion.* Physical Review E, 1994. **49**(6): p. 5158-5163.

17. Cui, B.X., H. Diamant, B.H. Lin, and S.A. Rice, *Anomalous hydrodynamic interaction in a quasi-two-dimensional suspension.* Physical Review Letters, 2004. **92**(25): p. 258301.

18. Han, A.P., G. Schurmann, G. Mondin, R.A. Bitterli, N.G. Hegelbach, N.F. de Rooij, and U. Staufer, *Sensing protein molecules using nanofabricated pores.* Applied Physics Letters, 2006. **88**(9): p. 093901.

19. Muthukumar, M., *Translocation of a confined polymer through a hole.* Physical Review Letters, 2001. **86**(14): p. 3188-3191.

20. Shah, R.K., J.W. Kim, J.J. Agresti, D.A. Weitz, and L.Y. Chu, *Fabrication of monodisperse thermosensitive microgels and gel capsules in microfluidic devices.* Soft Matter, 2008. **4**(12): p. 2303-2309.

21. Fidalgo, L.M., G. Whyte, D. Bratton, C.F. Kaminski, C. Abell, and W.T.S. Huck, *From microdroplets to microfluidics: Selective emulsion separation in microfluidic devices.* Angewandte Chemie-International Edition, 2008. **47**(11): p. 2042-2045.

22. Chu, L.Y., A.S. Utada, R.K. Shah, J.W. Kim, and D.A. Weitz, *Controllable monodisperse multiple emulsions.* Angewandte Chemie-International Edition, 2007. **46**(47): p. 8970-8974.

23. Tu, H.L., L. Hong, S.M. Anthony, P.V. Braun, and S. Granick, *Brush-sheathed particles diffusing at brush-coated surfaces in the thermally responsive PNIPAAm system.* Langmuir, 2007. **23**(5): p. 2322-2325.

24. Crocker, J.C. and D.G. Grier, *Methods of digital video microscopy for colloidal studies.* Journal of Colloid and Interface Science, 1996. **179**(1): p. 298-310.

25. Lancon, P., G. Batrouni, L. Lobry, and N. Ostrowsky, *Drift without flux: Brownian walker with a space-dependent diffusion coeffcient.* Europhysics Letters, 2001. **54**(1): p. 28-34.

26. Liron, N. and S. Mochon, *Stokes Flow for a Stokes-Let between 2 Parallel Flat Plates.* Journal of Engineering Mathematics, 1976. **10**(4): p. 287-303.

27. Pawar, Y. and J.L. Anderson, *Hindered Diffusion in Slit Pores - an Analytical Result.* Industrial & Engineering Chemistry Research, 1993. **32**(4): p. 743-746.

28. Blake, J.R., *Image System for a Stokeslet in a No-Slip Boundary.* Proceedings of the Cambridge Philosophical Society-Mathematical and Physical Sciences, 1971. **70**(Sep): p. 303.

29. Chung, K., J.K. Cho, E.S. Park, V. Breedveld, and H. Lu, *Three-Dimensional in Situ Temperature Measurement in Microsystems Using Brownian Motion of Nanoparticles.* Analytical Chemistry, 2009. **81**(3): p. 991-999.

30. Pecora R., *Dynamic light scattering*, (Plenum Press, New York, 1985).

CHAPTER 6

CONCLUSIONS AND RECOMMENDATIONS

6.1 Conclusions

In this thesis, we primarily focused our attention on investigating the dynamics, phase behavior, intermolecular forces, and hydrodynamics of colloidal suspensions of multi-responsive pNIPAm-*co*-AAc microgels. Chapter 1 was intended to give a general introduction to the reader who is not familiar with the subjects of this thesis, in particular the various forces that play a role in colloidal systems, the interaction potential and phase behavior, and the role of microgels as a model system for soft colloids.

Capitalizing on the fact that micron size colloidal systems are readily accessible with conventional instruments like optical microscopy, in Ch. 2 we introduced PTVM as a useful experimental technique for various colloidal systems. We then applied PTVM to dilute colloidal suspensions to measure various physical properties: hydrodynamic particle radius R_H, sample temperature, and micro-structure of the suspending complex fluid. Firstly, we measured R_H for polystyrene colloidal particles and validated the methodology by comparing results with PCS and subsequently investigated the swelling-transition of pH-responsive pNIPAm-*co*-AAc microgel as a function of pH. This study confirmed the pH-responsive changes of R_H for pNIPAm-*co*-AAc microgels upon pH change. We also successfully investigated the reversible and reproducible dynamics of swelling/deswelling of pH-responsive microgels upon pH change *in situ* by coupling with microdialysis cell, which allows direct control over solvent composition. Secondly, PTVM was used to measure the local temperature in microfluidic devices. The method provided accurate and reproducible temperature measurements in 2D (in-plane) and 3D

(out-of plane) temperature gradients in microfluidics devices with an experimental accuracy better than ± 1 °C. The results of the 2D and 3D studies were in good agreement with predictions from numerical models. Lastly, we investigated the changes in rheological properties of PEO-PPO-PEO triblock copolymer solutions during temperature-induced gelation with oscillatory macro-rheology and with micro-rheology via PTVM. While macro-rheology provided a two-step gelation transition, micro-rheology via PTVM only captured the secondary transition and revealed that it is characterized by heterogeneous microscopic phase separation. Based on the observations, we proposed a gelation mechanism at molecular level.

After demonstrating the efficacy of PTVM for studying dilute colloidal suspensions, we shifted our attention to concentrated particle suspensions. Specifically, in Ch. 3, the phase behavior of soft pH-responsive pNIPAm-*co*-AAc microgels was investigated by using PTVM, coupled with the microdialysis cell to control pH. The results showed that microgel suspensions exhibit the same equilibrium phases as hard sphere suspensions: liquid, crystal and liquid/crystal coexistence. In comparison with hard spheres, the liquid/crystal coexistence region for microgels was much broader, and it shifted and expanded to higher effective volume fractions with increased degree of microgel swelling (pH). The unique behavior is most likely caused by the deformability, compressibility, and complex interparticle interactions of the microgels. In addition, we determined the location of a non-equilibrium, kinetically trapped jammed phase in the phase diagram. Surprisingly, the boundary between non-jammed and jammed states was located in the middle of the equilibrium liquid/crystal coexistence domain, further highlighting the complex nature of the interparticle interactions. Finally, all microgel crystals grown in the microdialysis cell resulted in RHCP (random hexagonally close packed) structures.

After finding unusual phase behavior of pNIPAm-*co*-AAc microgels upon pH change, we decided to directly probe the underlying interparticle interactions. In Ch. 4,

we measured the pairwise interparticle potential $u(r)$ between pNIPAm-*co*-AAc colloidal microgels in a quasi 2D suspension. We confirmed the existence of a weakly attractive potential below the pKa of AAc, which shifts to a purely repulsive interparticle potential changed above the pKa. From these results, we concluded that the pH-dependent long-range interaction arises mainly from rearrangement/reorientation of multiple weak hydrogen bonds between acid/amide groups on dangling polymer chains. The weakness of the interaction ($< 1\ k_BT$) explains why cooperative behavior of multiple particles is required to form stable attractive structures.

The studies of phase behavior and interparticle interaction revealed striking differences between hard spheres and pNIPAm-*co*-AAc microgels. Thus, it was reasonable to pose another question: does the softness of microgels have an effect on the hydrodynamics of these particles when they are geometrically confined. In chapter 5, we investigated the hindered Brownian diffusion of hard and soft colloidal spheres between parallel walls over a wide range of degrees of confinement. As expected, we found that the hydrodynamic coupling of colloidal particles with confining walls suppresses their lateral diffusion significantly. While the experimental results for hard spheres were in excellent agreement with numerical predictions from existing models, soft pNIPAm-co-AAc microgels exhibited significantly enhanced mobility under confinement, which cannot be explained with current numerical models.

6.2 Recommendations

The projects described in the previous chapters have raised several interesting questions that warrant additional experimental work beyond the scope of this thesis:

1. In chapter 4, the interparticle interactions between microgels were described but it needs more thoughtful evaluation. Our experiments highlighted an interesting feature of the microgels: tunability of the interparticle potential from weakly attractive to purely repulsive. While charged silica particles can successfully be described with DLVO theory [1, 2], and purely repulsive interactions have effectively been modeled through inverse power law potentials [3], our result clearly show that the pH responsive microgels cannot be captured by these models. More quantitative experiments should be performed, for example by varying ionic strength, to provide a solid experimental basis for the development of alternative models that describe the interaction potential of these colloids.

2. The phase behavior of pNIPAm-*co*-AAc ionic microgels at I = 15 mM was described in Ch. 3. However, in this study we have not fully explored the entire range of multi-responsiveness of the microgels. Other parameters of interest are ionic strength and the crosslink density of the microgels, which determines their softness. A more detailed multi-dimensional phase diagram can be obtained by exploring these additional parameters.

3. We showed that crystallization in the microdialysis cell always results in RHCP crystal structures. Because the microdialysis cell provides direct control over effective volume fraction and gravitational effects are minimal, we might be able to use the system to study the crystallization kinetics for other crystal structures. For instance, by utilizing patterned substrates as a template for colloidal crystals, we can guide crystal growth into certain structures. Another suggestion is to insert electrodes into the microdialysis cell to generate electric fields that could facilitate desired crystal growth.

4. When impurities are present in crystallizing systems, they can either act as nucleation seed or as a defect that hinders crystallization. Especially when the size of the impurity is larger than, but of the same order as the diameter of crystalling particles, the curvature of

the impurity can cause geometric frustration [4, 5]. However, the dynamics of crystallization in the presence of such impurities have not reported yet. By using microgel suspensions in combination with artificial impurities of known size, one can investigate the effect of impurities on crystallization dynamics in the microdialysis cell and study phenomena like defect propagation. These experiments would not only offer fundamental information regarding colloidal crystallization, but could also be used as inspiration for new methods for the fabrication of ordered colloidal structures.

REFERENCES

1. Vondermassen, K., J. Bongers, A. Mueller, and H. Versmold, *Brownian-Motion - a Tool to Determine the Pair Potential between Colloid Particles.* Langmuir, 1994. **10**(5): p. 1351-1353.

2. Denton, A.R., *Effective interactions and volume energies in charged colloids: Linear response theory*. Physical Review E, 2000. **62**(3): p. 3855-3864.

3. Prestipino, S., F. Saija, and P.V. Giaquinta, *Phase diagram of softly repulsive systems: The Gaussian and inverse-power-law potentials.* Journal of Chemical Physics, 2005. **123**(14): p. 144110.

4. de Villeneuve, V.W.A., R.P.A. Dullens, D.G.A.L. Aarts, E. Groeneveld, J.H. Scherff, W.K. Kegel, and H.N.W. Lekkerkerker, *Colloidal hard-sphere crystal growth frustrated by large spherical impurities.* Science, 2005. **309**(5738): p. 1231-1233.

5. de Villeneuve, V.W.A., L. Derendorp, D. Verboekend, E.C.M. Vermolen, W.K. Kegel, H.N.W. Lekkerkerker, and R.P.A. Dullens, *Grain boundary pinning in doped hard sphere crystals.* Soft Matter, 2009. **5**(12): p. 2448-2452.